Advances in Disjunctive and Time-Optimal Predictive Control Methods

by

Richard L Sutherland, Jr

A dissertation submitted in partial fulfillment
of the requirements for the degree of
Doctor of Philosophy
(Aerospace Engineering)
in the University of Michigan
2019

Doctoral Committee:

Associate Professor Anouck R. Girard, Co-Chair
Professor Ilya V. Kolmanovsky, Co-Chair
Professor Anthony Bloch
Dr. Frederick A. Leve
Dr. Christopher D. Petersen

Richard L Sutherland, Jr

rlsu@umich.edu

ORCID iD: 0000-0002-0494-9251

Dedication

To my parents,
to Dr. Lauren Soblosky,
to my friends and colleagues.

ACKNOWLEDGMENTS

I would like to acknowledge and express my enormous gratitude for the patience and insights of my advisors, including my co-chairs Prof. Ilya Kolmanovsky and Prof. Anouck Girard but also including the members of my committee and collaborators Dr. Fred Leve of AFOSR and Dr. Chris Petersen of AFRL. The feedback, advice, and guidance I have received from all of you over the past few years has been invaluable in reaching this point.

Further, I would like to acknowledge the support of my friends and colleagues in the Department of Aerospace Engineering at the University of Michigan, especially those within my prelim cohort.

TABLE OF CONTENTS

LIST OF FIGURES

LIST OF APPENDICES

LIST OF ABBREVIATIONS

BFP Body-Fixed Principal

CM Center of Mass

CP Center of Pressure

DARE Discrete-Time Algebraic Riccati Equation

DCM Direction Cosine Matrix

DSC Disjunctive Sensing and Control

EOMs Equations of Motion

INMS Ion-and-Neutral Mass Spectrometer

KKT Karush-Kuhn-Tucker

LQR Linear Quadratic Regulator

LVLH Local Vertical, Local Horizontal

MILP Mixed-Integer Linear Program

MPC Model Predictive Control

PD Proportional-Derivative

ABSTRACT

This dissertation addresses two kinds of problems. The first kind, Disjunctive Sensing and Control (DSC), is a particular variant of a hybrid control problem type that arose from a complication when working on a small satellite attitude control system in which the magnetic actuators and sensors could not function at the same time as magnetic actuation would inject unacceptable levels of sensor noise. The second class of problems involves time-optimal waypoint-following Model Predictive Control (MPC), inspired by missions such as fast-slewing imaging spacecraft, which must capture as many ground images as possible before their orbit and the Earth's rotation move the target out of line of sight. In this dissertation, novel approaches are developed to address each problem, and simulations are presented to illustrate their effectiveness. Specific contributions are as follows.

Firstly, the small satellite problem is analyzed in detail. The control goal is defined, the Equations of Motion (EOMs) are derived, the magnetic actuator/sensor conflict is described, and an LQR control scheme is developed that alternates between actuation and estimation, allowing these conflicting subsystems to still successfully achieve the mission objective. The spacecraft configuration with the additional passive stabilization mechanism in the form of panels that induce restorative air drag torques is considered as well as the design of an MPC controller to handle actuation constraints.

Secondly, inspired by the satellite problem, the DSC problem is treated in detail. The two subsystems, i.e., the sensing and actuation subsystems, are assumed to be linked by a binary decision variable that activates either subsystem at the expense of the other. Contractivity sufficient conditions are derived which can facilitate the construction of periodic

switching sequences that guarantee boundness and convergence properties of the closed-loop system trajectories and of the error covariance as well as the enforcement of chance constraints in steady-state. Additional methods are proposed to speed up the search for periodic sequences that satisfy the contractivity conditions. Spacecraft relative motion simulation case studies are reported to demonstrate the effectiveness of the technique.

Next, time-optimal waypoint-following MPC is considered for which a Mixed-Integer Linear Program (MILP) approach is proposed. The MILP formulation complements the ability of MPC-based controllers to explicitly handle state constraints. Several different scenarios are considered for spacecraft attitude control, including multiple waypoints, exclusion zones, and the addition of flexible mode states to the attitude dynamics. Simulation results are reported.

Finally, the non-uniqueness of the solution to the time-optimal MPC problem in the discrete-time setting is addressed and it is shown that it can lead to the loss of closed-loop Lyapunov stability. As a remedy, a secondary objective function is minimized after the optimal time horizon has been determined; this lexicographic optimization yields a unique solution which is shown to restore Lyapunov stability. Spacecraft relative motion simulation case studies are reported which illustrate closed-loop stability and robustness to unmeasured disturbances of the minimum-time MPC with the lexicographic optimization.

CHAPTER 1

Introduction

1.1 Disjunctive Sensing and Control (DSC)

DSC is a particular class of control problems for Hybrid Dynamical Systems [2]. Hybrid dynamical systems combine continuous evolution with discrete switching and jumps. In a continuous-time (resp., discrete-time) hybrid system, the state evolution is described by one set of differential (resp., difference) equations until certain conditions, referred to as the *jump* conditions, are satisfied, at which time instant the system *switches* to a new set of governing equations. The system then remains in this new dynamic mode until such time as another jump condition is satisfied. These jump conditions can be set by constraints on the system, by prescribed time intervals, or by the actions of an operator.

Hybrid systems have a long history of study [3], but have seen a significant surge in interest with the increasing role of computers in control systems. They can be used to model a wide range of scenarios; some examples of hybrid systems include a simple bouncing ball [4] (illustrated in Figure 1.1), an electrical circuit with switches or diodes [5], and a gain-scheduled missile [6].

Hybrid systems require careful treatment; even with a family of systems that share an equilibrium point and are individually each asymptotically stable, a poorly implemented switching logic can sometimes destabilize the overall hybrid system. Conversely, a family of systems that are each unstable can sometimes be stabilized with a carefully-designed

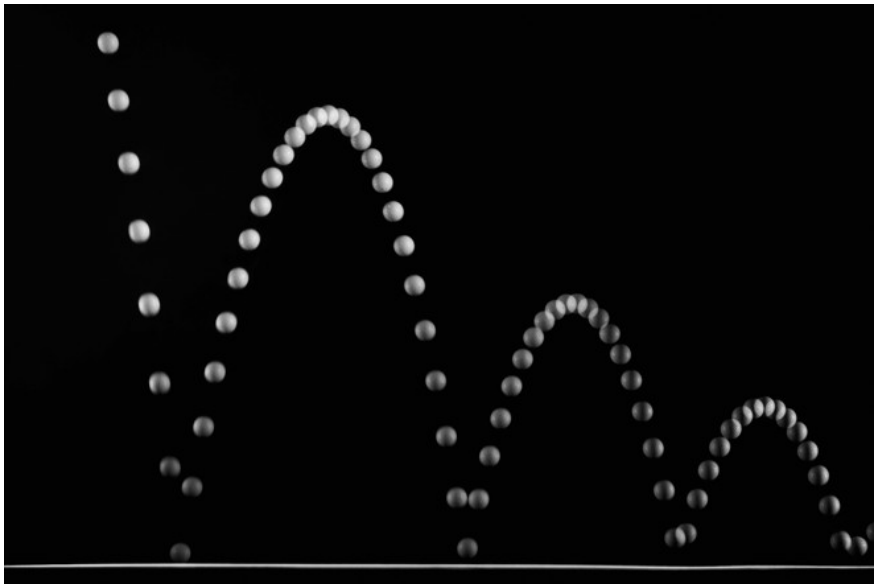

Figure 1.1: Strobe-photo capture of a bouncing ball. The jump conditions in this hybrid system are prescribed by physical constraints, i.e., the collisions between the ball and the ground [1].

switching logic [7].

What distinguishes DSC within the broader class of hybrid control problems is that in DSC, when the actuator subsystem is active, the measurement subsystem is inactive, and vice versa. This switching logic is illustrated in Figure 1.2. When the associated subsystem is inactive, either tracking error or estimation error can grow unbounded. Thus, the switching logic must be designed with care in order to ensure boundness and closed-loop stability.

1.2 Time-Optimal Predictive Control

In predictive control, inputs to a closed-loop system are selected based on the the prediction and optimization of the behavior of that system over a specified time horizon. A popular technique is Model Predictive Control (MPC) [8], in which the system's response is predicted with a dynamic model. System inputs are then selected based on the solution to an optimization problem formulated over a receding time horizon; however, in MPC, only the

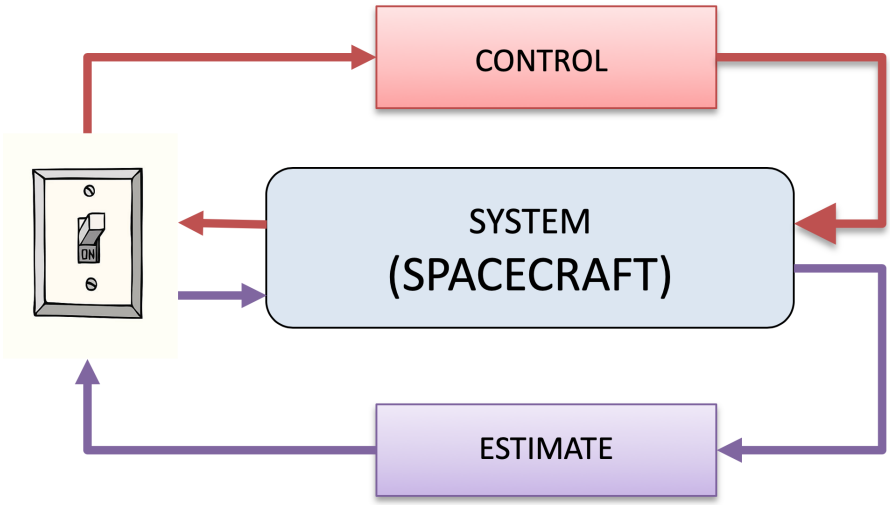

Figure 1.2: Visualization of disjunctive sensing and control. The system can be set to actuate or to measure, but both subsystems cannot be active at the same time.

control inputs for the current time instant, the "first move" in the optimal control sequence, are applied. Future control inputs are determined by new solutions to the optimization problem at each additional time step in turn. MPC is an attractive option in predictive control as it allows for the explicit handling of multiple state and input constraints, and, as a closed-loop approach, can accommodate disturbance effects.

In general, however, if the dynamic model is non-linear, if the optimization problem is non-convex, or if the prediction horizon is large, then computations to obtain control inputs at each time-step can be quite involved [9]. These factors are especially critical for the time-optimal approach considered in this work, as the optimization problems become non-convex when exclusion zones/obstacles are added and the prediction horizon must be long enough to encompass the entire trajectory to ensure a time-optimal solution.

One approach to time-optimality as well as the addition of exclusion zones is to treat the problem by converting it into a Mixed-Interger Linear Program (MILP). A MILP is a linear program in which some of the variables are constrained to only take integer values. As mentioned above, the introduction of integer-only variables makes the optimization problem non-convex; given a problem with multiple solutions, points in between those so-

lutions are in general non-integer valued and therefore infeasible [10]. In addition, MILP problems are known to be $\mathcal{NP}$-complete [11], and thus there is no guarantee that the problem can be solved in a time bounded by a polynomial function of the number of decision variables and the constraints.

However, methods exist that are known to efficiently converge to solutions. The most popular such method, Branch-and-Bound [12], is known to give a globally optimal solution by solving a sequence of relaxed linear programs in which the integer variables are allowed to take non-integer values. Due to the $\mathcal{NP}$-completeness property, this approach cannot be guaranteed to terminate with a globally-optimal solution without searching the entire space of feasible solutions. However, with good heuristics, in particular a warm-start approach in which previous known solutions serve as a starting point in searching for new solutions [13], this method can be practically useful for finding globally-optimal solutions in reasonable computation times. Other solution methods exist, such as Genetic Algorithms [14] and Tabu Search [15], that are generally based on a heuristic random-search approach; the randomness helps to avoid solver iterations terminating in a local, i.e. non-global, minimum.

Despite the computational challenges, the MILP framework is attractive as it offers great flexibility in constructing and solving problems, and it integrates well with the MPC framework in the handling of explicit constraints. In addition to classic optimization problems such as Time Scheduling [16] and Traveling Salesman [17] problems, in which the goal is to minimize a target quantity, the MILP framework can also handle problems such as drift counteraction [18–22], in which the goal is to maximize a target quantity, in particular the time before the state violates constraints. The MILP methods extend even to scenarios such as collision avoidance in unmanned formation flight [23].

1.3 Contributions and Dissertation Outline

The contributions of this dissertation include advancements in theory, methodology, and applications and address the two primary topics discussed above, the DSC problem and the time-optimal predictive control problem. The majority of the content of this dissertation has been originally published in or submitted to scientific journals [24, 25] and conference proceedings [26–29]. The specific contributions are listed below.

- Development of a controller for a cubesat which exploits magnetic actuation to maintain pointing on a circular orbit at a gravity gradient unstable equilibrium.
- Analysis of closed-loop properties of the cubesat with the additional passive attitude stabilization mechanism which exploits air drag panels to complement the active magnetic controller.
- Development of the solution to the general DSC problem in the non-deterministic setting.
- Development of sufficient conditions that ensure stability in the DSC problem.
- The development of MILP-based solution to the time-optimal waypoint following problem for a spacecraft, with the capability of dealing with constraints arising from non-convex obstacles and flexible appendages.
- A methodology and conditions to ensure Lyapunov stability with minimum-time MPC through lexicographic optimization.
- Development of a method using convex hulls to determine the minimum prediction horizon needed in discrete-time minimum-time control problems.

The dissertation is organized as follows. In Chapter 2, the QB50 cubesat attitude control problem is described in detail. Specific control objectives are defined, the models that

govern the system are derived, and analysis of controllability properties is presented. The magnetic actuation system is augmented with a passive drag-based actuation system, and the stability properties of the closed-loop system are analyzed. Simulations are presented that demonstrate the controller's efficacy.

In Chapter 3, motivated by sensing and control considerations for the magnetically actuated satellite and by other spacecraft control applications, a more general disjunctive sensing and control problem is studied, and stability/boundness conditions are derived that can be easily checked. Simulations are presented that illustrate the closed-loop operation of the system under the DSC switching controller.

In Chapter 4, the time-optimal waypoint following MPC problem is introduced, along with MILP methods for tracking waypoints and avoiding keep-out zones in the state space. The results are first applied to the case of the rigid spacecraft attitude control. The dynamics are then augmented with a set of flexible appendage modes, and through the use of simulations it is shown that the controller can keep the flexible modes of the system within prescribed constraints while the spacecraft performs agile minimum-time maneuvering.

In Chapter 5, the time-optimal MPC framework is revisited in search of ways to ensure closed-loop Lyapunov stability of the equilibrium as well as quickly determine the time horizon in MILP. A two-step approach is followed, solving the minimum-time problem on the first pass and then solving a related lexicographic problem on the second pass. It is shown that under suitable assumptions, the two-step procedure yields Lyapunov stability of the target equilibrium. A convex hull method is discussed to obtain functional characterizations of value sets from which the state can be steered to the target in a given number of steps. Finally, simulations are presented that demonstrate the operation of the system under the MPC controller.

Concluding remarks and discussion of future avenues of research appear in Chapter 6.

CHAPTER 2

Magnetic Control

2.1 The QB50 Scenario

This chapter considers the development of an attitude control system, with application to two of the QB50 satellites designed to conduct a survey of the upper atmosphere at low-Earth orbit altitudes [30, 31]. See Figure 2.1. The primary enabler for this survey mission is a constellation of forty 2U cubesats, each equipped with an INMS sensor mounted to one of the 1U faces. To function correctly, this sensor must be kept pointed to within a 20° half-angle cone of the velocity vector. The key challenge in maintaining this attitude is that it corresponds to the cubesat being near a gravity gradient unstable equilibrium. The goal of this chapter is to demonstrate controllability of the linearized time-varying dynamic system and to design a controller for the attitude of a 2U cubesat using first magnetic torque rod actuators alone and in combination with a hardware modification that involves an additional set of four air drag panels. The passive air drag panels are introduced to enhance, in combination with a magnetic rod actuator controller, the satellite's stability and disturbance rejection characteristics.

2.2 Problem Formulation

The cubesat kinematics are expressed through an Euler angle parameterization. The dynamics are characterized using Euler's equation, and incorporate the effects of gravity gra-

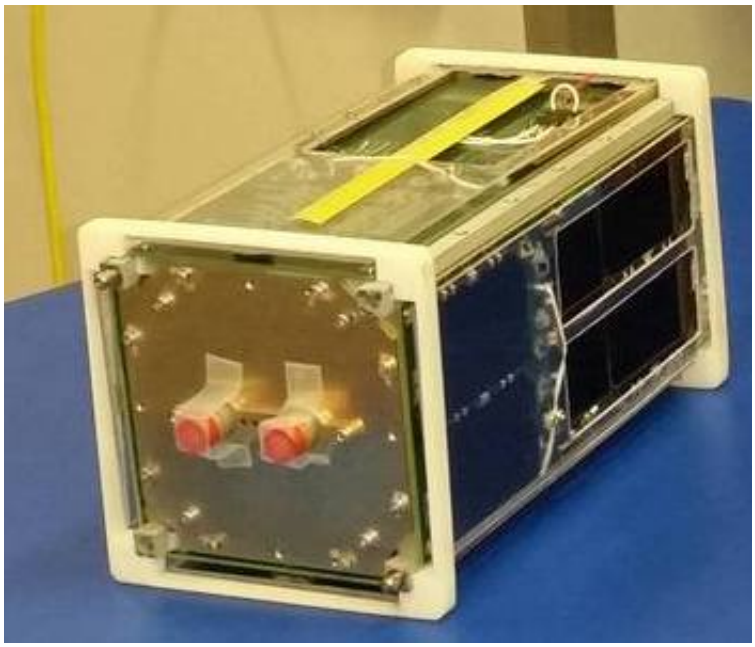

Figure 2.1: Front face of one of the 2U cubesats, featuring the INMS sensor array. This face must be kept pointed within a 20° half-angle cone of the satellite's orbital velocity vector for the array to function correctly. Two of the air drag panels are visible in their undeployed configurations.

dient torque. Controlling the satellite's attitude via magnetic actuators alone is an attractive option; magnetic rods are compact in size, have no moving parts, and consume only electricity, which can be supplied by batteries and solar panels. The drawback to purely magnetic actuation, however, is that the system is instantaneously underactuated due to the inability to exert a torque parallel to the direction of the magnetic field vector. However, unlike underactuated systems involving reaction wheel or thruster failures [32–35], in this system the unactuated axis is not fixed with respect to the body but rotates as the satellite traverses its orbit. System controllability can be demonstrated by taking into account the time-varying unactuated axis in tandem with the gravity gradient torque.

Much prior work has been done to investigate the use of magnetic torques in spacecraft attitude control. However, that work has largely focused on the use of magnetic torque in spin-stabilized spacecraft [36, 37] or in gravity gradient stabilized spacecraft [38, 39]. The satellite considered in this example is not gravity gradient stabilized; in fact, the de-

sired attitude corresponds to a gravity gradient unstable equilibrium, so a control law is needed that establishes pointing despite being hindered, rather than aided, by the gravity gradient torque. While destablizing in our configuration, it is interesting that the gravity gradient torque, on the other hand, facilitates the satellite controllability and the overcoming of the effects of underactuation. Previous approaches have been proposed that exploit the quasi-periodicity of the magnetic field in controller design [40]. These approaches typically pursue time-averaged solutions of the changing magnetic field to precompute control gains offline; however, these solutions can grow less accurate over time and may require that the satellite be sent updated time-averaged parameters. This work uses magnetic field readings to calculate control gains online. Previous work on passive aerodynamic stability treated small-area drag surfaces [41] with a tendency to twist and deform, whereas our satellite is equipped with larger drag plates that should be less prone to performance-degrading deformation. In this chapter, the LQR controller design is based on a linearized, discrete-time model that accounts for the effect of the air drag plates, for which the controllability analysis results are also established. As in [26], before applying the LQR controller and linearizing the model, we use a nonlinear state and control transformation from [42]. Simulation results for the case of an MPC controller that is capable of explicitly enforcing control constraints are also presented.

2.3 Theoretical Results

Our first step in developing a controller is to derive the EOMs for the system. We define the body-fixed frame as follows: The $\hat{\boldsymbol{\imath}}_b$-axis aligns with the INMS sensor array, seen as the small red attachments to the front face in Figure 1. The $\hat{\boldsymbol{k}}_b$-axis aligns with the satellite's radio antenna, seen as the yellow strip on the "top" face in Figure 1, following its deployment; at that time, the antenna will stand perpendicular to the cubesat body. Finally, the $\hat{\boldsymbol{\jmath}}_b$-axis completes the frame according to the right-hand rule, with the unit vector given

by $\hat{\boldsymbol{\jmath}}_b = \hat{\boldsymbol{k}}_b \times \hat{\boldsymbol{\imath}}_b$. We also assume this frame to be a principal frame and refer to it as the Body-Fixed Principal (BFP) frame.

2.3.1 Euler Angle Attitude Parameterization

To stabilize the satellite to the desired attitude, the controller must account for six states: three independent attitude parameters and three independent angular velocity rates. The satellite's inertial measurement unit gives its angular velocity outputs in terms of Euler angle rates and, in addition, the contributions of the drag panels to the satellite dynamics are simplified by the use of an Euler angle parameterization. Thus, we choose to work with Euler angles to describe the EOMs.

The goal of ram pointing is equivalent to aligning the chosen satellite BFP frame with the non-inertial LVLH frame with $\hat{\boldsymbol{\imath}}_L$, $\hat{\boldsymbol{\jmath}}_L$, $\hat{\boldsymbol{k}}_L$ being unit vectors, in which $\hat{\boldsymbol{\imath}}_L$ points along the orbital track (parallel to the orbital velocity vector), $\hat{\boldsymbol{k}}_L$ points toward the focus of the orbit (opposite to the orbital radius vector), and $\hat{\boldsymbol{\jmath}}_L$ completes the frame according to the right-hand rule, with the unit vector given by $\hat{\boldsymbol{\jmath}}_L = \hat{\boldsymbol{k}}_L \times \hat{\boldsymbol{\imath}}_L$ (opposite to the orbital angular momentum vector). See Figure 2.2 for a visual representation. When properly aligned, the INMS sensor achieves ram pointing while keeping the satellite's antenna pointed towards the Earth.

The Direction Cosine Matrix (DCM) of the satellite's body fixed frame relative to the LVLH frame is represented using a 3-2-1 Euler angle rotation sequence, such that:

$$\mathbf{O}_{bL} = \mathbf{O}_1(\phi)\mathbf{O}_2(\theta)\mathbf{O}_3(\psi), \tag{2.1}$$

where

$$\mathbf{O}_1(\phi) = \begin{bmatrix} 1 & 0 & 0 \\ 0 & \cos\phi & \sin\phi \\ 0 & -\sin\phi & \cos\phi \end{bmatrix} = \begin{bmatrix} 1 & 0 & 0 \\ 0 & c_\phi & s_\phi \\ 0 & -s_\phi & c_\phi \end{bmatrix},$$

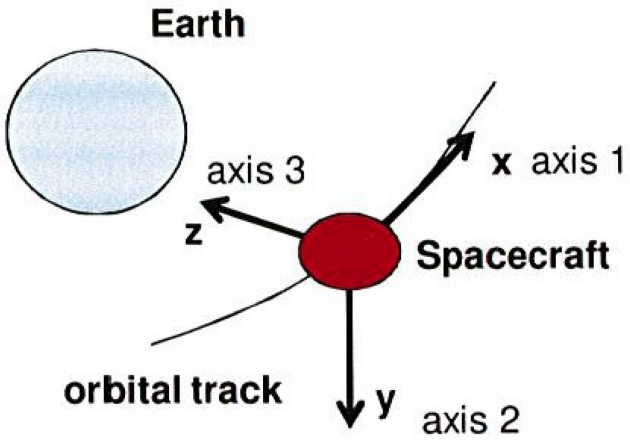

Figure 2.2: LVLH frame; planet and spacecraft view.

$$\mathbf{O}_2(\theta) = \begin{bmatrix} \cos\theta & 0 & -\sin\theta \\ 0 & 1 & 0 \\ \sin\theta & 0 & \cos\theta \end{bmatrix} = \begin{bmatrix} c_\theta & 0 & -s_\theta \\ 0 & 1 & 0 \\ s_\theta & 0 & c_\theta \end{bmatrix},$$

$$\mathbf{O}_3(\psi) = \begin{bmatrix} \cos\psi & \sin\psi & 0 \\ -\sin\psi & \cos\psi & 0 \\ 0 & 0 & 1 \end{bmatrix} = \begin{bmatrix} c_\psi & s_\psi & 0 \\ -s_\psi & c_\psi & 0 \\ 0 & 0 & 1 \end{bmatrix},$$

where we use the shorthand c and s to designate cosine and sine of the argument given in the subscript. When all three angles are at zero, which is the target equilibrium, the $\hat{\boldsymbol{\imath}}_b$-axis aligns with the velocity vector and the $\hat{\boldsymbol{k}}_b$-axis points in the nadir direction.

The drawback of 3-2-1 Euler angles is the kinematic singularity at $\cos\theta = 0$, i.e., $\theta = \pm 90^\circ$, which presents known difficulties for the control design [43]; thus, we require that the pitch angle be within the $-90^\circ < \theta < 90^\circ$ range before beginning actuation. In the event that the initial attitude violates this constraint, we can sidestep the singularity by rotating about each axis by $\pm 180^\circ$, thereby recasting the attitude to an equivalent set of Euler angle parameters. This procedure is equivalent to the methods described in, for example, Slabaugh [44] or Weiss [45] for finding an equivalent set of Euler angles with

$|\theta| < 90°$. While in theory the pitch angle could still possibly violate the constraint window some time after actuation begins despite initially satisfying it, in simulations this did not lead to any further actuation problems. We note that the singularity problem could also be alleviated by the use of a different attitude parameterization such as quaternions or reduced quaternions, which push the singularity to the furthest point away from the origin, which serves as the equilibrium point. However, in this application, we choose to pursue the Euler angle parameters due to the need to interface with the cubesat's legacy hardware, in particular the onboard attitude module. In addition, the Euler parameters lead to an easier representation of the aerodynamic drag moment when the drag panels are included in the calculations. We leave the treatment of alternative attitude parameterizations to future work.

2.3.2 Kinematics

The angular velocity, i.e., the axis and rate of rotation, of the body frame relative to an inertial frame can be decomposed as the sum of the intermediate angular velocity physical vectors:

$$\vec{\boldsymbol{\omega}}^{bg} = \vec{\boldsymbol{\omega}}^{bL} + \vec{\boldsymbol{\omega}}^{Lg}. \tag{2.2}$$

We resolve this expression in the BFP frame to produce the following expression:

$$\boldsymbol{\omega}_b^{bg} = \boldsymbol{\omega}_b^{bL} + \boldsymbol{\omega}_b^{Lg} = \boldsymbol{\omega}_b^{bL} + \mathbf{O}_{bL}\boldsymbol{\omega}_L^{Lg}. \tag{2.3}$$

The LVLH frame rotates, relative to an inertial frame, at a rate given by the orbital motion n. This rate is constant due to the circular orbit assumption. In the chosen coordinate

system, $\boldsymbol{\omega}_L^{Lg} = [0 \ -n \ 0]^T$. Then,

$$\begin{bmatrix} \omega_1 \\ \omega_2 \\ \omega_3 \end{bmatrix} = C_{\phi\theta} \begin{bmatrix} \dot{\phi} \\ \dot{\theta} \\ \dot{\psi} \end{bmatrix} + \mathbf{O}_{bL} \begin{bmatrix} 0 \\ -n \\ 0 \end{bmatrix}, \tag{2.4}$$

where

$$C_{\phi\theta} = \begin{bmatrix} 1 & 0 & -s_\theta \\ 0 & c_\phi & s_\phi c_\theta \\ 0 & -s_\phi & c_\phi c_\theta \end{bmatrix},$$

and

$$\mathbf{O}_{bL} = \begin{bmatrix} c_\theta c_\psi & c_\theta s_\psi & -s_\theta \\ s_\phi s_\theta c_\psi - c_\phi s_\psi & s_\phi s_\theta s_\psi + c_\phi c_\psi & s_\phi c_\theta \\ c_\phi s_\theta c_\psi + s_\phi s_\psi & c_\phi s_\theta s_\psi - s_\phi c_\psi & c_\phi c_\theta \end{bmatrix}.$$

We invert (2.4) to solve for the Euler angle rates:

$$\begin{bmatrix} \dot{\phi} \\ \dot{\theta} \\ \dot{\psi} \end{bmatrix} = C_{\phi\theta}^{-1} \left(\begin{bmatrix} \omega_1 \\ \omega_2 \\ \omega_3 \end{bmatrix} + n \begin{bmatrix} c_\theta s_\psi \\ s_\phi s_\theta s_\psi + c_\phi c_\psi \\ c_\phi s_\theta s_\psi - s_\phi c_\psi \end{bmatrix} \right), \tag{2.5}$$

where

$$C_{\phi\theta}^{-1} = \left(\frac{1}{c_\theta} \right) \begin{bmatrix} c_\theta & s_\phi s_\theta & c_\phi s_\theta \\ 0 & c_\phi c_\theta & -s_\phi c_\theta \\ 0 & s_\phi & c_\phi \end{bmatrix}.$$

2.3.3 Dynamics

Having derived the equations for the kinematics, we turn to the dynamics, which can be modeled with Euler's equation,

$$\mathbf{J}_b^{\mathcal{B}c} \dot{\boldsymbol{\omega}}_b^{bg} + S[\boldsymbol{\omega}_b^{bg}] \mathbf{J}_b^{\mathcal{B}c} \boldsymbol{\omega}_b^{bg} = \boldsymbol{\tau}_b^{\mathcal{B}c}, \tag{2.6}$$

where all quantities have been resolved in BFP frame, $\boldsymbol{\tau}_b^{\mathcal{B}c}$ represents the external torque on body $\mathcal{B}$ about its center of mass, and the matrix $S[\boldsymbol{\omega}_b^{bg}]$ denotes the skew-symmetric matrix formed of the components of $\boldsymbol{\omega}_b^{bg}$ and given by

$$S[\boldsymbol{\omega}_b^{bg}] = S\left(\begin{bmatrix}\omega_1\\ \omega_2\\ \omega_3\end{bmatrix}\right) = \begin{bmatrix}0 & -\omega_3 & \omega_2\\ \omega_3 & 0 & -\omega_1\\ -\omega_2 & \omega_1 & 0\end{bmatrix}. \tag{2.7}$$

Since the BFP frame is a principal frame, $\mathbf{J}_b^{\mathcal{B}c}$ is

$$\mathbf{J}_b^{\mathcal{B}c} = \begin{bmatrix}J_1 & 0 & 0\\ 0 & J_2 & 0\\ 0 & 0 & J_3\end{bmatrix}, \tag{2.8}$$

where J_1, J_2, and J_3 are the principal moments of inertia. The torque acting on the body can be further decomposed into the magnetic control torque, gravity gradient torque, and disturbance torque,

$$\boldsymbol{\tau}_b^{\mathcal{B}c} = \boldsymbol{\tau}_b^{\mathcal{B}c,mt} + \boldsymbol{\tau}_b^{\mathcal{B}c,gg} + \boldsymbol{\tau}_b^{\mathcal{B}c,dist}. \tag{2.9}$$

2.3.3.1 Magnetic Torque

The net magnetic dipole generated by the torque rods interacts with the Earth's magnetic field to produce a torque according to the following law:

$$\vec{\boldsymbol{\tau}}^{\mathcal{B}c,mt} = \vec{\boldsymbol{m}} \times \vec{\boldsymbol{b}}, \tag{2.10}$$

where $\vec{\boldsymbol{b}}$ denotes the external magnetic field vector and $\vec{\boldsymbol{m}}$ denotes the magnetic moment. Resolving the torque in the BFP frame, we obtain

$$\boldsymbol{\tau}_b^{\mathcal{B}c,mt} = -S[\boldsymbol{b}_b]\mathbf{m}_b, \tag{2.11}$$

where we have replaced the vector cross-product operation with the equivalent skew-symmetric matrix representation,

$$S\left(\begin{bmatrix} b_1 \\ b_2 \\ b_3 \end{bmatrix}\right) = \begin{bmatrix} 0 & -b_3 & b_2 \\ b_3 & 0 & -b_1 \\ -b_2 & b_1 & 0 \end{bmatrix}. \tag{2.12}$$

Note that rank$(S[\boldsymbol{b}_b]) = 2$, which affirms that the system is instantaneously underactuated with magnetic torque alone.

2.3.3.2 Gravity Gradient Torque

The Earth's gravitational field exerts a force on the satellite that can be modeled by an inverse-square distance law. Hence, the force is slightly greater on the portions of the satellite that are closer to the Earth than on those portions that are further away. This differential, though small, produces a torque on the satellite's body approximated by [46]

$$\boldsymbol{\tau}_b^{\mathcal{B}c,gg} = 3n^2 S[\hat{\boldsymbol{r}}_b] J_b^{\mathcal{B}c} \hat{\boldsymbol{r}}_b, \tag{2.13}$$

where a circular orbit is assumed for the satellite. The radial unit vector $\hat{\boldsymbol{r}}_b$ points opposite to the $\hat{\boldsymbol{k}}_L$ vector; hence, $\hat{\boldsymbol{r}}_b$ can be expressed as

$$\hat{\boldsymbol{r}}_b = \mathbf{O}_{bL}(-\hat{\boldsymbol{k}}_L) = \mathbf{O}_{bL} \begin{bmatrix} 0 \\ 0 \\ -1 \end{bmatrix}.$$

Thus,

$$\boldsymbol{\tau}_b^{\mathcal{B}c,gg} = 3n^2 \begin{bmatrix} (J_2 - J_3)\, c_\phi s_\phi c_\theta^2 \\ (J_3 - J_1)\, c_\phi c_\theta s_\theta \\ (J_1 - J_2)\, s_\phi c_\theta s_\theta \end{bmatrix}. \tag{2.14}$$

There exist multiple configurations in which this torque vanishes, two stable ($c_\theta = 0$) and several unstable ($s_\theta = s_{2\phi} = 0$). As the desired equilibrium attitude for the satellite is close to one of the unstable configurations, the gravity gradient torque tends to destabilize the satellite's attitude, and thus becomes a significant factor in our treatment of the system dynamics.

2.3.4 Control Analysis and Control Law Design for the Satellite Without Drag Panels

The magnetic torque cross-product expression (2.10) indicates that the component of the dipole parallel to the magnetic field generates zero torque. Thus, to obtain maximum control torque, we seek a dipole moment that minimizes the magnitude of the projection $\vec{\boldsymbol{m}} \cdot \vec{\boldsymbol{b}} = \boldsymbol{m}_b^T \boldsymbol{b}_b$. Following Lovera and Astolfi [42], we prescribe a dipole moment of the form:

$$\mathbf{m}_b = -\left(\frac{S[\boldsymbol{b}_b]}{\boldsymbol{b}_b^T \boldsymbol{b}_b}\right) \mathbf{u}, \tag{2.15}$$

where $\mathbf{u} \in \mathbb{R}^3$ is a control input vector. This dipole law constrains $\mathbf{m}_b$ to be perpendicular to $\boldsymbol{b}_b$, thus fixing $\mathbf{m}_b^T \boldsymbol{b}_b = 0$. The magnetic input torque can then be expressed as

$$\boldsymbol{\tau}_b^{\mathcal{B}c,mt} = \left(\frac{S[\boldsymbol{b}_b] S[\boldsymbol{b}_b]}{\boldsymbol{b}_b^T \boldsymbol{b}_b}\right) \mathbf{u}. \tag{2.16}$$

Lovera and Astolfi [42] use a Proportional-Derivative (PD) control law to prescribe the new control input vector $\mathbf{u}$; we choose instead to apply LQR theory to obtain the controller as it can be applied systematically to different spacecraft configurations.

2.3.5 Linearized Equations of Motion

We first linearize the EOMs about the desired equilibrium state $\mathbf{x}_{eq} = [0, 0, 0, 0, -n, 0]^T$ to get linearized EOMs in the form

$$\dot{\mathbf{x}} = A_c\mathbf{x} + B_c(t)\mathbf{u},$$

with

$$A_c = \begin{bmatrix} 0 & 0 & n & 1 & 0 & 0 \\ 0 & 0 & 0 & 0 & 1 & 0 \\ -n & 0 & 0 & 0 & 0 & 1 \\ -3n^2J_{23} & 0 & 0 & 0 & 0 & -nJ_{23} \\ 0 & 3n^2J_{31} & 0 & 0 & 0 & 0 \\ 0 & 0 & 0 & -nJ_{12} & 0 & 0 \end{bmatrix}, \tag{2.17}$$

where $J_{12} := (J_1 - J_2)/J_3$, $J_{23} := (J_2 - J_3)/J_1$, and $J_{31} := (J_3 - J_1)/J_2$, and

$$B_c(t) = \begin{bmatrix} \mathbf{0}_{3\times 3} \\ \\ \left(\mathbf{J}_b^{\mathcal{B}c}\right)^{-1} \frac{S[\boldsymbol{b}_b(t)]S[\boldsymbol{b}_b(t)]}{\boldsymbol{b}_b^T(t)\boldsymbol{b}_b(t)} \end{bmatrix}. \tag{2.18}$$

The complete derivation of the linearized EOMs is found in Appendix A. Note that $\mathbf{b}_b(t)$ in (2.18) is ideally the nominal magnetic field at the linearization point. However, in our implementation, we use the measured magnetic field values in (2.18), which are determined by the onboard magnetomer readings. While this makes little difference in terms of model accuracy near the linearization point, this approach allows us to implement the controller with gains computed online without strong coupling to the nominal orbital position or the need to either store nominal values of $\mathbf{b}_b$ or compute them offline and store them in memory. This also improves the robustness in case of deployment errors or orbit decaying due to the influence of the air drag. In either case, $\mathbf{b}_b$ in (2.18) depends on time t, as does $B_c(t)$. The

matrices $A_c, B_c(t)$ at any fixed time instant t do not constitute a controllable pair without the assumption of relative pointing, e.g., they violate the controllability rank condition for time-invariant systems under inertial pointing, i.e., for $n = 0$.

2.3.5.1 Controllability of the Time-Varying Linearized System

Having derived the linearized EOMs, we now demonstrate that the linearized system, which is time-varying, is controllable on any time interval of non-zero length. Yang [47] reduces the problem of complete controllability by magnetic torque rods to a small number of sufficient conditions:

- The satellite is not located on the magnetic Equator.
- Assuming the above holds, then
  1. $J_2 \neq J_3$,
  2. $6J_3\,(J_3 - J_1) \neq J_2\,(J_1 - J_2 + J_3)$.

The considered cubesat has an inertia matrix of $\mathbf{J}_b^{\mathcal{B}c} = \text{diag}(3654338, 9060235, 8813148)$ g·mm^2. As it is to be ejected from the ISS, it will operate with an initial altitude of 415 km and at an inclination of $51.6°$, with an orbital period of 5570 s. At this inclination, the satellite is away from the plane of the magnetic Equator, and also satisfies the controllability constraints on the J_i's above, confirming that the linearized time-varying system is controllable. This implies that, in the absence of control constraints, there exists a control input that drives the state to the origin over any specified time interval.

2.3.6 LTV Controllability

The controller uses magnetic rods, thus the $B(t)$ matrix depends on the Earth's magnetic field and the system is time-varying. While for implementation, we rely on measured magnetic field values, for the controllabilty analysis here, we approximate the magnetic

field by assuming a tilted dipole model, with periodicity equal to the satellite's orbital period T; following Psiaki [40], the magnetic field approximation takes the following form,

$$\begin{bmatrix} b_1(t) \\ b_2(t) \\ b_3(t) \end{bmatrix} = \frac{\mu_f}{a^3} \begin{bmatrix} \cos(nt)\sin(i_m) \\ -\cos(i_m) \\ 2\sin(nt)\sin(i_m) \end{bmatrix}, \tag{2.19}$$

where μ_f is the strength of the dipole field, a is the semimajor axis, n is the mean motion, i_m is the inclination of the orbit with respect to the magnetic equator, and $t \in [0,\ T]$ is measured from the crossing of the ascending node of the magnetic Equator. We then show that the LTV system is controllable on the interval $[0,\ T]$, under a few conditions.

Theorem 2.1: The linearized system is controllable on the interval $[0,\ T]$ if the following conditions hold:

1) The satellite's orbital plane is not aligned with the magnetic Equator,

2) $J_2 \neq J_3$,

3) $J_3\left(6(J_3 - J_1) + 2\Gamma\right) \neq J_2\left(J_1 - J_2 + J_3 - 2\Gamma\right)$.

The proof is similar to the method in Yang [47] and is found in Appendix C. The properties are easily checked, as the principal moments J_1, J_2, and J_3 are determined early in the satellite design phase and Γ is simple to calculate from properties of the panel angle and orbital altitude. Note that if $\Gamma \to 0$, for example, if the panel area or the atmospheric density had a value of zero, then the last condition specializes to the controllability result for the spacecraft without panels.

In Figure 2.3, the air drag panels are added to the simulation in Figure 2.4, with drag coefficient $C_D = 2$ and atmospheric density $\rho \approx 2.81 \times 10^{-12}$ kg/m^3. The convergence is slowed, but the cubesat detumbles properly as the augmented controller does reject the unmodeled disturbance, demonstrating that the additional restorative torques from the panels

help to overcome the unmodeled disturbance that destabilized the system previously.

2.4 LQ Control

The control design is based on LQR theory applied to a discrete-time model that is obtained by converting (2.17)-(2.18) to discrete-time. We apply a Zero-Order Hold method to carry out the discretization. Let $t \in \mathbb{R}_{\geq 0}$ be the current time instant and A_c, $B_c(t)$ defined in (2.17), (2.18). For $\Delta t > 0$, the discrete-time model predicts the state $\mathbf{x}_k$ at time $t+k\Delta t, k \in \mathbb{Z}_{\geq 0}$, according to the following model with the "frozen-in-time" magnetic field:

$$\begin{aligned} \mathbf{x}_{k+1} &= A_d \mathbf{x}_k + B_d(t)\mathbf{u}_k, \\ A_d &= e^{A_c \Delta t}, \\ B_d(t) &= -A_c^{-1}\left(\mathbf{I}_6 - A_d\right) B_c(t), \\ \mathbf{x}_0 &= \mathbf{x}(t). \end{aligned} \tag{2.20}$$

where "frozen-in-time" means that the slowly-time-varying term $B(t)$ is assumed to remain constant over the entire discrete-time step. The pair $(A_d, B_d(t))$ can be verified to be controllable for all t for our orbit and choices of Δt we have used. For the difference equation (2.20), we define the infinite-horizon cost functional J:

$$J(t) = \sum_{k=0}^{\infty} \left(\mathbf{x}_k^T Q \mathbf{x}_k + \mathbf{u}_k^T R \mathbf{u}_k\right), \tag{2.21}$$

where $R = R^T \in \mathbb{R}^3$ is a positive definite matrix, and $Q = Q^T \in \mathbb{R}^6$ is a positive semi-definite matrix satisfying the usual detectability assumption. Then, the optimal feedback control sequence $\mathbf{u}_k = -K(t)\mathbf{x}_k$ that minimizes $J(t)$ has the solution:

$$K(t) = \left(R + B_d(t)^T P(t) B_d(t)\right)^{-1} B_d(t)^T P(t) A_d, \tag{2.22}$$

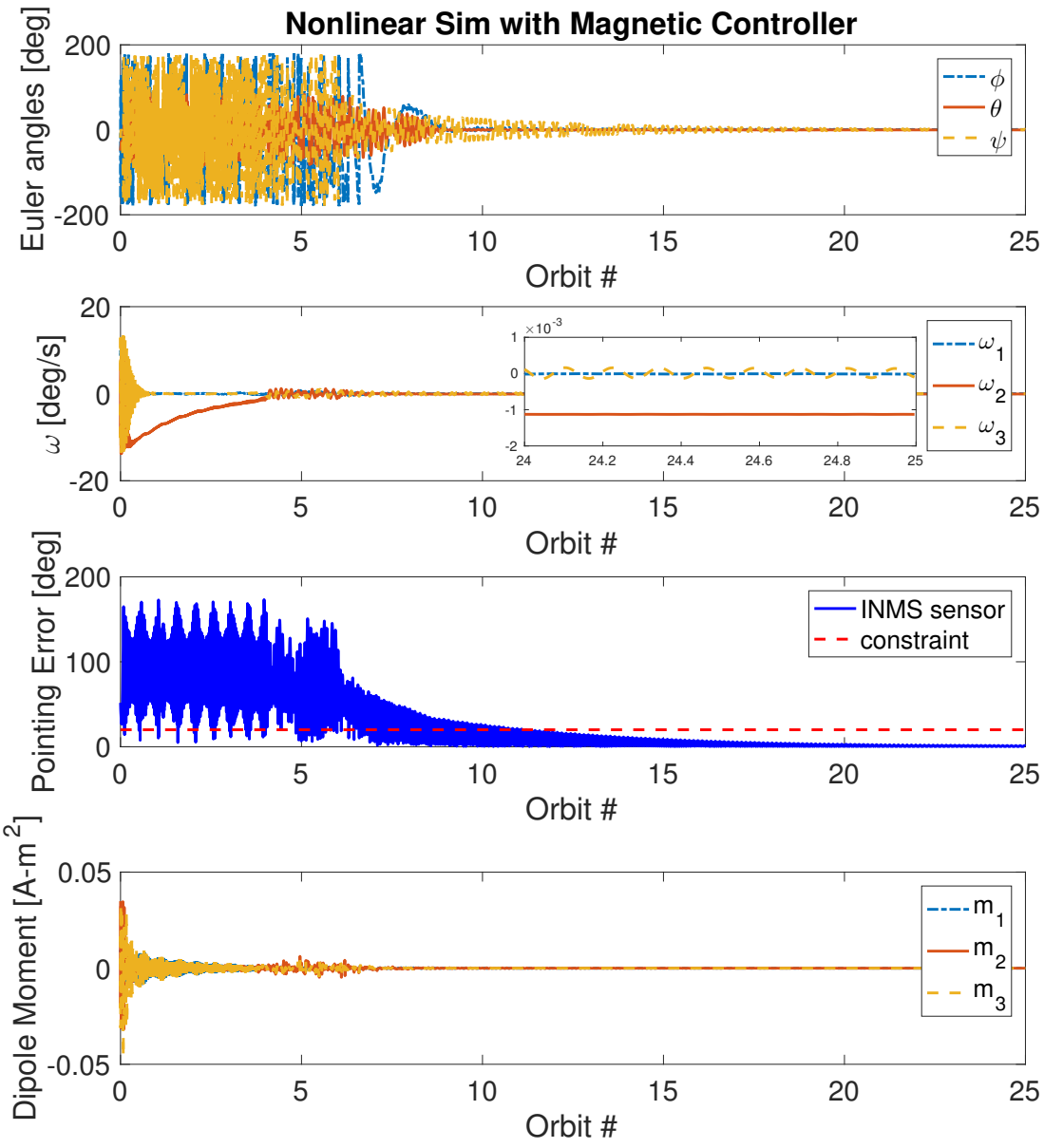

Figure 2.3: Simulation results using the control design based on the relinearized dynamics, to include the panels, with the same constant disturbance torque as in Figure 2.4.

$$P(t) = A_d^T P(t) A_d + Q - A_d^T P(t) B_d(t) K(t). \tag{2.23}$$

Note that (2.23) can have multiple solutions; the $P(t)$ of interest to us is the unique positive definite solution. Also note that $B_d(t)$ changes throughout the orbit, thus (2.23) is solved at different instants t in time and the gain $K(t)$ in (2.22) is time-varying. The control $\mathbf{u}(t+\sigma) = K(t)\mathbf{x}(t)$ is applied for $0 \leq \sigma < \Delta t$ and then recomputed. A fast update scheme for the solution of the Algebraic Riccati Equation in response to changes in the magnetic field vector can be defined, see Appendix B. An alternative approach to solving the Riccati Equation can be found in Yang [48]; this method uses the approximate periodicity of the magnetic field to construct periodic solutions offline to (2.23) at each time step. We choose to calculate the solutions online, as the time steps in this problem are very small compared to the period of the orbit and storing that many solutions would consume an excessive amount of the satellite's memory.

Though there are no explicit constraints placed on the optimal control solution, in practice there do exist implicit control constraints in the form of magnetic torque rod saturation. In the LQR control formulation, these constraints are taken into account indirectly; if at least one component violates the constraint, the control input is rescaled such that its largest component is equal to the saturation limit while remaining parallel to the calculated dipole vector. In this way, the dipole vector remains perpendicular to the magnetic field vector, for maximum torque generation. In Section 2.5, we extend the LQR controller to a MPC-based controller that has the additional capability of being able to explicitly handle these control saturation constraints.

2.4.1 Passive Air Drag Control

The magnetic torque rod controller works well in the ideal case, but can struggle to maintain the pointing constraint in the presence of unmodeled disturbance torques, as seen in Figure 2.4 when a constant magnitude unmodeled disturbance torque is added to the system.

As magnetic rods alone do not appear to provide strong disturbance rejection capability, a solution that takes advantage of hardware and control interplay has been adopted. Specifically, the cubesat was augmented with a set of four drag panels, to supplement the magnetic torque with passive aerodynamic stabilizing torque. We note that in a different application to a flying wind turbine [49], a solution that exploits passive aerodynamic stabilization to enhance an underactuated system has also been proposed.

The symmetry of the drag panels serves to move the satellite's Center of Pressure (CP), which in the original design coincided with the Center of Mass (CM), such that the CP falls behind the CM in the target configuration represented in Figure 2.5. This effect enhances the disturbance rejection capability of the system, as the drag force on the panels creates a net torque along the CP-CM moment arm that acts to return the satellite to the equilibrium state if perturbed away from it [50].

As the panels add additional torque inputs, they change the satellite's dynamics. Thus, in order to apply the LQR controller, the equations of motion must be relinearized to properly reflect these changes. From the circular orbit assumption, the orbital velocity vector satisfies $\hat{\boldsymbol{v}}_L = [1,\ 0,\ 0]^T$, and we can apply the orientation matrix $\mathbf{O}_{bL}$ to resolve it in the BFP frame,

$$\begin{aligned}\hat{\boldsymbol{v}}_b &= \begin{bmatrix} c_\theta c_\psi & \sim & \sim \\ s_\phi s_\theta c_\psi - c_\phi s_\psi & \sim & \sim \\ c_\phi s_\theta c_\psi + s_\phi s_\psi & \sim & \sim \end{bmatrix} \begin{bmatrix} 1 \\ 0 \\ 0 \end{bmatrix} \\ &= \begin{bmatrix} c_\theta c_\psi \\ s_\phi s_\theta c_\psi - c_\phi s_\psi \\ c_\phi s_\theta c_\psi + s_\phi s_\psi \end{bmatrix} \approx \begin{bmatrix} 1 \\ \phi\theta - \psi \\ \theta + \phi\psi \end{bmatrix} \approx \begin{bmatrix} 1 \\ -\psi \\ \theta \end{bmatrix},\end{aligned} \tag{2.24}$$

where $\hat{\boldsymbol{v}}_b$ is simplified by first a small angle approximation and then the discarding of higher-order terms.

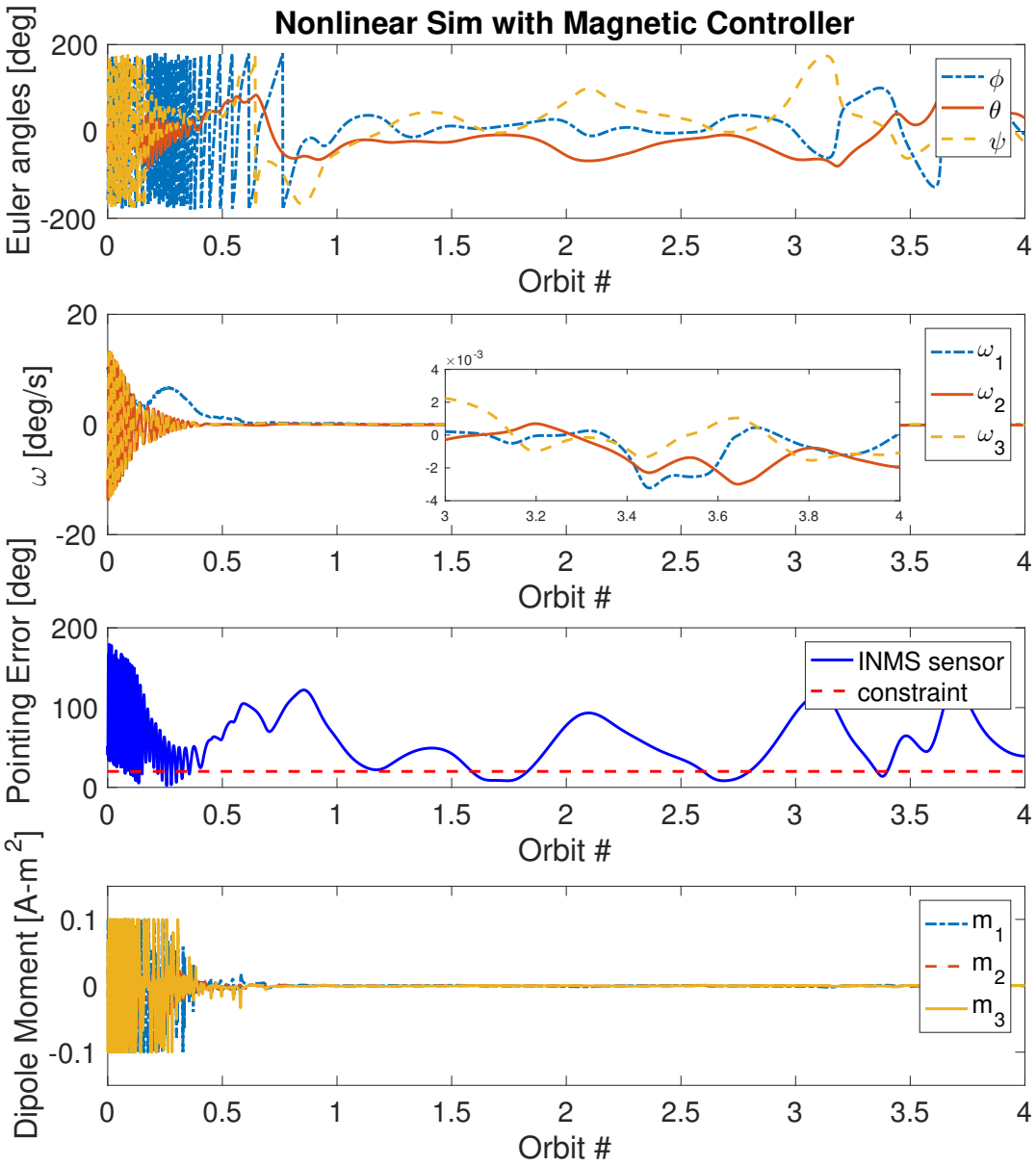

Figure 2.4: Simulation of the closed-loop system with the LQR control law for the magnetic torque rods with an unmodeled disturbance torque of constant 10^{-8} N·m magnitude.

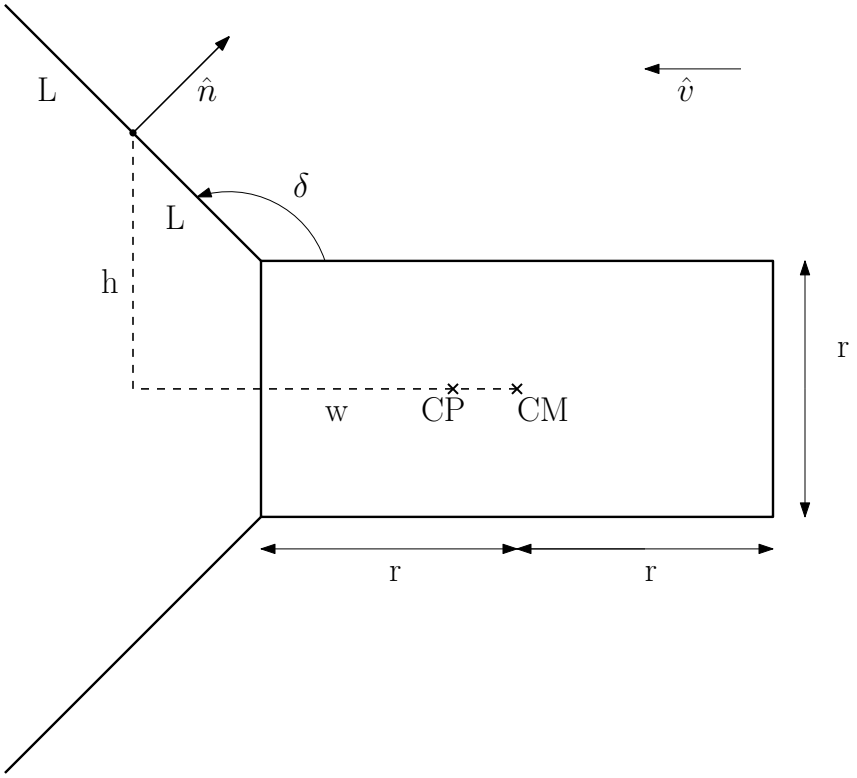

Figure 2.5: Drag panel model following deployment. The satellite has four such panels but, for clarity, only two panels are depicted here.

Each panel is assumed to contribute a torque of the form

$$\left(\boldsymbol{\tau}_b^{ad}\right)_i = \left(\mathbf{r}_b\right)_i \times \left(\mathbf{F}_b^{ad}\right)_i, \tag{2.25}$$

where $\left(\mathbf{F}_b^{ad}\right)_i$ is the air drag force on the i^{th} panel, $\left(\mathbf{r}_b\right)_i$ is the distance from the satellite's center of mass to the center of the i^{th} panel, and

$$\boldsymbol{\tau}_b^{ad} = \sum_{i=1}^{4} \left(\boldsymbol{\tau}_b^{ad}\right)_i. \tag{2.26}$$

The force exerted by the air drag acts opposite to the orbital velocity vector, and is modeled as

$$\begin{aligned} \left(\mathbf{F}_b^{ad}\right)_i &= (0.5\rho v^2 \mathcal{A}_i C_D)(-\hat{\boldsymbol{v}}_b) \\ &= (0.5\rho n^2 a^2 \mathcal{A}_i C_D)(-\hat{\boldsymbol{v}}_b), \end{aligned} \tag{2.27}$$

where ρ represents the atmospheric density at altitude, estimated by use of a table in Gombosi [51], and C_D is the drag coefficient. The circular orbit assumption is used to conclude that $v = na$, with a being the orbital radius, and the effective panel area $\mathcal{A}_i = (\hat{\boldsymbol{n}}_i \cdot \hat{\boldsymbol{v}})\mathcal{A}$ is equal to the actual panel area scaled by the dot product of the outward facing unit normal

vector and the unit velocity vector. Thus, the torque has the following components,

$$
\begin{aligned}
(\mathbf{r}_b)_1 &= \begin{bmatrix} -w \\ 0 \\ -h \end{bmatrix}, \quad \left(\mathbf{F}_b^{ad}\right)_1 = n^2 f\left(s_\delta + c_\delta\theta\right) \left(\begin{bmatrix} -1 \\ \psi \\ -\theta \end{bmatrix} \right), \\
(\mathbf{r}_b)_2 &= \begin{bmatrix} -w \\ 0 \\ h \end{bmatrix}, \quad \left(\mathbf{F}_b^{ad}\right)_2 = n^2 f\left(s_\delta - c_\delta\theta\right) \left(\begin{bmatrix} -1 \\ \psi \\ -\theta \end{bmatrix} \right), \\
(\mathbf{r}_b)_3 &= \begin{bmatrix} -w \\ -h \\ 0 \end{bmatrix}, \quad \left(\mathbf{F}_b^{ad}\right)_3 = n^2 f\left(s_\delta - c_\delta\psi\right) \left(\begin{bmatrix} -1 \\ \psi \\ -\theta \end{bmatrix} \right), \\
(\mathbf{r}_b)_4 &= \begin{bmatrix} -w \\ h \\ 0 \end{bmatrix}, \quad \left(\mathbf{F}_b^{ad}\right)_4 = n^2 f\left(s_\delta + c_\delta\psi\right) \left(\begin{bmatrix} -1 \\ \psi \\ -\theta \end{bmatrix} \right),
\end{aligned}
\tag{2.28}
$$

where $f = 0.5\rho a^2 \mathcal{A} C_D$ and δ is constrained to be in the interval [90°, 180°]. Taking the cross products and summing to get an approximation of the air drag torque $\boldsymbol{\tau}_b^{ad}$,

$$
\boldsymbol{\tau}_b^{ad} = 0.5\rho n^2 a^2 \mathcal{A} C_D \begin{bmatrix} 0 \\ (2hc_\delta - 4ws_\delta)\theta \\ (2hc_\delta - 4ws_\delta)\psi \end{bmatrix}. \tag{2.29}
$$

For the 2U cubesat depicted in Figure 2.5, $w = r - Lc_\delta$ and $h = 0.5r + Ls_\delta$, thus,

$$\begin{aligned}\boldsymbol{\tau}_b^{ad} &= n^2 f \begin{bmatrix} 0 \\ (2hc_\delta - 4ws_\delta)\theta \\ (2hc_\delta - 4ws_\delta)\psi \end{bmatrix} \\ &= 4n^2 rf \left(c_\delta - 4s_\delta + 3(\frac{L}{r})s_{2\delta} \right) \begin{bmatrix} 0 \\ \theta \\ \psi \end{bmatrix} = n^2 \Gamma \begin{bmatrix} 0 \\ \theta \\ \psi \end{bmatrix},\end{aligned} \tag{2.30}$$

where $\Gamma = 4rf\left(c_\delta - 4s_\delta + 3(\frac{L}{r})s_{2\delta}\right)$. The linearized dynamic contribution of $\left(\mathbf{J}_b^{\mathcal{B}c}\right)^{-1}\boldsymbol{\tau}_b^{ad}$ then takes the form

$$\left(\mathbf{J}_b^{\mathcal{B}c}\right)^{-1} d\boldsymbol{\tau}_b^{ad} = \begin{bmatrix} 0 & 0 & 0 & 0 & 0 & 0 \\ 0 & \frac{n^2\Gamma}{J_2} & 0 & 0 & 0 & 0 \\ 0 & 0 & \frac{n^2\Gamma}{J_3} & 0 & 0 & 0 \end{bmatrix} \begin{bmatrix} d\phi \\ d\theta \\ d\psi \\ d\omega_1 \\ d\omega_2 \\ d\omega_3 \end{bmatrix}, \tag{2.31}$$

where $d(\cdot)$ denotes the deviation from the nominal values. Incorporating this contribution into the previously linearized equations of motion $\dot{x} = Ax + Bu$, A now takes the form

$$A = \begin{bmatrix} 0 & 0 & n & 1 & 0 & 0 \\ 0 & 0 & 0 & 0 & 1 & 0 \\ -n & 0 & 0 & 0 & 0 & 1 \\ 3n^2 J_{32} & 0 & 0 & 0 & 0 & nJ_{32} \\ 0 & 3n^2 J_{31} + \frac{n^2\Gamma}{J_2} & 0 & 0 & 0 & 0 \\ 0 & 0 & \frac{n^2\Gamma}{J_3} & nJ_{21} & 0 & 0 \end{bmatrix}. \tag{2.32}$$

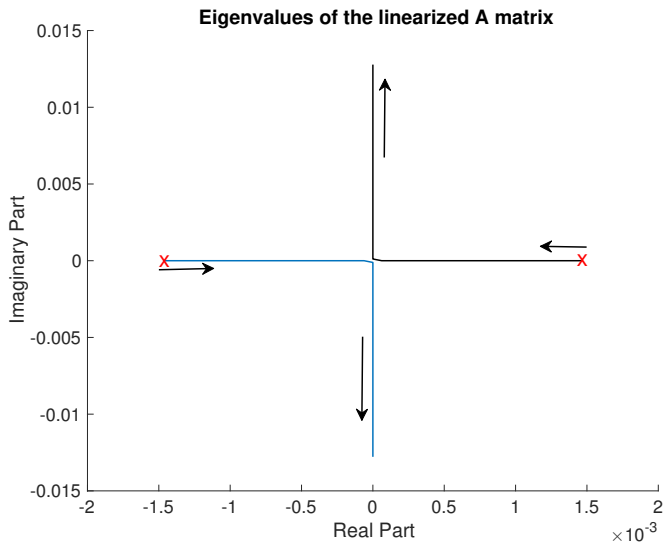

Figure 2.6: Eigenvalues of the A matrix as a function of panel area. The crosses denote the pair of real eigenvalues that correspond to zero panel area. As panel area increases, this pair of real eigenvalues migrate first to the $j\omega$-axis and then outward along the axis, eliminating the unstable mode.

Notable about this modified A matrix is that, for sufficiently large values of Γ, all eigenvalues of A lie on the $j\omega$-axis, whereas for $\Gamma = 0$ there exists an unstable positive real eigenvalue, as seen in Figure 2.6. Further, the panel deployment angle directly influences the eigenvalues of the system and its "stiffness", i.e., the ability to resist disturbances. See Figure 2.7. For proper disturbance rejection, the panels should be designed such that Γ exceeds the threshold at which there exists an eigenvalue in the open right-half plane.

2.4.2 Simulation Results

After several tuning experiments with the goal of obtaining good performance, the weighting matrices Q and R for the LQR cost functional have been chosen as $Q = \text{diag}(10^{-8}, 10^{-8}, 10^{-8}, 10^{-4}, 10^{-4}, 10^{-4})$ and $R = \text{diag}(10^{8}, 10^{8}, 10^{8})$. The initial attitude of the satellite is $\phi(0) = -35°$, $\theta(0) = -75°$, and $\psi(0) = 75°$. It is estimated that the magnitudes of the post-ejection tumble rates would be approximately $10°$ per second in each axis, thus the satellite is given an initial angular velocity of $\omega_1(0) = -10°/\text{s}$, $\omega_2(0) = 10°/\text{s}$,

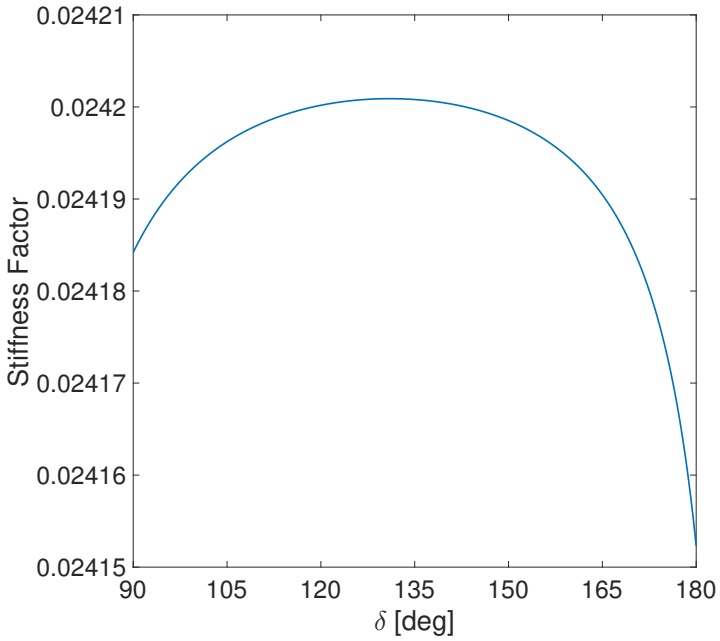

Figure 2.7: Square root of the magnitude of the smallest-magnitude eigenvalue of the linearized panel system as a function of the panel angle. As all eigenvalues for this particular panel size lie on the $\jmath\omega$-axis, this can be treated as a measure of the "stiffness" of the system. For our particular satellite, the panels have their strongest effect at $\delta = 131°$.

and $\omega_3(0) = -10°/\text{s}$. The orbital period of 5570 s yields an orbital angular velocity of $n = 1.13 \times 10^{-3}$ rad/s. The simulation time steps are of magnitude $\Delta t = 4$ s, and model the on-board software switches between magnetic torque and magnetic sensing. Note that, while the switch is modeled as being instantaneous, in reality there are non-zero ramp up and decay periods between each use of the magnetic torque rods that would introduce an additional perturbing effect; however, for this application such periods were on the order of milliseconds, much shorter than the simulation time steps. The Earth's magnetic field is modeled using the tilted dipole approximation of Wertz [52], updated with the 2015 International Geomagnetic Reference Field IGRF-12 [53] coefficients. The controller saturation limit is $u_{max} = 0.1$ A·m^2. The control goal is to drive the pointing angle, i.e., the angle between $\hat{\boldsymbol{\imath}}_b$ and the satellite's velocity vector, to within the $\pm 20°$ constraint. The controller successfully achieves the commanded equilibrium, without unwinding. As shown in Figure 2.8, the cubesat experiences many rotations about its roll and yaw axes while detumbling,

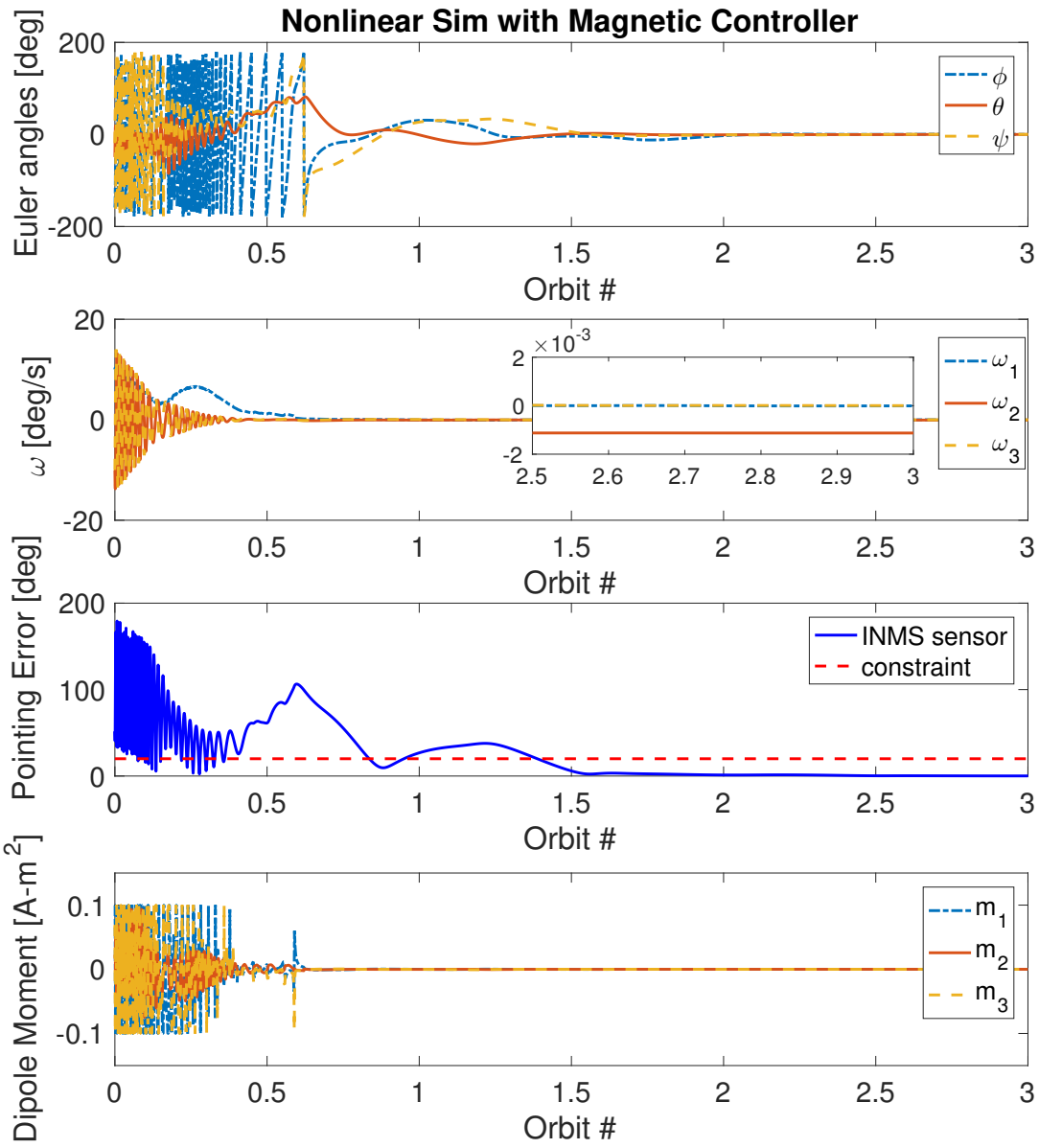

Figure 2.8: Simulation of the closed-loop system with the LQR control law for the magnetic torque rods with no sensor noise or unmodeled disturbance torques.

but does reach and remain within the required pointing angle constraint inside of two orbits. The pointing error of the INMS sensor approaches zero, indicating that it is correctly oriented.

2.5 MPC Control Results

We compare the results of the simulated LQR controller to those of a simulated MPC controller with the same weights as the LQR controller. Unlike the LQR controller, the MPC-based controller has the additional capability of explicitly handling control constraints, such as the magnetic torque rod saturation described in Section 2.4.

2.5.1 Discrete Time Conversion

To develop our predictive controller, a discrete-time approximation to the continuous-time dynamics is implemented. The discretization is performed under the assumption that the magnetic field is constant during each control actuation step; this assumption is reasonable, especially over the short prediction horizon, on the order of seconds, that we consider, as the field, while time-varying, is only slowly-varying, with a period of approximately 24 hours.

A zero-order hold, identical to that used in (2.20), is applied to discretize the continuous-time dynamics of the satellite with drag panels system and predict the future state $\mathbf{x}_{k+1}$ according to the "frozen-in-time" magnetic field $B_d(t)$.

At each sampling step, the controller then minimizes the now finite-horizon cost functional

$$J(t) = \mathbf{x}_N^T P(t) \mathbf{x}_N + \sum_{k=0}^{N-1} \left(\mathbf{x}_k^T Q \mathbf{x}_k + \mathbf{u}_k^T R \mathbf{u}_k \right), \tag{2.33}$$

with prediction horizon N and subject to the discrete-time dynamics in (2.20), as well as to the constraint

$$|\mathbf{u}_k|_\infty \leq u_{max}, \tag{2.34}$$

where $P(t)$ is the unique positive definite solution to the associated Discrete-Time Algebraic Riccati Equation,

$$\begin{aligned} P(t) &= A_d^T P(t) A_d + Q - A_d^T P(t) B_d(t) K(t), \\ K(t) &= \left(R + B_d(t)^T P(t) B_d(t)\right)^{-1} B_d(t)^T P(t) A_d. \end{aligned} \tag{2.35}$$

The controller implements the first control action and then recomputes a new minimizing control sequence at the next sampling time instant.

2.5.2 Simulation Results

The MPC controller uses the same weights as in the LQR controller. The discrete-time steps are of length $\Delta t = 4$ sec, and the prediction horizon is held at $N = 5$. All other parameters are identical to those used to generate the simulation results in Figure 2.3. The predictive controller provides faster convergence than the LQR controller, at the added cost of additional computation complexity and power consumption that may present challenges to a resource-limited cubesat platform.

2.6 Summary

This chapter described the design of pointing controllers to enable the QB50 satellites' scientific mission. The two LQR controllers exploit the magnetic torque rod actuators to regulate both attitude and angular velocity states, and the second such controller complements the augmented passive drag panels. Both controllers have been shown to provide convergence to the desired pointing configuration in nonlinear model simulations; the second controller, however, has demonstrated greater robustness to unmodeled disturbance torques. A finite-horizon predictive controller is shown to provide faster convergence than the LQR controllers while maintaining the robustness to disturbance torques.

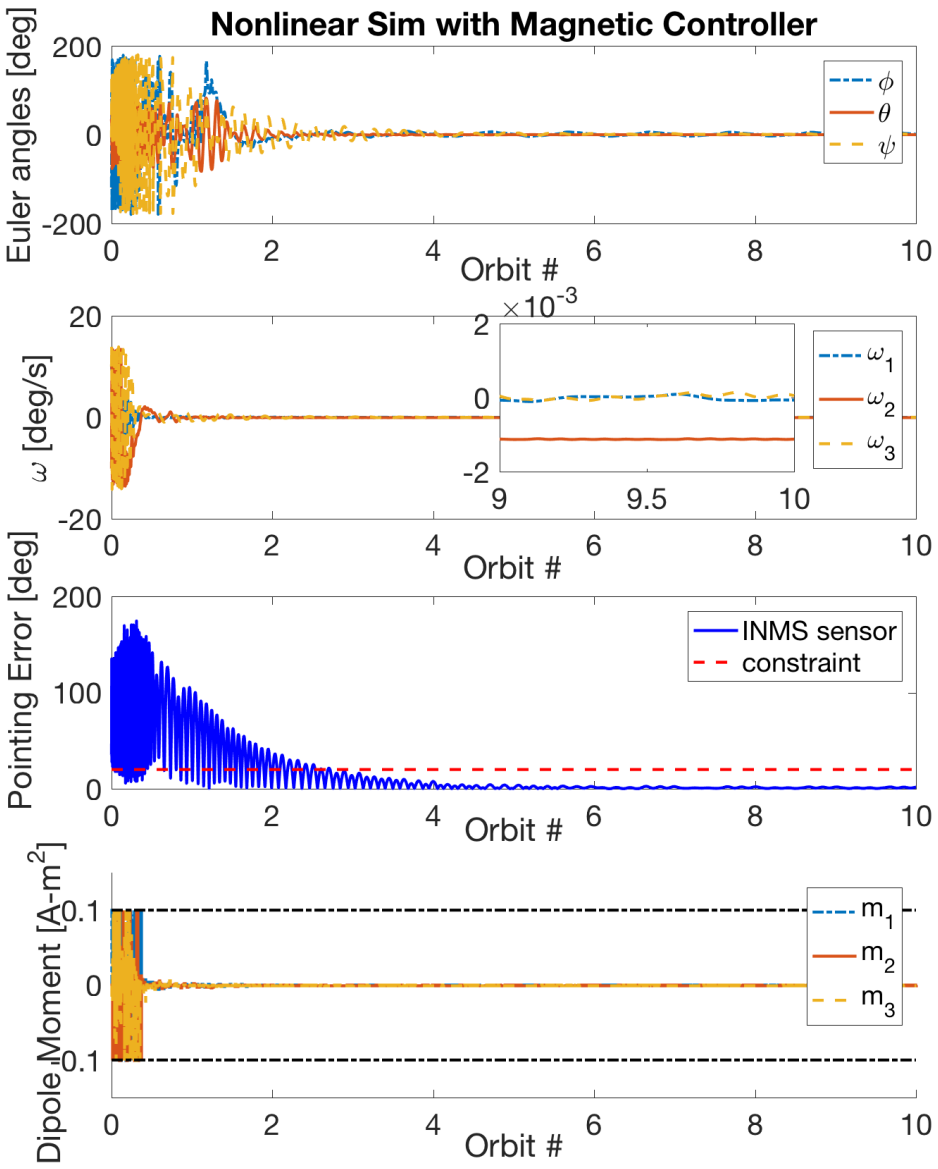

Figure 2.9: Simulation results using the predictive control design based on the re-linearized dynamics, to include the panels, with the same constant disturbance torque as in Figure 2.4.

CHAPTER 3

Disjunctive Sensing and Control

3.1 Motivation

A common assumption in control theory is that sensing and actuation can be performed simultaneously. In this chapter, we consider the case of *disjunctive* sensing and actuation, in which, at any given time step, either a sensor or an actuator can be operated but not both. Thus, a switching policy between sensing and actuation needs to be determined that achieves the specified mission objectives.

The motivation for considering this class of problems comes from spacecraft control applications. Specifically, magnetic fields generated by magnetic actuators may interfere with the magnetic sensors used for attitude sensing, see e.g., [54]. In larger satellites, magnetometers may be placed on a boom to reduce the electromagnetic interference from the magnetic actuators and other equipment onboard the spacecraft. Such a solution is not feasible for the smaller and cheaper class of cubesats, where the magnetic actuators must be deactivated and the residual field then allowed to decay before recording an accurate attitude reading. Other situations in which simultaneous sensing and actuation are not viable include vision-based rendezvous, docking, and relative motion maneuvering [55], in which the plume or vibration from spacecraft thrusters may interfere with cameras or other sensitive navigation equipment. Further, Kalman Filters are frequently deactivated while thrusters are firing, inducing a natural switching of subsystems.

For this problem, we consider the eventual enforcement of probabilistic chance state constraints of the form

$$\forall k \geq k^*, \text{ Prob}(\{x_k \in X\}) \geq 1 - \delta, \tag{3.1}$$

where X is the set prescribed by the constraints of the problem, $0 \leq \delta < 1$, and $k^* \in \mathbb{Z}_+$ is sufficiently large. In spacecraft applications, X may represent a region in the state space in which scientific measurements can be reliably taken by the onboard instrumentation, see, for instance, the case study in [26] and [24]. In this case study, the state constraints do not need to be satisfied during initial transients but must be satisfied eventually to enable the equipment to function.

In this chapter, we treat a disjunctive sensing and actuation problem for systems that can be represented by discrete-time linear models with stochastic process disturbance and measurement noise inputs. A procedure to construct a periodic switching sequence between sensing and actuation is described and closed-loop boundedness and convergence properties when such a sequence is applied are analyzed.

The given problem falls within the general class of switched system stabilization problems in which a part of the dynamics represents the propagation of the estimated state and of the estimation error covariance matrix. Stability of switched systems has been studied extensively, see e.g., [56] and [57]. We note that if the system is open-loop unstable then, to guarantee either boundedness of states or boundedness of state estimates based on dwell time conditions, sufficient dwell time in each mode (sensing or actuation) is necessary. In addition, sensing and actuation intervals need to be suitably interlaced to achieve both goals simultaneously.

Techniques developed for stability analysis and control of discrete-time periodic systems [58–60] are also relevant given our search for a periodic switching sequence. In event triggered and self-triggered control [61] and in sensor networks, sensor scheduling

and sensor tasking [62, 63], sensors may be deactivated when confidence in the estimated states is high; however, the situation in which the sensors and the actuators cannot be used simultaneously does not appear to be treated.

3.2 Problem Formulation

Consider a system represented by a discrete-time linear model with stochastic state disturbance and measurement noise inputs, given by

$$\begin{aligned} x_{k+1} &= Ax_k + Bu_k + w_k, \\ y_k &= Cx_k + \nu_k, \end{aligned} \tag{3.2}$$

where x_k is a vector state and u_k is a vector control. The variables w_k and ν_k are, respectively, the state disturbance and the measurement noise inputs, each assumed to be a sequence of zero-mean, independent (and jointly independent) identically distributed (i.i.d.) random variables with $\mathbb{E}[w_k w_k^{\mathrm{T}}] = \Sigma_w = \Sigma_w^{\mathrm{T}}$, $\mathbb{E}[\nu_k \nu_k^{\mathrm{T}}] = \Sigma_\nu = \Sigma_\nu^{\mathrm{T}}$.

For this scenario, a fixed gain state feedback is considered,

$$u_k = u_T + K(\hat{x}_k - x_T), \tag{3.3}$$

where $\hat{x}_k$ is the state estimate generated by a fixed gain observer of the form

$$\hat{x}_{k+1} = A\hat{x}_k + \eta_k B u_k + (1 - \eta_k) L(y_k - C\hat{x}_k). \tag{3.4}$$

The binary variable $\eta_k \in \{0, 1\}$ represents the system operating mode. When $\eta_k = 1$, the control is applied to the system. When $\eta_k = 0$, the control is deactivated ($u_k = 0$) and the sensed output, y_k, is obtained. The target equilibrium is denoted by x_T, and it is assumed that the feedforward control input, u_T, supports it in steady-state in the absence of w_k and with $\eta_k = 1$, i.e., $x_T = Ax_T + Bu_T$.

In a typical control design process, due to the Separation Principle, the gains K and L would be determined without consideration of the interference between actuation and sensing (possibly by different engineers) and then a coordination mechanism introduced by specifying $\eta_k,\ k = 0, 1, \ldots$. In this setting, offline-generated N-periodic switching sequences, $\{\eta_k\}$, with $\eta_k = \eta_{k+N}$ for all $k \in \mathbb{Z}_{\geq 0}$, $N \in \mathbb{Z}_{>0}$, are of particular interest, so that their repeated application leads to the attainment of the control objectives, including eventual satisfaction of state constraints. This approach, based on the application of the offline generated periodic sequence, has low computational footprint and is appealing in view of limited computing power and restrictive electrical power consumption budgets onboard of small spacecraft.

3.3 Admissible Sequences

Suppose that $\{\eta_k\}$ is fixed and define $\bar{A}_k = A + \eta_k BK,\ \ \tilde{A}_k = A + (1 - \eta_k)LC$. The evolution of the state, x_k, and of the state estimation error, $e_k = x_k - \hat{x}_k$, are driven by

$$\begin{aligned} x_{k+1} &= Ax_k + \eta_k BK\hat{x}_k + w_k \\ &= \bar{A}_k x_k - \eta_k Be_k + \eta_k Bu_T + w_k, \end{aligned} \tag{3.5}$$

and

$$\begin{aligned} e_{k+1} &= [A + (1 - \eta_k)LC]\, e_k + w_k + (1 - \eta_k)L\nu_k \\ &= \tilde{A}_k e_k + w_k + (1 - \eta_k)L\nu_k. \end{aligned} \tag{3.6}$$

In simulations, we assume that $x_T = 0$ (and so $u_T = 0$). Based on (3.6) and assumed independence and zero mean properties of the stochastic disturbance, w_k, and measurement noise, ν_k, the error covariance matrix $P_k = \mathbb{E}[e_k e_k^{\mathrm{T}}]$ satisfies

$$P_{k+1} = \tilde{A}_k P_k \tilde{A}_k^{\mathrm{T}} + R_k, \tag{3.7}$$

$$R_k = \begin{bmatrix} (1-\eta_k)L & \mathbf{I} \end{bmatrix} \begin{bmatrix} \Sigma_\nu & \mathbf{0} \\ \mathbf{0} & \Sigma_w \end{bmatrix} \begin{bmatrix} (1-\eta_k)L^{\mathrm{T}} \\ \mathbf{I} \end{bmatrix}. \tag{3.8}$$

Definition 3.1: Let A, B be defined as in (3.2), K, L be defined as in (3.3), (3.4), and $\bar{A}_k$, $\tilde{A}_k$ be defined as above, with none of $\bar{A}_k$, $\tilde{A}_k$ nilpotent. An N-periodic sequence of binary integers $\{\eta_0, \eta_1, \cdots, \eta_{N-1}\}$, where, for all $k \in \mathbb{Z}_{\geq 0}$, $\eta_k \in \{0, 1\}$ and $\eta_{k+N} = \eta_k$, is called *admissible* if the following contractivity conditions hold:

$$\rho(\bar{A}_{N-1}\bar{A}_{N-2}\cdots\bar{A}_0) = \bar{q}_A < 1, \tag{3.9}$$

$$\rho(\tilde{A}_{N-1}\tilde{A}_{N-2}\cdots\tilde{A}_0) = \tilde{q}_A < 1, \tag{3.10}$$

where $\rho(\cdot)$ denotes the spectral radius operator. A non-periodic sequence of binary integers $\{\eta_0, \eta_1, \dots\}$ is admissible if:

$$\lim_{k\to\infty} \rho(\bar{A}_k\bar{A}_{k-1}\cdots\bar{A}_0) = 0, \tag{3.11}$$

$$\lim_{k\to\infty} \rho(\tilde{A}_k\tilde{A}_{k-1}\cdots\tilde{A}_0) = 0. \tag{3.12}$$

The constraint against nilpotent matrices ensures that the limits in (3.11) and (3.12) approach zero rather than "jump" to zero. These definitions are consistent with the properties of discrete-time state transition matrices found in, for example, Chen [64].

Lemma 3.1: If an admissible sequence exists, then a periodic admissible sequence exists.

Proof: Let $s = \{\eta_0, \eta_1, \dots, \eta_k, \dots\}$ be an admissible sequence. If s is periodic, then done. Thus, assume s is non-periodic. By definition, $\lim_{k\to\infty} \rho(\bar{A}_k\bar{A}_{k-1}\cdots\bar{A}_0) = 0$, thus, for each $\bar{\epsilon} > 0$, there exists $\bar{N} \in \mathbb{N}$ such that, for all $k > \bar{N}$, $\rho(\bar{A}_k\bar{A}_{k-1}\cdots\bar{A}_0) < \bar{\epsilon}$, and, by similar argument, for each $\tilde{\epsilon} > 0$ there exists $\tilde{N}$ such that, for all $k > \tilde{N}$, $\rho(\tilde{A}_k\tilde{A}_{k-1}\cdots\tilde{A}_0) < \tilde{\epsilon}$. Choose k such that $\max\{\bar{\epsilon}, \tilde{\epsilon}\} < 1$. Then, $\rho(\bar{A}_k\bar{A}_{k-1}\cdots\bar{A}_0) < 1$, and $\rho(\tilde{A}_k\tilde{A}_{k-1}\cdots\tilde{A}_0) <$

1, therefore $s_k = \{\eta_0, \eta_1, \ldots, \eta_k\}$ is admissible by construction and, when applied repeatedly, is periodic with period $k+1$. ■

3.3.1 Limits of the Mean and Error Covariance Matrix Sequences

Note first that $\mathbb{E}[\nu_k] = 0$, $\mathbb{E}[w_k] = 0$ and hence (3.5), (3.6) imply that the state and estimation error mean, $\mu_{x,k} = \mathbb{E}[x_k]$ and $\mu_{e,k} = \mathbb{E}[e_k]$, respectively, satisfy

$$\mu_{x,k+1} = \bar{A}_k \mu_{x,k} - \eta_k B \mu_{e,k} + \eta_k B u_T, \tag{3.13}$$

$$\mu_{e,k+1} = \tilde{A}_k \mu_{e,k}, \tag{3.14}$$

where $\bar{A}_k$ and $\tilde{A}_k$ are periodic with the same period, N, as η_k.

Proposition 3.1: Suppose that (3.9) and (3.10) hold. Then, as $k \to \infty$, $\mu_{e,k} \to 0$ and $\mu_{x,k} \to \mu^{\mathrm{s}}_{x,k}$ exponentially, where $\{\mu^s_{x,k}\}$ is the unique N-periodic solution of (3.13) with $\mu_{e,k} \equiv 0$. Furthermore, if $u_T = 0$ then $\mu^s_{x,k} = 0$.

Sketch of the proof: The proof follows from Proposition 4.5 in [65] by noting that the characteristic multipliers (eigenvalues of N-step state transition matrix) of the combined time-periodic system (3.13)-(3.14), which is upper triangular, are inside the unit disk if (3.9) and (3.10) hold. ■

The next result summarizes the properties of the error covariance matrix sequence.

Proposition 3.2: Suppose that (3.10) holds. Then the error covariance matrix, P_k, is bounded and, as $k \to \infty$, converges to the unique N-periodic solution of (3.7), $\{P^{\mathrm{s}}_k\}$, with $P^{\mathrm{s}}_{k+N} = P^{\mathrm{s}}_k$. In addition, for any $n \in \mathbb{Z}_{\geq 0}$,

$$\left(\|P_{N(n+1)}\| - \frac{\gamma}{1-\tilde{q}_A^2} \right) \leq \tilde{q}_A^2 \left(\|P_{Nn}\| - \frac{\gamma}{1-\tilde{q}_A^2} \right), \tag{3.15}$$

where

$$\gamma \geq \|\tilde{A}_{N-1} \cdots \tilde{A}_1 R_0 \tilde{A}_1^{\mathrm{T}} \cdots \tilde{A}_{N-1}^{\mathrm{T}} + \cdots + \tilde{A}_{N-1} R_{N-2} \tilde{A}_{N-1}^{\mathrm{T}} + R_{N-1}\|.$$

Sketch of the proof: The proof of the error covariance matrix convergence follows by applying similar arguments in discrete-time as the ones on p. 58 of [58] for the continuous-time case. The bound (3.15) follows by expressing P_N in terms of P_0 and $R_0, \cdots R_{N-1}$ based on (3.7) and applying the triangular inequality. ■

Remark 3.1: The steady-state periodic solution, P_k^s, of (3.7) can be computed by solving the conventional discrete-time Lyapunov equation for the evolution of the *lifted* system error covariance matrix, i.e., of $P^l = \text{diag}\{P_0^s, \cdots, P_{N-1}^s\}$, which is directly obtained from (3.7).

Remark 3.2: Note that (3.15) implies that $\limsup_{k\to\infty} \|P_{Nk}\| \leq \gamma/(1-\tilde{q}_A^2)$.

Remark 3.3: The results in Propositions 3.1 and 3.2 generalize to non-constant N-periodic feedback and observer gains, i.e., K and L are replaced by K_k, and L_k, where $K_{k+N} = K_k,\ L_{k+N} = L_k$ for all $k \in \mathbb{Z}_{\geq 0}$, under the same conditions (3.9) and (3.10). However, analysis results benefit from both $\bar{A}_k$ and $\tilde{A}_k$ having only two possible values each, which is the case when the gains are constant.

3.4 Dwell Time Conditions

We can take advantage of the dwell time conditions for stability analysis of hybrid systems to develop simpler sufficient conditions that can inform procedures for faster determination of admissible switching sequences. The discussion of the dwell time conditions follows Theorem 4.1 in [66] and its proof.

Let $\bar{\Omega}_0 = A$ and $\bar{\Omega}_1 = A + BK$, and consider the condition (3.9). By Gelfand's theorem [67], $\lim_{k\to\infty} \|\Omega^k\|^{\frac{1}{k}} = \rho(\Omega)$, for any matrix Ω and norm $\|\cdot\|$. This implies that

there exist constants c_0, c_1, that do not depend on k, such that for any $k \geq 1$,

$$\|\bar{\Omega}_0^k\|^{\frac{1}{k}} \leq c_0 \rho(\bar{\Omega}_0), \quad \|\bar{\Omega}_1^k\|^{\frac{1}{k}} \leq c_1 \rho(\bar{\Omega}_1). \tag{3.16}$$

As the tail of $\|A^k\|^{\frac{1}{k}}$ is strictly non-increasing for any consistent matrix norm, there exists a finite k^* such that $\|A^{k^*}\|^{\frac{1}{k^*}} \geq \|A^k\|^{\frac{1}{k}}$ for all $k \geq 1$. Then,

$$c_i = \frac{\|\bar{\Omega}_i^{k^*}\|^{\frac{1}{k^*}}}{\rho(\bar{\Omega}_i)}.$$

Note that $c_0 \geq 1$ and $c_1 \geq 1$ since $\|A\| \geq \rho(A)$ for any A. Let $c = \max\{c_0, c_1\}$, $n_0 < N$ be the total time spent in the mode $\eta = 0$, $n_1 = N - n_0$ be the total time spent in the mode $\eta = 1$, and n_s be the number of mode "blocks" in the sequence, equivalent to the number of switches plus one. Then, $\|\bar{A}_{N-1}\bar{A}_{N-2}\cdots\bar{A}_0\| \leq c^{n_s}\rho(\bar{\Omega}_0)^{n_0}\rho(\bar{\Omega}_1)^{n_1}$, and (3.9) holds if

$$c^{n_s}\rho(\bar{\Omega}_0)^{n_0}\rho(\bar{\Omega}_1)^{n_1} \leq \bar{q}_A < 1. \tag{3.17}$$

A frequent situation is that $\bar{\Omega}_0$ (no actuation) is unstable and $\rho(\bar{\Omega}_0) > 1$, while $\bar{\Omega}_1$ is stable and $\rho(\bar{\Omega}_1) < 1$. Then (3.17) dictates that there must be sufficient time spent in the actuation mode and, furthermore, there must be sufficient dwell time (not too many switches) so that n_s and c^{n_s} are small.

Taking the logarithm of the left hand side of (3.17), it follows that (3.9) holds if

$$n_s \log c + n_0 \log \bar{\rho}_0 + n_1 \log \bar{\rho}_1 < 0, \tag{3.18}$$

where $\bar{\rho}_0 = \rho(\bar{\Omega}_0)$, $\bar{\rho}_1 = \rho(\bar{\Omega}_1)$. When finding admissible sequences, it is therefore possible to first restrict the search to sequences for which n_0, n_1 and n_s satisfy the condition (3.18). Note that $\bar{q}_A$ in (3.17) is an estimate of the rate of convergence of the state. Hence, ensuring that the left hand side of (3.18) is as negative as possible promotes increasing the

convergence rate to x_T; this may, however, increase the estimation error.

Similar analysis can be applied in the case of (3.10). Let $\tilde{\rho}_0 = \rho(\tilde{\Omega}_0)$, $\tilde{\rho}_1 = \rho(\tilde{\Omega}_1)$ where $\tilde{\Omega}_0 = A + LC$ and $\tilde{\Omega}_1 = A$. Then, $\|\tilde{A}_{N-1} \cdots \tilde{A}_0\| \leq c^{n_s} \rho(\tilde{\Omega}_0)^{n_1} \rho(\tilde{\Omega}_1)^{n_0} \leq \tilde{q}_A < 1$. By taking the logarithm of this expression, we can see that (3.10) holds if

$$n_s \log c + n_1 \log \tilde{\rho}_0 + n_0 \log \tilde{\rho}_1 < 0. \tag{3.19}$$

The condition (3.19) complements (3.18) and can facilitate the initial fast search for admissible sequences.

Remark 3.4: Conditions (3.18) and (3.19) together are sufficient, but not necessary, to also satisfy conditions (3.9) and (3.10).

3.5 Reducible and Irreducible Sequences

The search for admissible sequences can be made faster by discarding sequences that replicate a known inadmissible subsequence.

Definition 3.2: A sequence $\{s_N\}$ of length $N \in \mathbb{Z}_{>0}$ is called *reducible* if there exists a subsequence $\{s_k\}$ of length $k \in \mathbb{Z}_{>0}$ such that $k < N$, N is a multiple of k, and $\{s_N\} = \{s_k\} \oplus \{s_k\} \oplus \cdots \oplus \{s_k\}$, N/k times, where $\oplus$ is used to denote sequence concatenation. A sequence which is not reducible is called *irreducible*.

Proposition 3.3: Every (non-empty) sequence $\{s_N\}$ contains a unique irreducible subsequence $\{s_n\}$.

Proof: If $\{s_N\}$ is irreducible, then we are done. Thus, assume $\{s_N\}$ to be reducible. There exists then $k_1 \in \mathbb{N}$ such that $k_1 < N$, N is a multiple of k_1, and $\{s_N\} = \{s_{k_1}\} \oplus \ldots \oplus \{s_{k_1}\}$, concatenated N/k_1 times. If $\{s_{k_1}\}$ is irreducible, then done, as no shorter subsequences exist and no subsequence longer than $\{s_{k_1}\}$ can be irreducible. If $\{s_{k_1}\}$ is reducible, then there exists $k_2 \in \mathbb{N}$ such that $k_2 < k_1$, k_1 is a multiple of k_2, and $\{s_{k_1}\} = \{s_{k_2}\} \oplus \ldots \oplus \{s_{k_2}\}$, concatenated k_1/k_2 times. The same argument for $\{s_{k_1}\}$

above now repeats for $\{s_{k_2}\}$. The sequence $\{k_1, k_2, ...\}$ eventually terminates in some k_n as each k_i is strictly smaller than the previous, and reaches an absolute minimum value $k_n \geq 1$ after a finite number of iterations. The process eventually yields an irreducible subsequence $\{s_{k_n}\}$ of $\{s_N\}$ that is of minimum length (no irreducible subsequences of smaller length exist). As this subsequence consists of the first k_n elements of $\{s_N\}$, it is also unique, as only one such subsequence is possible for a given n. ■

In practice, we need only focus on these irreducible sub-sequences. This is summarized by the following:

Proposition 3.4: A binary sequence $\{s_N\}$ is admissible if and only if the associated irreducible subsequence $\{s_n\}$ is admissible.

Proof: Assume that $\{s_N\} = \{s_n\} \oplus \{s_n\} \oplus \cdots \oplus \{s_n\}$, where $n \mid N$, and consider the condition (3.9). Let $\rho(\{s_n\})$ denote the spectral radius of the product of the matrices, $\bar{A}_k = (A + \eta_k BK)$, $k = 1, ..., n-1$, corresponding to the switching sequence, $\{s_n\} = \{\eta_0, ..., \eta_{n-1}\}$. The properties of the spectral radius of a matrix power imply that $\rho(\{s_N\}) = \rho(\{s_n\})^{N/n}$. Hence $\rho(\{s_N\}) < 1$ if and only if $\rho(\{s_n\}) < 1$. This implies the result. ■

Any reducible admissible sequence can be formed by propagating an irreducible admissible sequence forward in time. Thus, when investigating sequences of length N for admissibility, all sequences for which we have already evaluated the associated irreducible sub-sequence can be discarded.

To check a sequence $\{s_N\}$ for reducibility, we employ the following algorithm:

1. Let $D = \{d : \ d \mid N \text{ and } d < N\}$, i.e., the set of proper divisors of N.

2. If there exists $d \in D$ such that, for every $1 \leq n \leq N - d$, the sequence satisfies $s_n = s_{n+d}$, where $s_n \in \{s_N\}$, then the sequence is reducible.

3. Otherwise, the sequence is irreducible.

Remark 3.5: If N is prime, then $D = \{1\}$ and the only reducible sequences are the sequence of zeros and the sequence of ones. Under our initial assumption that both actu-

ation and sensing actions are required, these two sequences can immediately be discarded as inadmissible.

3.6 Chance Constraints

Consider now the chance constraint (3.1). Define $z = \begin{bmatrix} x^{\mathrm{T}} & e^{\mathrm{T}} \end{bmatrix}^{\mathrm{T}}$ and $\zeta = \begin{bmatrix} \nu^{\mathrm{T}} & w^{\mathrm{T}} \end{bmatrix}^{\mathrm{T}}$. Then,

$$z_{k+1} = \breve{A}_k z_k + \breve{\Gamma}_k \zeta_k + \breve{G}_k u_T, \tag{3.20}$$

where

$$\breve{A}_k = \begin{bmatrix} \bar{A}_k & -\eta_k BK \\ \mathbf{0} & \tilde{A}_k \end{bmatrix}, \; \breve{\Gamma}_k = \begin{bmatrix} \mathbf{0} & \mathbf{I} \\ (1-\eta_k)L & \mathbf{I} \end{bmatrix},$$

and

$$\breve{G}_k = \begin{bmatrix} \mathbf{0} \\ \eta_k B \end{bmatrix}.$$

Under contractivity conditions (3.9) and (3.10), repeat the analysis in Propositions 3.1 and 3.2 for (3.20). Let $\breve{P}_k = \mathbb{E}[(z_k - \mu_{z,k})(z_k - \mu_{z,k})^{\mathrm{T}}]$, where $\mu_{z,k} = \mathbb{E}[z_k]$. Then,

$$\breve{P}_{k+1} = \breve{A}_k \breve{P}_k \breve{A}_k^{\mathrm{T}} + \breve{\Gamma}_k \begin{bmatrix} \Sigma_\nu & \mathbf{0} \\ \mathbf{0} & \Sigma_w \end{bmatrix} \breve{\Gamma}_k^{\mathrm{T}}, \tag{3.21}$$

and $\breve{P}_k \to \breve{P}_k^{\mathrm{s}}$ as $k \to \infty$, where $\breve{P}_k^{\mathrm{s}}$ is the unique N-periodic solution to (3.21). Then, the steady-state covariance matrix satisfies $\breve{P}_{x,k}^{\mathrm{s}} = \begin{bmatrix} \mathbf{I} & \mathbf{0} \end{bmatrix} \breve{P}_k^{\mathrm{s}} \begin{bmatrix} \mathbf{I} & \mathbf{0} \end{bmatrix}^{\mathrm{T}}$. Thus, x_k converges to x_k^{s}, a cyclostationary process with the N-periodic mean, $\mu_{x,k}^{\mathrm{s}}$, and N-periodic covariance matrix, $P_{x,k}^{\mathrm{s}}$.

As no assumption on the actual probability density functions of w_k and ν_k is made, we resort to the multivariate Chebyshev's inequality [68, 69] to treat the chance constraint,

which states

$$\text{Prob}\left((x_k - \mu^{\text{s}}_{x,k})^{\text{T}}(P^{\text{s}}_{x,k})^{-1}(x_k - \mu^{\text{s}}_{x,k}) \leq \alpha_x^2\right) \geq 1 - \frac{n_x}{\alpha_x^2}, \tag{3.22}$$

where n_x is the dimension of x and $0 < \alpha_x \leq 1$.

Given $\delta > 0$, choose $\alpha_x = \sqrt{n_x/\delta}$. Suppose that for $k = 0, 1, \ldots, N-1$, the following condition is verified:

$$\mu^{\text{s}}_{x,k} \in X \sim \mathcal{E}\left(\mathbf{0}, \frac{1}{\alpha_x^2}(P^{\text{s}}_{x,k})^{-1}\right), \tag{3.23}$$

where $\mathcal{E}(\mathbf{0}, S) = \{x : \ x^{\text{T}} S x \leq 1\}$ is an ellipsoidal set and $\sim$ denotes the Pontryagin set difference. Then, in steady-state, the chance constraint (3.1) holds.

Remark 3.6: The steady-state periodic solution, $\breve{P}^{\text{s}}_k$, can be computed by solving the conventional discrete-time Lyapunov equation for the evolution of the *lifted* system error covariance matrix, i.e., of $\breve{P}^l = \text{diag}\{\breve{P}^{\text{s}}_0, \cdots, \breve{P}^{\text{s}}_{N-1}\}$, which is directly obtained from (3.21).

3.7 Optimal Control Approach

Since multiple admissible sequences may exist, we can select one by minimizing a cost functional. Consider the blended cost J that penalizes the estimation, the control objective, and the control effort:

$$J = \frac{1}{N}\sum_{k=0}^{N-1}\left(\text{Tr}\left(R_e P^{\text{s}}_k\right) + \text{Tr}\left(R_x P^{\text{s}}_{x,k}\right) + r_\eta \eta_k\right), \tag{3.24}$$

where $R_e = R_e^{\text{T}} \succeq 0$, $R_x = R_x^{\text{T}} \succeq 0$ and $r_\eta \geq 0$ are weights. The $1/N$ factor in the cost functional normalizes for sequence length, ensuring that a given reducible/irreducible sequence pair yield the same cost.

Now, search over sequences of a fixed length, check for admissibility, then find the

admissible sequence that yields the lowest cost. If no admissible sequence exists, we then extend the sequence length and search again. The process is summarized by the following algorithm:

Algorithm 3.1 Sequence search up to length N

1: Fix sequence length $N \in \mathbb{Z}_{>0}$.
2: Form 2^N binary integer sequences.
3: For each sequence, determine the associated irreducible subsequence.
4: Check the conditions of admissibility for the irreducible subsequence using dwell-time conditions (3.18), (3.19) or directly based on (3.9), (3.10).
5: If subsequence is admissible, evaluate the cost functional (3.24).
6: If no such subsequence satisfies the conditions of admissibility, then increase N and return to Step 1.
7: If at least one such subsequence is found to be admissible, then select the sequence that minimizes the objective function J.

The equivalence of admissibility between a sequence and its associated irreducible subsequence is invoked after incrementing N in Step 6; if Step 3 produces an irreducible subsequence that has already been evaluated in a previous iteration, then it can be skipped.

3.8 Numerical Simulations

We consider a case study of spacecraft three dimensional relative motion control. The relative motion dynamics are modeled with the linearized Clohessy-Wiltshire [70] equations,

$$\begin{aligned} \ddot{x}_1 &= 3\omega^2 x_1 + 2\omega \dot{x}_2 + \frac{1}{m} u_1, \\ \ddot{x}_2 &= -2\omega \dot{x}_1 + \frac{1}{m} u_2, \\ \ddot{x}_3 &= -\omega^2 x_3 + \frac{1}{m} u_3, \end{aligned} \tag{3.25}$$

where m is the chaser vehicle's mass and ω is the mean motion of the target vehicle's orbit. We form a system of first-order equations with state vector $x_k = [x_{1,k}, x_{2,k}, x_{3,k}, \dot{x}_{1,k}, \dot{x}_{2,k}, \dot{x}_{3,k}]^{\mathrm{T}}$ and discretize using a Zero-Order Hold [71] with sampling period of $30\ sec$, chaser vehicle mass of $140\ kg$ and target vehicle mean motion of $\omega = 0.0010\ rad/sec$.

We choose $C = [\mathbf{I}_3 \;\; \mathbf{0}_{3\times 3}]$, which corresponds to relative position measurements. The goal in this scenario is to rendezvous the chaser vehicle with the target vehicle, i.e., to bring the chaser's state to the origin.

For this controller and observer, the feedback gain matrix K is computed using LQR by solving the Discrete-Time Algebraic Riccati Equation (DARE) and the observer gain matrix L computed by solving the dual DARE, with $Q = \mathbf{I}_6$ and $R = \mathbf{I}_3$ in each case.

The distributions of the measurement noise, ν_k, and of the state disturbance, w_k, are assumed to be Gaussian with covariance matrices $\Sigma_v = 10^{-2} \cdot \mathbf{I}_3$ and $\Sigma_w = 10^{-4} \cdot \mathbf{I}_6$.

The cost function (3.24) has been defined with $r_\eta = 0$, $R_e = \mathbf{I}$ and $R_x = \mathbf{0}$. These choices ensure accurate estimates of the relative position states.

We now construct a sequence that satisfies the sufficient conditions, and demonstrate that it leads to stable behavior.

For this example, $\rho(\bar{\Omega}_0) = 1.0063$, $\rho(\bar{\Omega}_1) = 0.2016$, $\rho(\tilde{\Omega}_0) = 0.0332$, and $\rho(\tilde{\Omega}_1) = 1.0063$.

Working with the Frobenius norm, $k^* = 1$ and

$$c = \frac{\|\bar{\Omega}_1\|_F}{\rho(\bar{\Omega}_1)} = \frac{10.4716}{0.2016} = 51.950.$$

Begin with the (inadmissible) sequence $s_2 = \{0, 1\}$, with $n_s = 2$, $n_0 = 1$, and $n_1 = 1$. Then, $n_s \log c + n_0 \log \bar{\rho}_0 + n_1 \log \bar{\rho}_1 = 6.3054$ and $n_s \log c + n_1 \log \tilde{\rho}_0 + n_0 \log \tilde{\rho}_1 = 4.5016$.

To satisfy the sufficient conditions, increase n_1 until (3.18) is satisfied, then increase n_0 until (3.19) is satisfied, then repeat as necessary until both inequalities are simultaneously satisfied. This process yields $n_0 = 3$ and $n_1 = 5$, as then, $n_s \log c + n_0 \log \bar{\rho}_0 + n_1 \log \bar{\rho}_1 = -0.0879$ and $n_s \log c + n_1 \log \tilde{\rho}_0 + n_0 \log \tilde{\rho}_1 = -2.2837$. Then, we simulate this new sequence, $s_8 = \{0, 0, 0, 1, 1, 1, 1, 1\}$, that we have constructed, using randomized initial conditions. An example trajectory appears in Figure 3.1.

The shortest admissible solution sequence is of length 4, and the optimum such se-

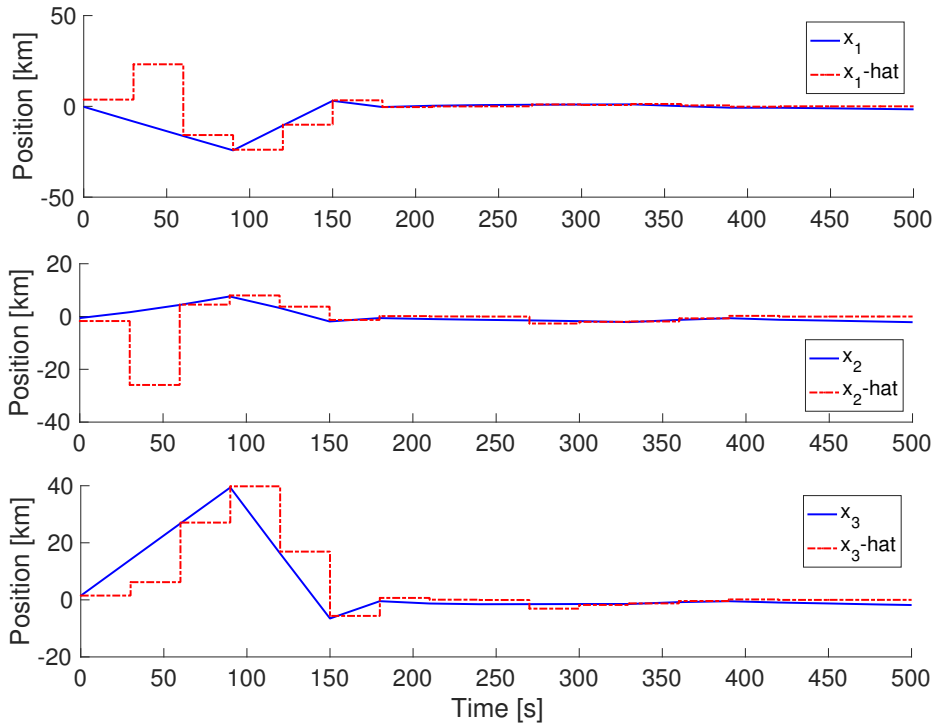

Figure 3.1: Simulation of the 8-step sequence s_8 that was constructed to satisfy the sufficient conditions.

quence is $S_4 = \{0, 0, 1, 1\}$, with $\bar{q}_A = 0.5879$ in (3.9) and $\tilde{q}_A = 0.0130$ in (3.10). When the algorithm treats sequences of length 7, the optimum sequence is $S_7 = \{0, 0, 1, 1, 1, 0, 0\}$, with $\bar{q}_A = 0.07594$ and $\tilde{q}_A = 3.796 \times 10^{-5}$. Figure 3.2 shows the results of propagating these control sequences forward.

In each case, the expected value of each state is successfully driven to the origin. Of note, when the algorithm treats sequences of length 8, the optimum sequence is $s_8 = \{0, 0, 1, 1, 0, 0, 1, 1\}$, a reducible sequence which has S_4 as its corresponding irreducible subsequence.

The remaining objective is to select an admissible sequence that also satisfies a specified chance constraint. For the relative motion scenario, suppose that we wish to establish a constraint on the steady-state of the form $X = \{x : \|x\|_\infty \leq b\}$, so that the chaser spacecraft remains within a box centered at the origin, of side length $2b$, with $\text{Prob}(X) \geq 0.95$. Consider again sequence S_4; invoking (3.23), with $\alpha_x = \sqrt{3/0.05}$, for each of

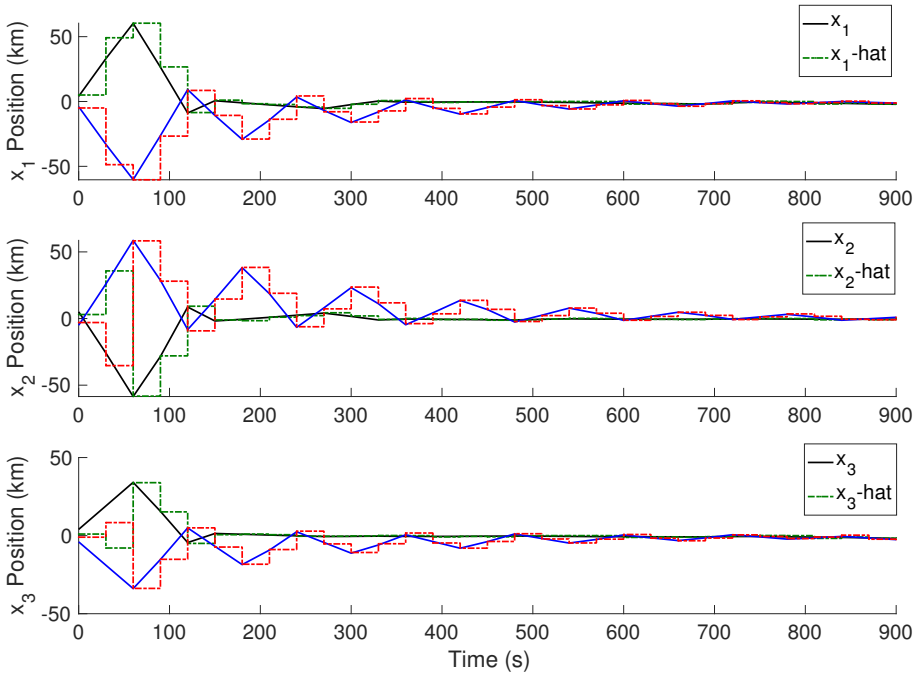

Figure 3.2: State responses when propagating the length 4 and length 7 optimal sense-control admissible sequences for the relative motion scenario.

$P^s_{x,0}, \ldots, P^s_{x,3}$ yields spheres with a minimum radius of $b = 2.79$ and a maximum radius of $b = 9.54$. Only the loosest of these constraints is guaranteed by (3.23), but even the tightest bound remains somewhat conservative. When we set $b = 2.5$, as demonstrated in Figure 3.3, the chance constraints are violated in no more than 4% of trajectories at any given time step over the course of two hundred simulation runs.

3.9 Summary

This chapter formulated and treated a problem in which simultaneous sensing and actuation was not possible. The solution involved the use of offline-constructed periodic switching sequences between sensing and actuation. When applied online, these sequences had desirable convergence properties. Approaches to simplify the check for admissibility of a sequence have been described based on the notion of reducible sequences and the use of

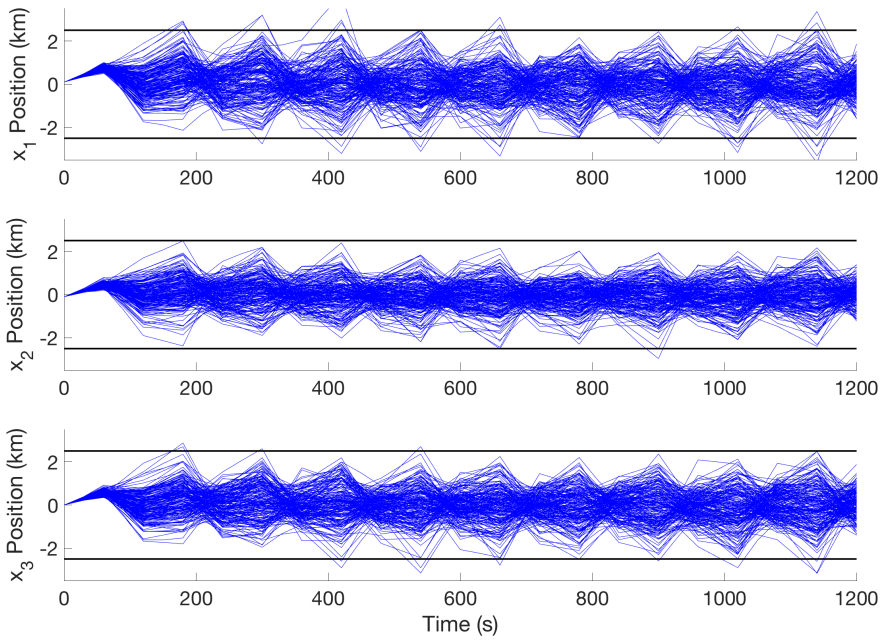

Figure 3.3: Two hundred simulated trajectories of the relative position of the chaser vehicle under the sequence S_4, subject to the box constraint $b = 2.5$ km and the chance constraint $\mathrm{P}(X) = 0.95$.

dwell time sufficient conditions. An example of applying the procedure to spacecraft relative motion control has been given in simulations.

CHAPTER 4

Waypoint-Following MPC in Minimum-Time

4.1 Motivation

In this chapter, motivated by applications to agile imaging satellites that must capture as many imaging sites as possible in minimum-time [72], we consider a problem in which a spacecraft must follow a series of prescribed attitude waypoints and reach each waypoint in minimum-time. In addition, the spacecraft attitude trajectory must avoid entering the specified exclusion zones in order to protect sensitive measurement equipment onboard the spacecraft.

To improve robustness to unmodeled dynamics and disturbances, rather than pursuing an open-loop solution, we implement a MPC [73, 74] strategy in which the first element of the solution sequence is applied to the spacecraft and the solution is then recomputed, with the state resulting after one step used as the initial condition.

Our MPC design is based on linearizing and then converting to discrete-time the continuous-time nonlinear attitude dynamics model of the spacecraft, and then formulating a MILP [75]. In this MILP, binary integer variables are used to indicate whether the trajectory has reached the target set around the destination waypoint at a given time instant, and these binary integer variables are optimized along with the control inputs over the prediction horizon. Such an approach can be extended to accommodate exclusion zone avoidance requirements that can be encoded with the help of additional binary integer variables and

constraints in the MILP. As compared to applying the minimum-time optimal control sequence open-loop, the use of MPC with the solution recomputed at every time instance compensates for the mismatch between the linear model and the nonlinear system.

In scenarios where a waypoint sequence is given, the minimum-time MPC solution is applied to reach the target sets corresponding to each waypoint in turn until the target set for the final waypoint is reached. The switching from the previous waypoint to the next waypoint in the sequence is effected upon reaching the target set of the previous waypoint, and a prediction horizon sufficient to reach the next waypoint is estimated. Our simulation results, based on the nonlinear spacecraft attitude dynamics model with disturbances, demonstrate that the controller is able to successfully track the sequence of waypoints without violating the exclusion zone constraints.

Since minimum-time MPC results in agile maneuvering of the spacecraft, depending on the level of spacecraft flexibility, spacecraft flexible modes could be significantly excited. To address this issue, we also demonstrate that a minimum-time MPC solution for the case of flexible spacecraft can be developed which accounts for the dynamics and constraints on spacecraft flexible modes.

A related approach of reducing the problem to an MILP was pursued in [76] where the objective was to guarantee a desired maneuver completion time rather than a minimum-time solution. In [77–79], a similar discrete-time MPC framework is developed for a time maximization problem of staying within a prescribed target set while counteracting drift. Minimum-time MPC solutions considered in [80–82] are based on continuous-time models and target state constraints. After a time re-scaling transformation, the resulting dynamic optimization problem over a fixed time interval is solved with respect to the control input and final time, where the final time appears as a multiplicative parameter in the re-scaled differential equations. The discrete-time framework for minimum-time MPC adopted in this section facilitates the onboard implementation of the resulting controller as a fixed controller update rate can be maintained. Furthermore, in this setting, the handling of state

constraints corresponding to the exclusion zone avoidance requirements can be performed through mixed integer programming techniques [83, 84].

4.2 Problem Formulation

Consider a discrete-time nonlinear system with the model given by

$$x_{k+1} = f(x_k, u_k), \tag{4.1}$$

where $k \in \mathbb{Z}_{\geq 0}$ denotes the discrete-time instant, $x_k \in \mathbb{R}^{n_x}$ denotes the state and $u_k \in \mathbb{R}^{n_u}$ denotes the control input.

Suppose the control constraints are given by

$$u_k \in U, \tag{4.2}$$

where U is a compact set. We let $\{u_k\} \in U_{\text{seq}}$ denote control sequences with elements $u_k \in U$. We also consider control policies which are mappings, $\pi : \mathbb{R}^{n_x} \to \mathbb{R}^{n_u}$. A control policy is admissible if the range of this mapping is the subset of U. The set of admissible control policies is denoted by U_{pol}.

Let $C \subset \mathbb{R}^{n_x}$ be a specified target set and let τ be the first time instant at which the trajectory enters C,

$$\tau(x_0, \{u_k\}) = \inf\{k : \ \phi_{\{u_k\}}(k, x_0) \in C, \ k \in \mathbb{Z}_{\geq 0}\}, \tag{4.3}$$

where $\phi_{\{u_k\}}(k, x_0)$ denotes the solution of (4.1) with the initial condition x_0 at the time instance $k \in \mathbb{Z}_{\geq 0}$ and under an admissible sequence $\{u_k\}$. Note that C is assumed to be robust control invariant; upon reaching C, we assume that there always exists a control that will keep the trajectory within C at all future times. In the sequel, when x_0 and $\{u_k\}$ are

clear from the context, we will use x_k to denote $\phi_{\{u_k\}}(k, x_0)$. Similar notations, $\phi_{\{\pi\}}(k, x_0)$, will be used to designate the closed-loop solution at the time instant k under the policy π and for the initial condition x_0. Note that for a given $\{u_k\}$, $\tau(x_0, \{u_k\})$ may not exist. In such a case, we set $\tau(x_0, \{u_k\}) = +\infty$.

The minimum-time problem to reach the target set C is now formulated as

$$\min_{\{u_k\} \in U_{\text{seq}}} \tau(x_0, \{u_k\}). \tag{4.4}$$

The value function of this problem is denoted by $\tau_{min}(x_0)$.

The following proposition provides sufficient conditions that can be used to determine the control policy based on dynamic programming.

Proposition 4.1: Suppose there exists a function $V : \mathbb{R}^{n_x} \to \mathbb{Z}_{\geq 0}$ and a control policy, $\pi^* \in U_{\text{pol}}$, such that

$$V(f(x, \pi^*(x))) - V(x) = -1, \tag{4.5}$$

$$V(f(x, \pi(x))) - V(x) \geq -1 \text{ for any } \pi \in U_{\text{pol}}, \tag{4.6}$$

$$V(x) > 0 \text{ if } x \notin C\ , \tag{4.7}$$

$$V(x) = 0 \text{ if } x \in C\ . \tag{4.8}$$

Then π^* is a (possibly non-unique) minimum-time optimal control policy.

Remark 4.1: Note that for V and π^* from Proposition 4.1, it follows that $V(x_0) = \tau_{min}(x_0)$ and if $V(x_0) = k$ then $\phi_{\pi^*}(k, x_0) \in C$.

Remark 4.2: If the function V satisfying Proposition 4.1 is known, control policies can be defined based on

$$u^*(x) \in \min_{u \in U} \{V(f(x, u))\}. \tag{4.9}$$

As an example, suppose $n_x = n_u = 1$, $f(x_k, u_k) = x_k + u_k$, $C = U = [-0.5,\ 0.5]$. In

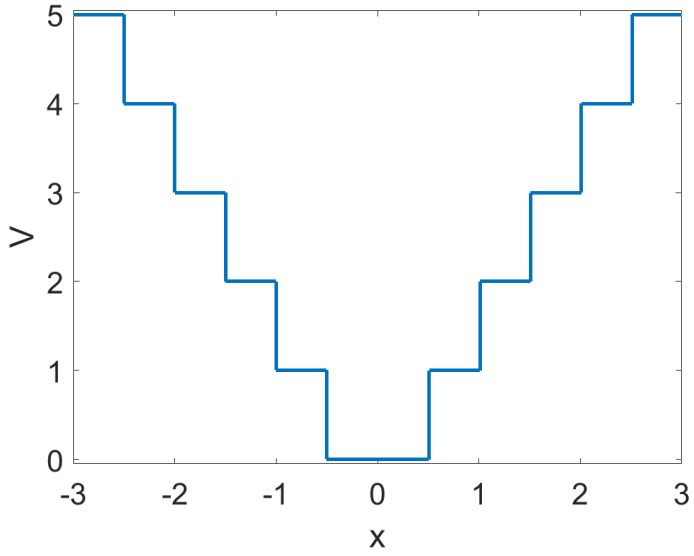

Figure 4.1: The value function of the minimum-time problem in the scalar example.

this case, an obvious control policy,

$$u^*(x) = \begin{cases} 0.5 & \text{if } x < 0.5, \\ 0 & \text{if } -0.5 \leq x \leq 0.5, \\ -0.5 & \text{if } x > 0.5 \end{cases}$$

and the value function $V(x)$ in Figure 4.1 satisfy the conditions of Proposition 4.1. The optimal control policy is non-unique. For instance, another optimal control policy is given in Figure 4.2 which is actually the minimum-norm selection that satisfies (4.9). For $x_0 = -1.8$, the closed-loop state trajectory with the former policy is a sequence, $\{-1.8,\ -1.3,\ -0.8,\ -0.3\}$, and with the latter control policy is a sequence $\{-1.8,\ -1.5,\ -1.0,\ -0.5\}$. In each case, it takes three steps to reach C.

While it may be possible to solve the dynamic programming problem in the low dimensional cases, using, e.g., value iteration, the treatment of higher dimensional problems requires a different approach, specifically, one based on model predictive control.

Let the control constraint set U and the target set C be polyhedral, and suppose the

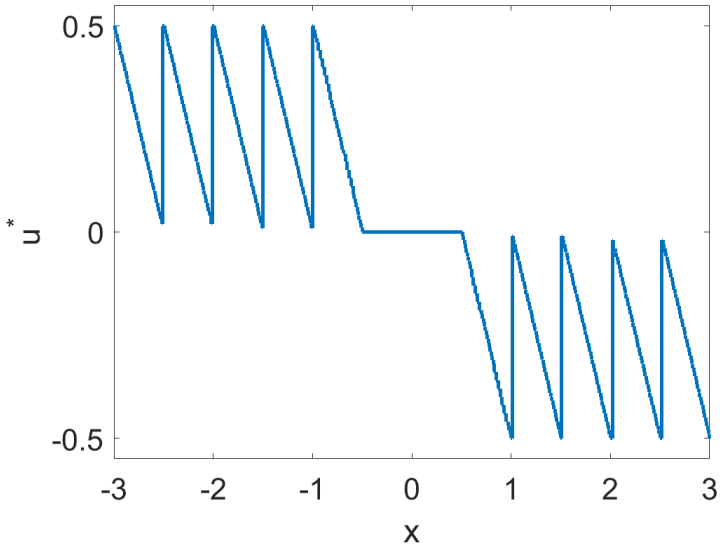

Figure 4.2: An optimal control policy in the scalar example.

model is linear, i.e.,

$$U = \{u \in \mathbb{R}^{n_u} : \ \Gamma u \leq \gamma, \ \gamma \in \mathbb{R}^{n_\gamma}\}, \tag{4.10}$$

$$C = \{x \in \mathbb{R}^{n_x} : \ Hx \leq h, \ h \in \mathbb{R}^{n_h}\}, \tag{4.11}$$

$$f(x_k, u_k) = Ax_k + Bu_k + d. \tag{4.12}$$

In what follows, we make a simplifying assumption that the target set C is control-invariant, i.e., the trajectory once it enters the set can always remain in the set with the feasible under constraints control input.

Consider the following optimization problem,

$$\sum_{k=\tau_{\rm lb}(x_0)}^{N} \delta_k \rightarrow \min_{\{\delta_k\},\{u_k\}} \tag{4.13}$$

subject to

$$x_{k+1} = Ax_k + Bu_k + d,$$

$$Hx_k \leq h + M\mathbf{1}_{n_h}\delta_k,$$

$$\delta_k \in \{0, 1\},$$

$$\Gamma u_k \leq \gamma,\ k = 0, 1, \cdots, N-1,$$

$$\delta_{k+1} \leq \delta_k,$$

where Hx_k and h define the polyhedral target set C, $\mathbf{1}_{n_h}$ is a $n_h \times 1$ vector of 1's, δ_k is a binary decision variable used to relax the inequality constraint, and $\tau_{\rm lb}(x_0) \in \mathbb{Z}_{\geq 0}$ denotes a known lower bound on the minimum-time; this can be estimated by solving the completely relaxed linear program or through a heuristic procedure where the dynamics are approximated by double integrators.

For $x_k \in C$, $Hx_k \leq h$ is satisfied and $\delta_k = 0$; otherwise, $\delta_k = 1$. The additional constraint $\delta_{k+1} \leq \delta_k$ ensures that once the target set is reached, then the state remains inside the target set for all future time steps. We exploit the lower bound $\tau_{\rm lb}(x_0)$ since this reduces the number of binary integer variables δ_k that need to be solved for, as for any $k < \tau_{\rm lb}(x_0)$, $\delta_k = 1$ in the solution. Note that problem (4.13) is a MILP that can be solved using standard numerical algorithms. We note also that the assumption of the target set being control-invariant can be relaxed but the resulting MILP will be more complicated. We leave the details to future publications.

Proposition 4.2: Suppose the solution to the minimum-time optimal control problem for (4.11)-(4.12) exists for a given x_0. Then for all sufficiently large $N > 0$ and $M > 0$, for the solution sequence to (4.13), $\{u_k^*\}$, it holds that $\tau(x_0, \{u_k^*\}) = \tau_{min}(x_0)$.

Remark 4.3: When solving (4.13) numerically, the initially chosen horizon N may not be sufficiently long to reach the target set. This can be detected if $\delta_N^* = 1$. In such a case, the horizon can be increased, e.g., by a fixed value, $N \leftarrow N + \Delta N$, and the problem can be re-solved.

The open loop solution sequence, $\{u_k^*\}$, of (4.13), determined for the given x_0 on the basis of the linearized model (4.12), if applied to the nonlinear model (4.1), may not lead to a trajectory that reaches the target set due to the model mismatch. To improve the robustness of the solution, the receding horizon control principle is used as in model predictive control. Hence we define a feedback law based on the first move of the solution sequence of (4.13) as

$$u_{MPC}(x_0) = u_0^*, \quad (u_0^* = u_0^*(x_0)). \tag{4.14}$$

Such a solution is referred to as the minimum-time MPC feedback law.

Remark 4.4: In the MPC setting, various warm start strategies can be devised to simplify the numerical implementation. For instance, if a feasible solution existed for a horizon N at a given time instant, a feasible solution should exist, assuming no disturbances or model mismatch, for a horizon of length $N - 1$ at the next time instant. This observation is exploited in our subsequent numerical computations.

Figure 4.3 illustrates the benefits of an MPC solution for a point mass moving on a plane, where the mass position dynamics are described by a pair of discrete-time double integrators for each axis and are subject to the control constraint $u \in U = [-1,\ 1] \times [-1,\ 1]$. A disturbance sequence that is additive to the control input is introduced for each axis which is sampled from the uniform distribution in the interval $[-0.05,\ 0.05]$. As Figure 4.3 shows, the trajectory that results from applying the initial control input sequence open-loop fails to reach the target set due to the perturbing effects of the unmeasured/unmodelled disturbances. However, the closed-loop trajectory with MPC is able to successfully reach the target set.

Remark 4.5: Extensions of the above MILP to the time-dependent case are straight-

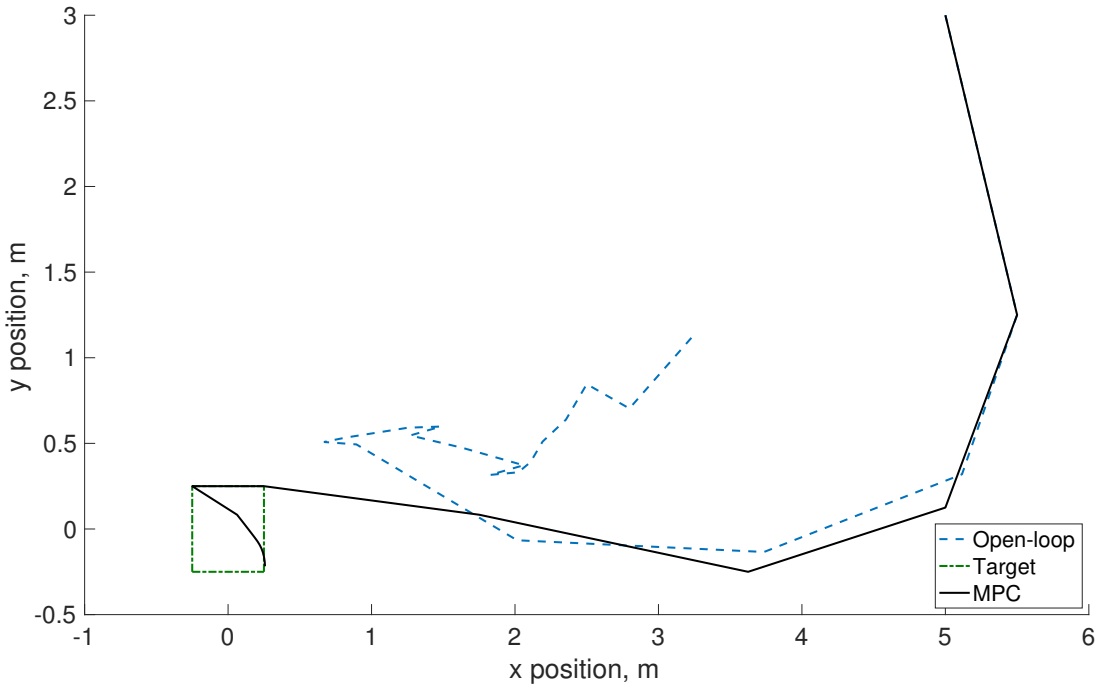

Figure 4.3: Trajectories when executing the initial control sequence open-loop vs re-solving for a new control at every step in the presence of unmodeled disturbances.

forward with A_k, B_k, d_k, H_k, h_k, Γ_k, γ_k, replacing A, B, d, H, h, Γ, γ, respectively.

The minimum-time MPC can be applied to waypoint following problems in a straightforward manner: Given a sequence of waypoints and associated target sets, one commands each target set sequentially to the minimum-time MPC controller until it is reached and then a switch to the next waypoint in the prescribed waypoint sequence is initiated.

4.3 Numerical Simulations

4.3.1 Satellite Attitude Slew with Exclusion Zones

Consider a nonlinear model for the spacecraft attitude dynamics relative to LVLH frame for a spacecraft on a circular orbit (see e.g. [30] and references therein for details). The

equations of motion are given by

$$\begin{bmatrix} \dot{\phi} \\ \dot{\theta} \\ \dot{\psi} \end{bmatrix} = \mathbf{C}_{\phi\theta}^{-1} \left(\begin{bmatrix} \omega_1 \\ \omega_2 \\ \omega_3 \end{bmatrix} + n \begin{bmatrix} c_\theta s_\psi \\ s_\phi s_\theta s_\psi + c_\phi c_\psi \\ c_\phi s_\theta s_\psi - s_\phi c_\psi \end{bmatrix} \right), \tag{4.15}$$

where

$$\mathbf{C}_{\phi\theta}^{-1} = \left(\frac{1}{c_\theta} \right) \begin{bmatrix} c_\theta & s_\phi s_\theta & c_\phi s_\theta \\ 0 & c_\phi c_\theta & -s_\phi c_\theta \\ 0 & s_\phi & c_\phi \end{bmatrix},$$

and

$$\begin{aligned} \dot{\omega}_1 &= J_{23}(\omega_2\omega_3 - 3n^2 c_\phi s_\phi c_\theta^2) + \frac{u_1}{J_1}, \\ \dot{\omega}_2 &= J_{31}(\omega_3\omega_1 + 3n^2 c_\phi c_\theta s_\theta) + \frac{u_2}{J_2}, \\ \dot{\omega}_3 &= J_{12}(\omega_1\omega_2 + 3n^2 s_\phi c_\theta s_\theta) + \frac{u_3}{J_3}, \end{aligned} \tag{4.16}$$

where $J_1 = 20$ kg·m^2, $J_2 = 50$ kg·m^2, $J_3 = 40$ kg·m^2 are principal moments of inertia, $J_{12} := (J_1 - J_2)/J_3$, $J_{31} := (J_3 - J_1)/J_2$, $J_{23} := (J_2 - J_3)/J_1$, and n represents low-Earth orbital mean motion of $2\pi/5400$ sec^{-1}. The three Euler angles (roll ϕ, pitch θ and yaw ψ) represent the orientation of the spacecraft body fixed frame with respect to the LVLH frame. The control inputs are moments u_1, u_2, u_3 about each body fixed axis.

The linearized model about the LVLH frame-resolved equilibrium $x_e = [0, 0, 0, 0, -n, 0]^{\mathrm{T}}$

takes the form,

$$A = \begin{bmatrix} 0 & 0 & n & 1 & 0 & 0 \\ 0 & 0 & 0 & 0 & 1 & 0 \\ -n & 0 & 0 & 0 & 0 & 1 \\ -3n^2 J_{23} & 0 & 0 & 0 & 0 & -nJ_{23} \\ 0 & 3n^2 J_{31} & 0 & 0 & 0 & 0 \\ 0 & 0 & 0 & -nJ_{12} & 0 & 0 \end{bmatrix}, \quad B = \begin{bmatrix} & \mathbf{0}_{3\times 3} & \\ J_1^{-1} & 0 & 0 \\ 0 & J_2^{-1} & 0 \\ 0 & 0 & J_3^{-1} \end{bmatrix}, \quad d = 0. \tag{4.17}$$

We convert the linearized model to discrete-time assuming a zero-order hold [71] and sampling period of $\Delta T = 0.5$ sec.

The closed-loop trajectories generated by the minimum-time MPC when applied to the continuous-time nonlinear spacecraft attitude dynamics model are shown in Figures 4.4 and 4.5. The spacecraft follows a sequence of two waypoints for which the target sets are shown in Figures 4.4 and 4.5 by the rectangular boxes and horizontal dashed lines, respectively. Note that the waypoints and the corresponding target sets are only defined in the roll-pitch-yaw subspace; the angular velocity components are not restricted. The saturation constraints on the control moments are given by $|u_i| \leq 0.2$ Nm, $i = 1, 2, 3$. Random unmeasured disturbance torques sampled from the uniform distribution over the interval $[-0.01,\ 0.01]$ have been added to the control moments about each axis to represent actuation errors. As observed from the simulated trajectories in Figures 4.4-4.6, the minimum-time MPC controller designed on the linearized discrete-time model is able to track the specified waypoints while respecting control constraints even when applied to the full non-linear continuous-time model and when disturbance torques are present. The computations were carried out on a MacBook laptop with a 2.5 GHz processor and 16 GB of memory using Matlab's *intlinprog* command to solve the MILP; the entire trajectory, including tracking both waypoints, was computed in 3.28 seconds.

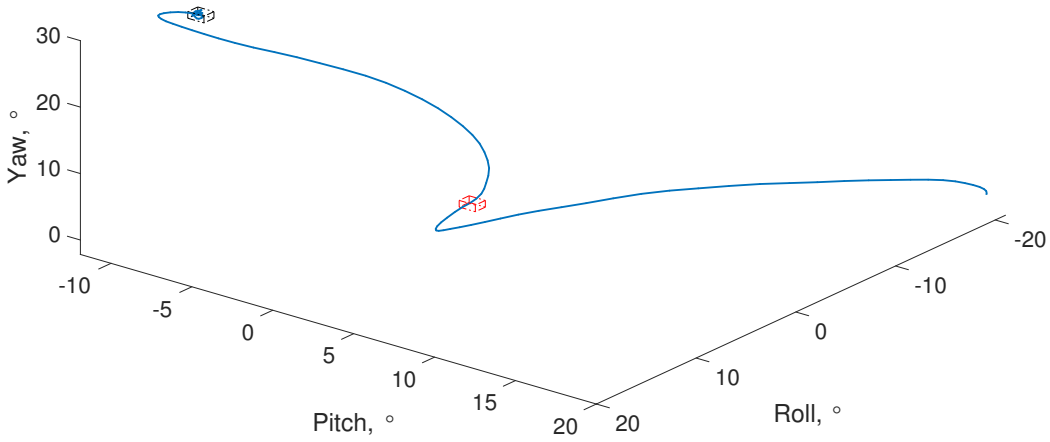

Figure 4.4: Attitude trajectory when controlled by the minimum-time MPC.

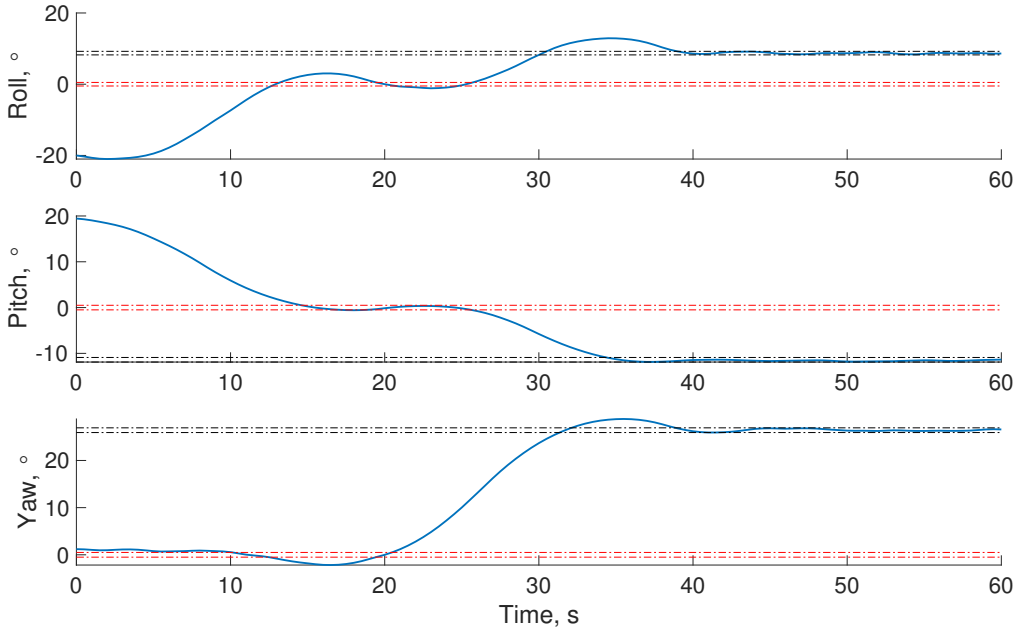

Figure 4.5: Time histories of the roll, pitch and yaw when controlled by the minimum-time MPC.

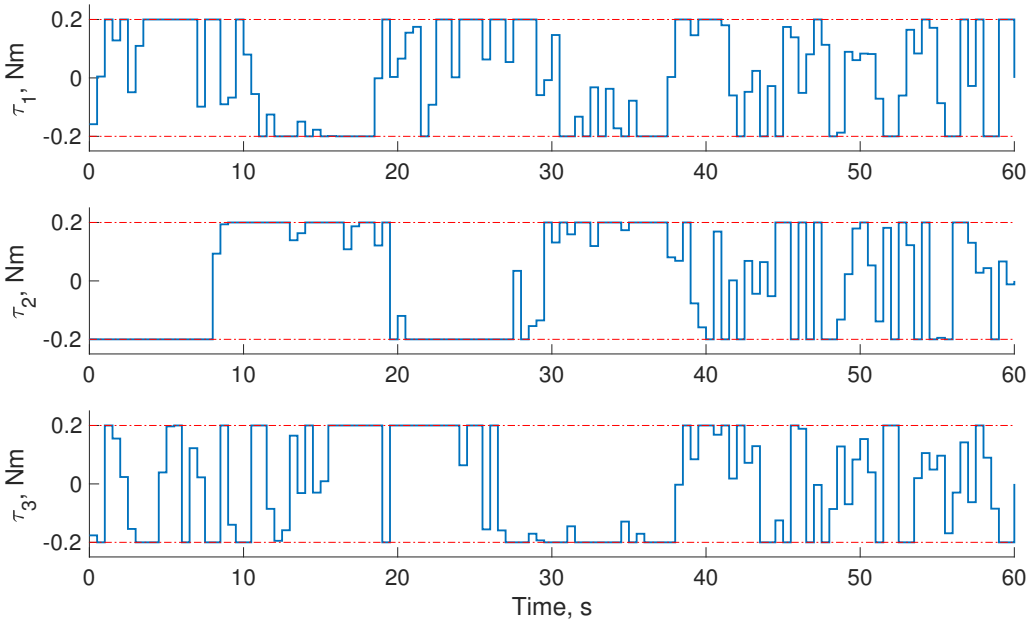

Figure 4.6: Time histories of the torque inputs when controlled by the minimum-time MPC.

4.4 Exclusion Zone Avoidance

The MILP can be augmented by exclusion zone constraints following the approach of [83, 85]. As an example, consider a rectangular exclusion zone avoidance requirement given by $(\phi, \theta, \psi) \notin [-\phi_l, \phi_u] \times [-\theta_l, \theta_u] \times [-\psi_l, \psi_u]$. To handle such an exclusion zone we augment our MILP with extra binary integer variables $\epsilon_{i,k} \in \{0, 1\}$ and constraints,

$$\begin{aligned}
\phi_k &\leq \phi_l + M\epsilon_{1,k}, \\
-\phi_k &\leq -\phi_u + M\epsilon_{2,k}, \\
\theta_k &\leq \theta_l + M\epsilon_{3,k}, \\
-\theta_k &\leq -\theta_u + M\epsilon_{4,k}, \\
\psi_k &\leq \psi_l + M\epsilon_{5,k}, \\
-\psi_k &\leq -\psi_u + M\epsilon_{6,k}, \\
\sum_{i=1}^{6} \epsilon_{i,k} &\leq 5,
\end{aligned} \tag{4.18}$$

where $M > 0$ is sufficiently large. The number of ϵ binary variables at each time step is equal to the number of faces of the exclusion zone polytope, with each $\epsilon = 1$ if the state lies "inside" the corresponding face and $\epsilon = 0$ otherwise. The final inequality ensures that the state remains outside of the exclusion zone, as the constraint is violated if and only if the state lies "inside" of every face simultaneously.

Figures 4.7-4.8 show the closed-loop simulation results with the nonlinear spacecraft attitude dynamics model and the exclusion zone represented by a cube centered at $(-5^\circ, -5^\circ, 5^\circ)$ with side length 5°. The initial attitude is $(-10^\circ, -10^\circ, 10^\circ)$ and the initial angular velocities are zero. The control moments here are limited to 0.1 Nm, and random unmeasured disturbance torques sampled from the uniform distribution over the interval $[-0.01,\ 0.01]$ Nm have been added to the control moments about each axis to represent actuation errors. The minimum-time MPC controller successfully controls the attitude to the waypoint at the origin, and then back to the waypoint corresponding to the initial state. The exclusion zone constraint violation is avoided. We note that when random disturbances are added, some trajectories generated at random may slightly violate the exclusion zone constraints. By slightly inflating these exclusion zones the violation of the original exclusion zone boundaries can be reduced.

In addition, when the exclusion zone is removed and the simulation re-run using identical initial conditions, the trajectory is noticeably different, as seen in Figures 4.9-4.10. In particular, the trajectory intersects the exclusion zone multiple times.

Accommodating additional exclusion zones results in a large increase in the binary decision variable count. The worst-case computation times increase exponentially as the number of these binary variables grows, which impedes the ability to compute the solution online. A mitigating approach used in [83] is to identify exclusion zones that do not lie between the current state and the target state, and discard those binary variables entirely until a new target state is assigned. Such a strategy can reduce the computational effort but requires a priori knowledge of all of the exclusion zones to decide which ones are "far

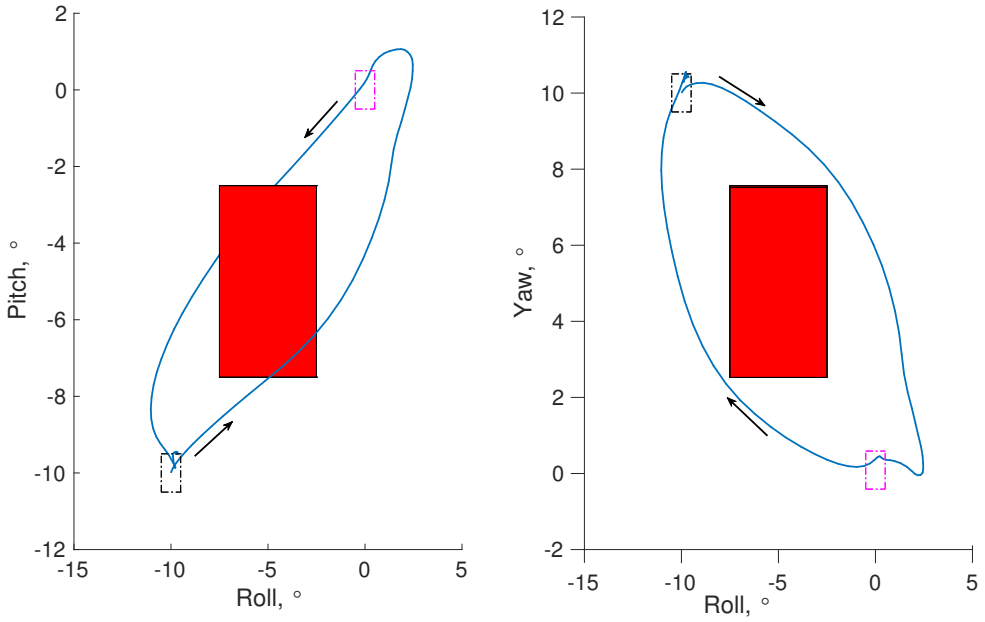

Figure 4.7: Closed-loop spacecraft attitude trajectory with a single exclusion zone. The dashed boxes correspond to the target sets around each waypoint. The solid red box is the exclusion zone.

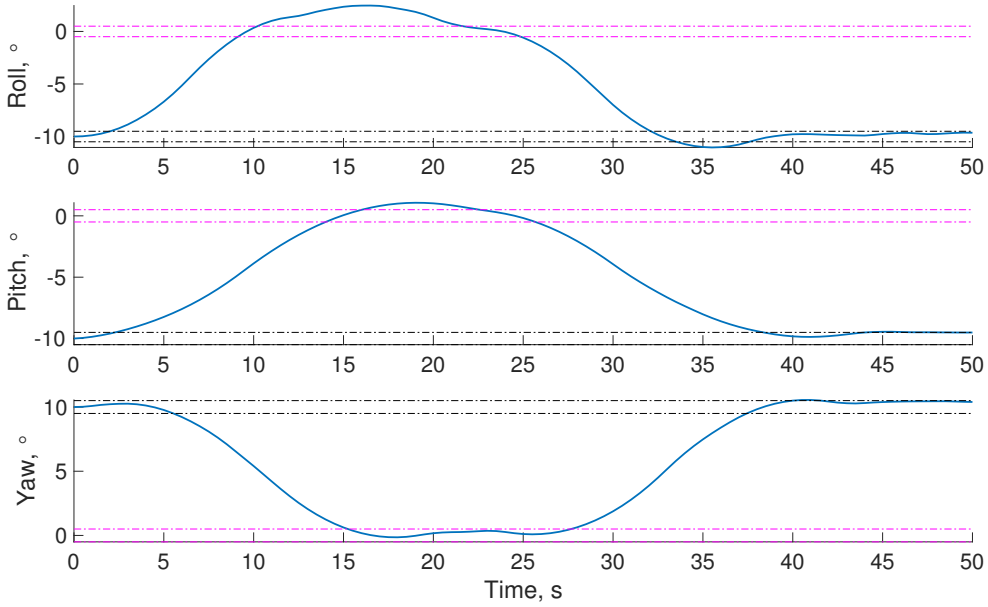

Figure 4.8: Time histories of the roll, pitch and yaw for the closed-loop simulations of the spacecraft attitude trajectory with a single exclusion zone. The dashed lines correspond to target sets.

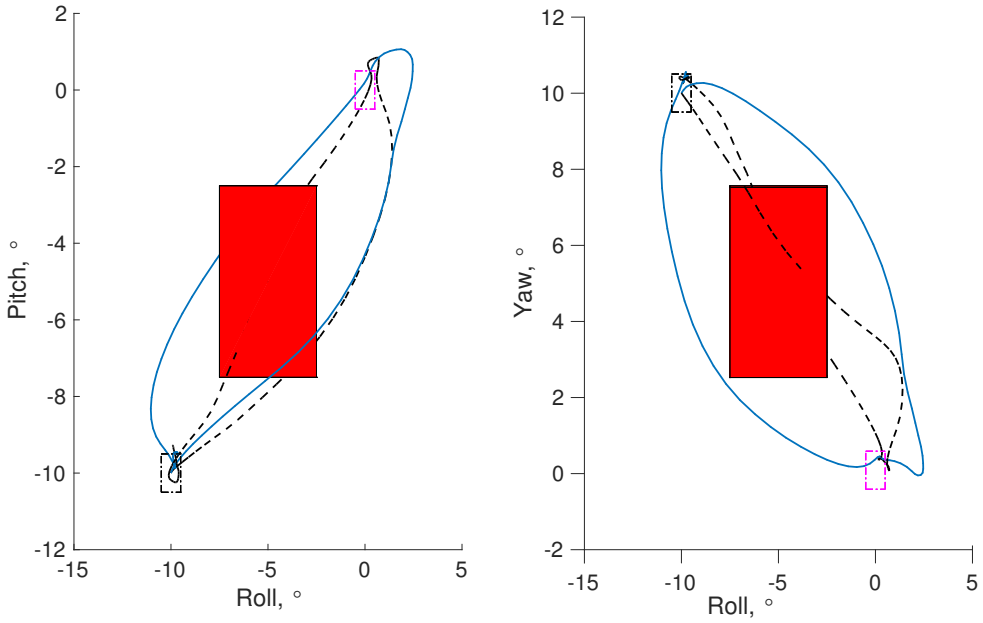

Figure 4.9: Closed-loop spacecraft attitude trajectory with the exclusion zone removed (dashed trajectories). The dashed boxes correspond to the target sets around way points. The solid red box is the exclusion zone.

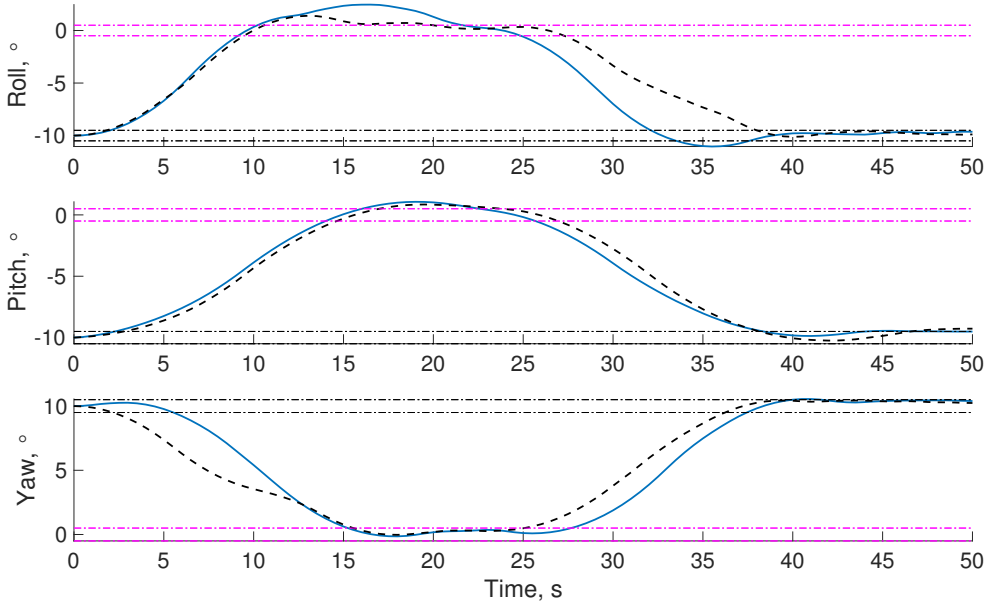

Figure 4.10: Time histories of the roll, pitch and yaw for the closed-loop simulations of the spacecraft attitude trajectory with the exclusion zone removed (dashed). The dashed lines correspond to target sets.

away" on each leg of the trajectory. Other possibilities include replacing a group of zones with their convex hull, reducing the prediction horizon by lengthening the time steps, or adding additional waypoints to allow for a shorter prediction horizon [86].

4.4.1 Satellite Attitude Slew with Flexible Modes

We now consider the application of the minimum-time MPC to a flexible spacecraft. As minimum-time maneuvers for agile satellites can be fairly aggressive, accounting for spacecraft flexibility effects in terms of deflections and loads can be important.

The orientation of the spacecraft frame relative to the reference LVLH frame is prescribed by the roll-pitch-yaw angles ϕ, θ and ψ. The angular velocity vector of the spacecraft frame relative to the reference frame expressed in the spacecraft frame is $\omega = [\omega_1, \omega_2, \omega_3]^{\mathrm{T}}$. The equations of motion [87] are given by (4.15) and

$$\begin{aligned} J\dot{\omega} + \omega^{\times} J\omega + \Delta^{\mathrm{T}}\ddot{\eta} &= \tau_{\mathrm{gg}} + u, \\ \ddot{\eta} + C_d\dot{\eta} + K\eta &= -\Delta\dot{\omega}, \end{aligned} \tag{4.19}$$

where $\eta \in \mathbb{R}^k$ is the vector of modal coordinates of flexible modes, k is the number of flexible modes included in the model, $\Delta \in \mathbb{R}^{k\times 3}$ is the coupling matrix between the rigid body modes and flexible modes, $C_d \in \mathbb{R}^{k\times k}$ is the matrix of damping ratios of the flexible modes, $K \in \mathbb{R}^{k\times k}$ is the stiffness matrix of the flexible modes, $\omega^{\times}$ is the skew-symmetric matrix of angular velocities,

$$\omega^{\times} = \begin{bmatrix} 0 & -\omega_3 & \omega_2 \\ \omega_3 & 0 & -\omega_1 \\ -\omega_2 & \omega_1 & 0 \end{bmatrix},$$

$u \in \mathbb{R}^3$ is the vector of control moments, and

$$\tau_{\text{gg}} = \begin{bmatrix} -3n^2(J_2 - J_3)c_\phi s_\phi c_\theta^2 \\ 3n^2(J_3 - J_1)c_\phi c_\theta s_\theta \\ 3n^2(J_1 - J_2)s_\phi c_\theta s_\theta \end{bmatrix}$$

represents the gravity gradient torque acting on the spacecraft,

From (4.19) it follows that

$$J\dot{\omega} + \omega^\times J\omega - \Delta^{\mathrm{T}}(C_d\dot{\eta} + K\eta + \Delta\dot{\omega}) = \tau_{\text{gg}} + u,$$
$$\ddot{\eta} + C_d\dot{\eta} + K\eta = -\Delta(J^{-1}(-\omega^\times J\omega - \Delta^{\mathrm{T}}\ddot{\eta} + \tau_{\text{gg}} + u)),$$

and

$$\begin{aligned} \dot{\omega} &= (J - \Delta^{\mathrm{T}}\Delta)^{-1}(-\omega^\times J\omega + \Delta^{\mathrm{T}}(C_d\dot{\eta} + K\eta) + \tau_{\text{gg}} + u), \\ \ddot{\eta} &= (\mathbf{I}_k - \Delta J^{-1}\Delta^{\mathrm{T}})^{-1}(-C_d\dot{\eta} - K\eta + \Delta J^{-1}(\omega^\times J\omega - \tau_{\text{gg}} - u)), \end{aligned} \tag{4.20}$$

where $\mathbf{I}_k$ denotes $k \times k$ identity matrix.

To apply minimum-time MPC, we will linearize these equations and then apply a zero-order hold discretization, following the procedure of Section 4.3.1. Note that our states are rigid body states, $(\phi,\ \theta,\ \psi,\ \omega_1,\ \omega_2,\ \omega_3)$, as well as the new flexible mode state variables that we have introduced in this section, $(\eta_1,\ \ldots,\ \eta_k,\ \dot{\eta}_1,\ \ldots,\ \dot{\eta}_k)$.

In the simulation example, we consider $k = 4$ flexible modes, and use the following parameter matrices based on [85, 88]:

$$\Delta = \frac{-1}{\sqrt{10}} \begin{bmatrix} 6.45637 & 1.27814 & 2.15620 \\ -1.25619 & 0.91756 & -1.67264 \\ 1.11687 & 2.48901 & -0.83674 \\ 1.23637 & -2.6581 & -1.12503 \end{bmatrix} \text{ kg}^{1/2} \cdot \text{m},$$

$C_d = \text{diag}(0.0086,\ 0.0190,\ 0.0487,\ 0.1275)$, sec^{-1} and $K = \text{diag}(0.59,\ 1.2184,\ 3.5093,\ 6.5004)$ sec^{-2}.

With four flexible modes, the linearization takes the form

$$\begin{aligned}
\begin{bmatrix} \dot{\omega}_1 \\ \dot{\omega}_2 \\ \dot{\omega}_3 \end{bmatrix} &= (J - \Delta^{\mathrm{T}}\Delta)^{-1} \left(\begin{bmatrix} D & \Delta^{\mathrm{T}}K & \Delta^{\mathrm{T}}C_d \end{bmatrix} x + u \right), \\
\begin{bmatrix} \ddot{\eta}_1 \\ \ddot{\eta}_2 \\ \ddot{\eta}_3 \\ \dot{\eta}_4 \end{bmatrix} &= (\mathbf{I}_4 - \Delta J^{-1}\Delta^{\mathrm{T}})^{-1} \left(\begin{bmatrix} \Delta D & -K & -C_d \end{bmatrix} x - \Delta J^{-1} u \right),
\end{aligned} \tag{4.21}$$

where $x = [\phi, \theta, \psi, \omega_1, \omega_2, \omega_3, \eta_1, \ldots, \eta_4, \dot{\eta}_1, \ldots, \dot{\eta}_4]^{\mathrm{T}}$ and D is given by,

$$D = \begin{bmatrix} -3n^2(J_2 - J_3) & 0 & 0 & 0 & 0 & -n(J_2 - J_3) \\ 0 & 3n^2(J_3 - J_1) & 0 & 0 & 0 & 0 \\ 0 & 0 & 0 & -n(J_1 - J_2) & 0 & 0 \end{bmatrix}.$$

Here, $n = 2\pi/5400$ sec^{-1} represents the mean orbital motion and $J_1 = 150$ kg $\cdot$ m^2, $J_2 = 50$ kg $\cdot$ m^2, $J_3 = 170$ kg $\cdot$ m^2 are the principal moments of inertia.

Note that, particularly in large space vehicles, there may exist many more than four flexible modes to consider; the relatively small number of modes in this example was chosen to maintain clarity of the presentation.

We simulate a rest-to-rest motion trajectory, with an initial attitude of $(\phi, \theta, \psi) = (-30^\circ, -30^\circ, 30^\circ)$ and the angular velocity and flexible mode states taking initial values of 0. The control input torque has a saturation limit of 0.2 N $\cdot$ m, and the flexible modes are constrained to a maximum of 1° kg$^{1/2}$ $\cdot$ m. The results of the simulation are found in Figures 4.11-4.14. The satellite executes the attitude change maneuver in minimum-time

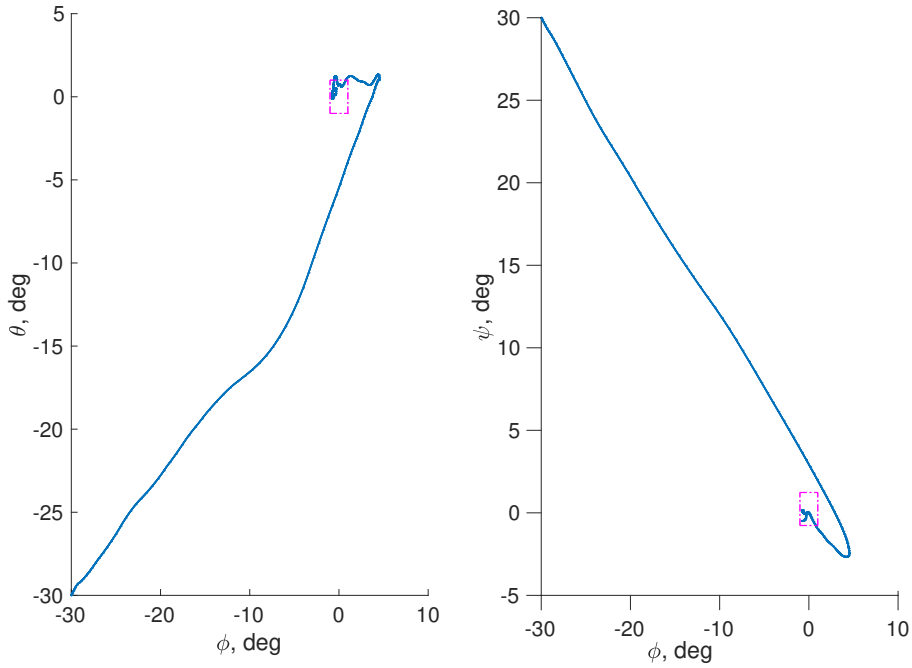

Figure 4.11: Attitude trajectory of flexible spacecraft under the minimum-time MPC controller.

while respecting the constraints on the flexible mode deflection magnitudes.

4.5 Summary

An MPC framework has been considered for minimum-time spacecraft attitude control in presence of exclusion zone constraints. The solution is based on a suitably formulated MILP for the linearized and converted to discrete-time model, and with the additional binary decision variables introduced to track whether the trajectory has reached the target set as well as to avoid entering non-convex exclusion zones. Simulation results based on the nonlinear model of a rigid spacecraft demonstrated that the controller is able to accomplish waypoint tracking and avoid the violation of exclusion zone constraints. The minimum-time MPC framework can be extended to the case of flexible spacecraft where, as demonstrated by our simulation results, the violation of constraints on elastic deflections

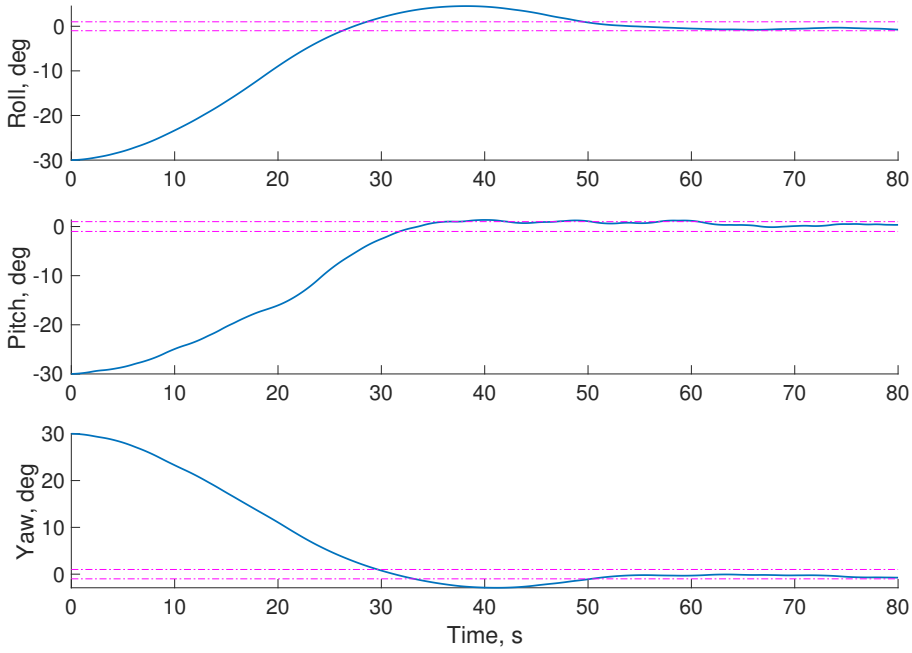

Figure 4.12: Time histories of roll, pitch, and yaw under the minimum-time MPC controller.

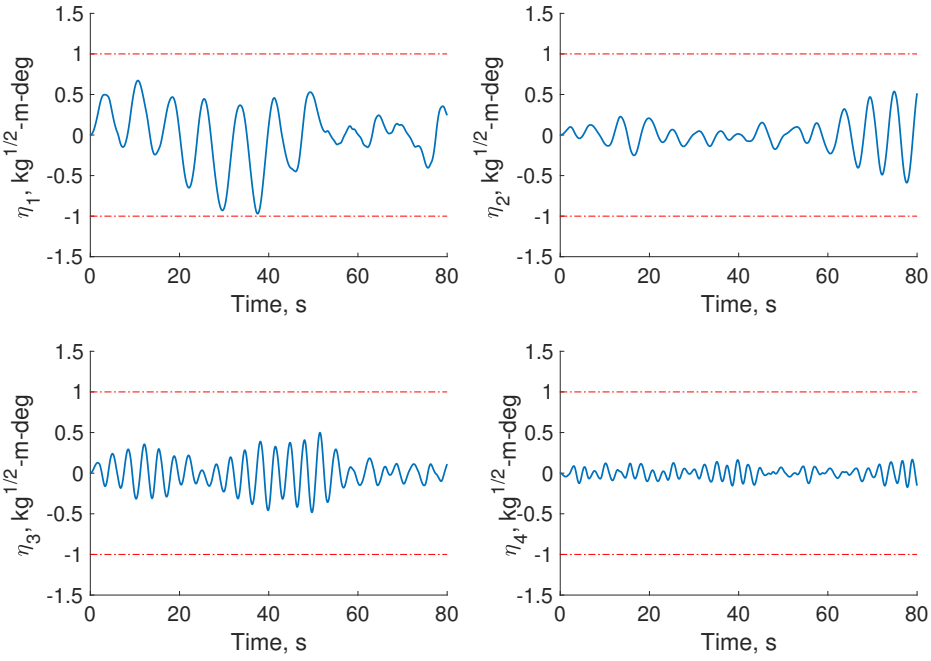

Figure 4.13: Modal coordinates of the flexible spacecraft under the minimum-time MPC controller.

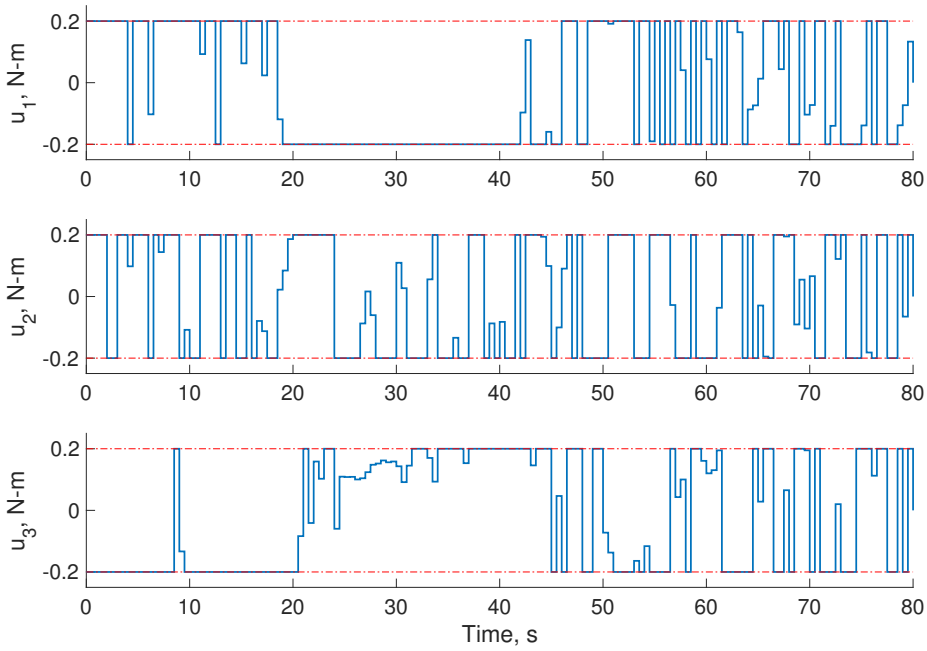

Figure 4.14: Control torque time histories for the flexible spacecraft under the minimum-time MPC controller.

and loads during the maneuvers can be avoided.

CHAPTER 5

Closed-loop Lyapunov Stability with Minimum-time MPC Feedback Laws for Discrete-time Systems

5.1 Motivation

There has been persistent interest in minimum-time MPC where the optimal control input to reach a target state or a target set in minimum-time is recomputed at discrete sampling instances subject to the current state as an initial condition and applied to the system for a period of time before the next re-computation takes place. As in the conventional MPC [73, 74], this process defines a feedback law which, as compared to the open-loop solution, is expected to improve robustness to unmodeled uncertainties and disturbances. The state and control constraints can be handled by including them in the optimization problem formulation and, under the assumption of no model mismatch, recursive feasibility and finite-time convergence are easily achieved.

Minimum-time MPC is motivated in part by applications to attitude control of agile imaging satellites where the time of pointing the spacecraft at a target must be minimized (see, e.g., [72]). Since minimum-time MPC provides finite-time (rather than asymptotic convergence), it is a convenient framework for waypoint following applications [28]. Other potential applications of minimum-time MPC involve systems that must be maneuvered in

finite time, e.g., helicopter ship landing (see, e.g., [89]) or spacecraft docking (see e.g., [90]).

Minimum-time MPC feedback laws can be developed either in continuous time or in discrete-time. The continuous-time setting is closest to the one of optimal control, in fact, minimum-time MPC can be viewed as an algorithmically defined [91] approximation of minimum-time optimal control. Consequently, minimum-time MPC inherits finite-time convergence and certain robustness properties (see, e.g., the discussion in [82]) from minimum-time optimal control. From the computational standpoint, a time re-scaling transformation can be used (see e.g., [80]) and the resulting dynamic optimization problem over a $[0, 1]$ time interval is solved with respect to the discretized (or parameterized) control input and final time, where the final time is a multiplicative parameter in the re-scaled differential equations.

The alternative setting for minimum-time MPC is discrete-time (see e.g., [92, 93]) which has important advantages from the implementation perspective in being able to maintain the fixed update rate for the controller. Computationally, discrete-time minimum-time MPC can be handled through mixed integer optimization [76, 94] and is straightforward to set up. An alternative approach in [95] is based on defining an equivalent objective function penalizing the 1-norm of the state with exponentially increasing weights. This formulation reduces the optimal control problem to a fixed-horizon problem while maintaining the time-optimality and without requiring mixed integer optimization. However, in this formulation, the initial prediction horizon must be chosen to be greater than the a priori unknown minimum-time horizon; this may result in having to repeatedly solve a larger optimal control problem than necessary. The computation of minimum-time MPC laws for piecewise-affine systems using multi-parametric programming is addressed in [96]. In [97], a discrete-time MPC framework is developed for a related time maximization problem of staying within a prescribed target set while counteracting drift.

In this chapter, we consider minimum-time MPC in a discrete-time setting with the

primary focus on achieving finite-time stabilization of a specified equilibrium point (rather than a set as in [98] and references therein). We illustrate with examples that while finite-time attractivity of the equilibrium is easily achievable with minimum-time MPC, Lyapunov stability of the closed-loop system at the equilibrium may not hold due to non-uniqueness of the optimal control sequence.

To recover Lyapunov stability, we propose an approach based on the lexicographic optimization [99–101]. In this approach, a secondary objective function is defined and minimized over the set of solutions that minimize the primary objective function (time-to-go). With the lexicographic approach we demonstrate that Lyapunov stability of the equilibrium is achievable under appropriate and reasonable assumptions.

5.2 Problem Formulation

The setting and properties of minimum-time MPC for a class of nonlinear discrete time systems are reviewed in this section. For completeness, and considering many of the basic facts have been shown for linear systems in the prior literature, we include a short, self-contained treatment along with the associated proofs.

Consider a system with a discrete-time nonlinear model given by

$$x_{k+1} = f(x_k, u_k), \tag{5.1}$$

where $k = 0, 1, 2, \cdots$ designates the time instance, x_k is an n_x-vector state, and u_k is an n_u-vector control.

The control constraints are imposed by specifying

$$u_k \in U \subset \mathbb{R}^{n_u}, \tag{5.2}$$

where the set U is assumed to be compact. The state constraints are given as

$$x_k \in X \subseteq \mathbb{R}^{n_x}. \tag{5.3}$$

Let $D_0 \subset X$ be a non-empty and compact target set. Often in applications, the target is a singleton, i.e., $D_0 = \{0\}$. This assumption will be made in subsequent sections when addressing closed-loop Lyapunov stability but not yet here.

Define a one step feasible set of states,

$$D_1 = \{x \in X : \exists u \in U, \text{ such that } f(x,u) \in D_0\}, \tag{5.4}$$

and, for $k > 1$, a k-step feasible set of states recursively as

$$D_k = \{x \in X : \exists u \in U, \text{ such that } f(x,u) \in D_{k-1}\}. \tag{5.5}$$

It is straightforward to prove that the set D_k consists of states that can be steered to the set D_0 in k steps without violating constraints; note, however, some of the states in D_k could also be steered into D_0 in a different number of steps. Formally, we have the following proposition.

Proposition 5.1: There exists a control sequence $\{u_0, u_1, \cdots, u_{k-1}\} \subset U$, such that $x_1 = f(x_0,u_0) \in X,\ x_2 = f(x_1,u_1) \in X, \cdots, x_k = f(x_{k-1},u_{k-1}) \in D_0$ if and only if $x_0 \in D_k$.

Proof: Suppose $x_0 \in D_k$. By definition of D_k, there exists $u_0 \in U$ such that $x_1 = f(x_0,u_0) \in D_{k-1} \subset X$. By definition of D_{k-1}, there exists $u_1 \in U$ such that $x_2 = f(x_1,u_1) \in D_{k-2} \subset X$. We can continue this process till u_{k-1} is found such that $x_k = f(x_{k-1},u_{k-1}) \in D_0$. The required sequence is $\{u_0, u_1, \cdots, u_{k-1}\}$. Suppose now that there exists a control sequence, $\{u_0, u_1, \cdots, u_{k-1}\} \subset U$, such that $x_1 = f(x_0,u_0) \in X,\ x_2 = f(x_1,u_1) \in X, \cdots, x_{k-1} = f(x_{k-2},u_{k-2}) \in X,\ x_k = f(x_{k-1},u_{k-1}) \in D_0$. Then $x_{k-1} \in$

D_1, $x_{k-2} \in D_2$, and so on, and finally, $x_0 \in D_k$. ■

Proposition 5.2: Suppose for all $x \in D_0$ there exists $u^0(x)$ such that $f(x, u^0(x)) \in D_0$. Then the sets D_k are nested, i.e., $D_k \subseteq D_{k+1}$.

Proof: The proof is by induction. By Proposition 5.1, for $x_0 \in D_k$, there exists a control sequence $\{u_0, u_1, \cdots, u_{k-1}\} \subset U$, such that $x_k \in D_0$ and $\{x_0, \cdots, x_k\} \subset X$. Let $u_k = u^0(x_0)$, and apply the control sequence, $\{u_0, u_1, \cdots, u_{k-1}, u_k\}$ to the system with the initial condition x_0. Then, $x_{k+1} = f(x_k, u_k) \in D_0$ and by Proposition 5.1, $x_0 \in D_{k+1}$. ■

Proposition 5.3: If the vector function f in (5.1) is continuous in both arguments ($f \in C(\mathbb{R}^{n_x} \times \mathbb{R}^{n_u} \to \mathbb{R}^{n_x})$) and X is closed, then the set D_k is closed for any k.

Proof: The proof is by induction. The set D_0 is compact and hence closed. Assume D_{k-1} is closed, $k \geq 1$. To show that D_k is closed, suppose there exists a sequence $\{x_j\} \subset D_k$, $x_j \to x^*$ as $j \to \infty$ and either (a) $x^* \notin X$ or (b) $f(x^*, u) \notin D_{k-1}$ for any $u \in U$. Since X is closed, (a) is not possible, hence we consider the possibility (b). Note that corresponding to each x_j, there exists $u_j \in U$ such that $f(x_j, u_j) \in D_{k-1}$. Since U is compact, from the sequence $\{u_j\}$ we can extract a convergent subsequence to some $u^* \in U$. Without loss of generality, assume that the whole sequence $\{u_j\}$ is convergent to u^* and the corresponding $\{x_j\}$ is convergent to x^*. Since f is continuous, $f(x_j, u_j) \to f(x^*, u^*) \notin D_{k-1}$. However, as $f(x_j, u_j) \in D_{k-1}$ and D_{k-1} is closed, this is a contradiction. ■

Note that the sets D_k may not be bounded (i.e., compact) without additional assumptions. For instance, consider the case for D_1 when $n_x = n_u = 1$, $D_0 = 0$, $X = \mathbb{R}$, $U = [-2, 2]$ and $f(x, u) = (e^{-x} - 1) + u$. In this case, $[0, +\infty[\subset D_1$ and D_1 is unbounded. To prevent D_k from being unbounded, the function f must grow unbounded as $x \to \infty$.

Definition 5.1: A vector function $f(x, u)$ is *coercive* in x if for any $\epsilon > 0$ there exists $\delta > 0$ such that $\|x\| > \delta$ implies $\|f(x, u)\| > \epsilon$ for all $u \in U$.

Proposition 5.4: If the assumptions of Proposition 5.3 hold and f is coercive in x, then the set D_k is compact.

Proof: The proof is by induction. Closeness has already been proven in Proposition

5.3, and we need to show boundness. The set D_0 is compact and hence bounded. Suppose D_{k-1} is compact (and hence bounded) for some $k \geq 1$, and suppose, contrary to what we need to prove, that D_k is unbounded. This means that there exists a sequence $\{x_j\}$ such that $\|x_j\| \to \infty$ and the corresponding sequence $\{u_j\}$ such that $f(x_j, u_j) \in D_{k-1}$. Since D_{k-1} is compact, $\|f(x_j, u_j)\|$ remains bounded as $x_j \to \infty$, which contradicts the coercitivity property $\|f\| > \epsilon$ in Definition 5.1. ■

Proposition 5.5: Suppose f is affine, of the form, $f(x, u) = L + Ax + Bu$, U is convex, X is convex, and D_0 is non-empty and convex. Then D_k is either empty or convex.

Proof: The proof is by induction. The set D_0 is non-empty and convex by the assumption made. If D_{k-1} is empty, then D_k is empty. Assume D_{k-1} is non-empty and convex and let $x^1, x^2 \in D_k \subset X$. Then there exist $u^1,\ u^2 \in U$ such that $f(x^1, u^1) \in D_{k-1} \subset X$ and $f(x^2, u^2) \in D_{k-1} \subset X$. Since f is an affine function $f(\lambda x^1 + (1-\lambda)x^2, \lambda u^1 + (1-\lambda)u^2) = \lambda f(x^1, u^1) + (1-\lambda) f(x^2, u^2) \in D_{k-1}$ by convexity of D_{k-1}, where $0 \leq \lambda \leq 1$. Since X is convex, $\lambda x^1 + (1-\lambda)x^2 \in X$. Thus $\lambda x^1 + (1-\lambda)x^2 \in D_k$ for $0 \leq \lambda \leq 1$. ■

We are now ready to define the minimum-time MPC for discrete-time nonlinear systems.

Definition 5.2: For an initial state x_0 and a given control sequence, $\{u_k\}$, the time-to-go τ is defined as

$$\tau(x_0, \{u_k\}) = \min\{i \in \mathbb{Z}_{\geq 0} |\ x_i \in D_0\}, \tag{5.6}$$

where $\{x_k\}$ is the corresponding to $\{u_k\}$ state sequence that satisfies (5.1), i.e., $x_{k+1} = f(x_k, u_k)$. In case no integer i satisfying (5.6) exists, $\tau(x_0, \{u_k\}) = +\infty$.

The minimum-time MPC problem for $x_0 \in X \setminus D_0$ is posed as follows:

$$\begin{aligned} &\text{Minimize } \tau(x_0, \{u_k\}) \text{ subject to } u_i \in U,\ x_i \in X, \\ &x_{i+1} = f(x_i, u_i),\ i = 0, \cdots, \tau(x_0, \{u_k\}). \end{aligned} \tag{5.7}$$

Let

$$\bar{D}_\infty = \bigcup_{k=0}^{\infty} D_k. \tag{5.8}$$

Now for $x_0 \in \bar{D}_\infty \setminus D_0$, let k^* be the smallest integer for which $x_0 \in D_{k^*}$, define

$$\tau^*(x_0) = k^*, \tag{5.9}$$

and select *any* minimum-time control sequence, $\{u_0^*, \cdots, u_{k-1}^*\}$. Define an MPC feedback law by the first action of this optimal control sequence,

$$u_{\text{MPC}}(x_0) = u_0^*. \tag{5.10}$$

Note that as the minimum-time control sequence may not be unique, different selections of the control sequence could lead to different MPC feedback laws. However, for any selection, the closed-loop trajectories for $x_0 \in \bar{D}_\infty$ converge to D_0 in finite-time.

Theorem 5.1: For any $x_0 \in \bar{D}_\infty \setminus D_0$, there exists an integer $k^* \geq 1$ such that closed-loop trajectories under the MPC feedback law (5.10) satisfy $x_k \in X$, $k = 0, \cdots, k^*$, $u_k \in U$, $k = 0, \cdots, k^* - 1$, $x_k \in D_{k^*-k}$, $k = 0, \cdots, k^* - 1$, and $x_{k^*} \in D_0$.

Proof: Since $x_0 \in \bar{D}_\infty \setminus D_0$ there exists the smallest integer $k^* \geq 1$ such that $x_0 \in D_{k^*}$. By Proposition 5.1, there exists a feasible control sequence steering the state trajectory into D_0 which is of minimum possible length, k^*. Let an optimal control sequence of the same length which defines the MPC law (5.10) be $\{u_0^*, \cdots u_{k^*-1}^*\}$. Then for $x_1^* = f(x_0, u_0^*)$, the sequence $\{u_1^*, \cdots u_{k^*-1}^*\}$ is feasible and steers the state into D_0 in $k^* - 1$ steps; hence by Proposition 5.1, $x_1^* \in D_{k^*-1} \setminus D_0$. Continuing this argument, with x_0 replaced by x_1^* and so on, it follows that $x_k \in D_{k^*-k}$, $k = 0, \cdots, k^* - 1$, and $x_{k^*} \in D_0$. ■

Thus any MPC feedback law defined according to (5.10) guarantees finite-time convergence into D_0 with the basin of attraction given by $\bar{D}_\infty$.

Furthermore, if there exists a terminal control law, $u^0(x)$, which makes D_0 invariant,

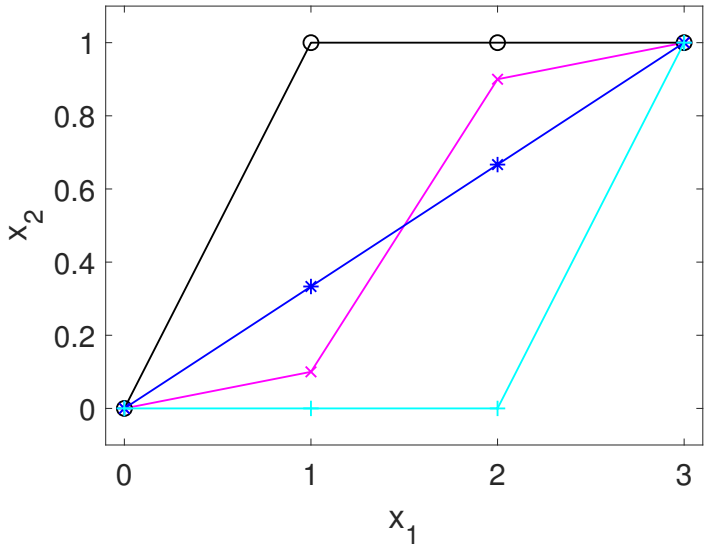

Figure 5.1: Minimum-time state trajectories for (5.12) on the phase plane.

i.e., $f(x, u^0(x)) \in D_0$ for any $x \in D_0$, then the switching dual mode feedback law,

$$u = \begin{cases} u_{\text{MPC}}(x) & \text{if } x \in \bar{D}_\infty \setminus D_0, \\ u^0(x) & \text{if } x \in D_0, \end{cases} \tag{5.11}$$

makes the set D_0 a finite-time attractor for the closed-loop trajectories with the basin of attraction given by $\bar{D}_\infty$.

As a simple illustration, consider a discrete-time system representing two scalar integrators with the model,

$$x_{k+1} = \begin{bmatrix} 1 & 0 \\ 0 & 1 \end{bmatrix} x_k + \begin{bmatrix} 1 & 0 \\ 0 & 1 \end{bmatrix} u_k, \; x_0 = \begin{bmatrix} 3 \\ 1 \end{bmatrix}, \tag{5.12}$$

and let $D_0 = 0$, $U = [-1, 1] \times [-1, 1]$, and $X = \mathbb{R}^2$. Then $x_0 \in D_3$ and there are infinitely-many feasible control sequences and corresponding state trajectories which result in $x_3 \in D_0$, see examples in Figures 5.1 and 5.2. Note that if $x_{1,0} = x_{2,0}$, then the minimum-time state trajectory and control sequences would be unique, but the set of such

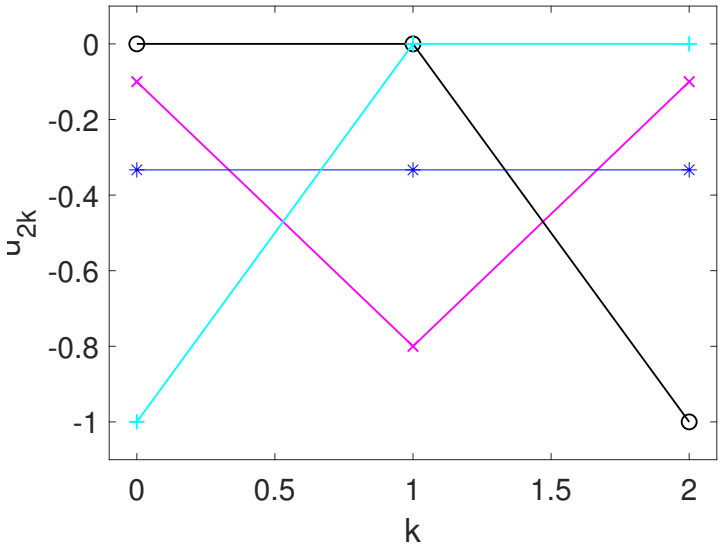

Figure 5.2: Minimum-time control sequences for (5.12) for the second input channel. The minimum-time sequence for the first input channel is $\{-1, -1, -1\}$.

initial conditions has measure zero. The implications of the non-uniqueness are discussed next.

5.3 Lexicographic Minimum-Time Control and Lyapunov Stability

We first construct an example that demonstrates lack of Lyapunov stability for the Minimum-time MPC. Consider the case $D_0 = 0$, $f(0,0) = 0$, and the origin is the target equilibrium which is made invariant with $u^o(x) = 0$.

Consider (5.1) with $f(x,u) = Ax + Bu$,

$$A = \begin{bmatrix} 0 & 0 & 0 \\ 0 & 1 & 0 \\ 1 & 0 & 0 \end{bmatrix}, \; B = \begin{bmatrix} 1 & 0 \\ 0 & 1 \\ 0 & 0 \end{bmatrix}. \tag{5.13}$$

Let $x_0 = [x_{01}, x_{02}, x_{03}]^{\mathrm{T}}$, $u_0 = [u_{01}, u_{02}]^{\mathrm{T}}$, and $u_1 = [u_{11}, u_{12}]^{\mathrm{T}}$. Then,

$$x_1 = \begin{bmatrix} u_{01} \\ x_{02} + u_{02} \\ x_{01} \end{bmatrix}, \quad x_2 = \begin{bmatrix} u_{11} \\ x_{02} + u_{02} + u_{12} \\ u_{01} \end{bmatrix}. \tag{5.14}$$

Consider $x_0 = [\delta, \delta, 0]^{\mathrm{T}}$ (i.e., $x_{01} = x_{02} = \delta,\ x_{03} = 0$), where $\delta \neq 0$. The minimum-time to the origin for such x_0 is $\tau^*(x_0) = 2$ and minimum-time control sequences are $\{u_0,\ u_1\}$ with $u_0 = [0,\ \alpha - \delta]^{\mathrm{T}}$, $u_1 = [0, -\alpha]^{\mathrm{T}}$, where α can be arbitrary as long as control constraints are satisfied. For instance, if the control constraints are $\|u\|_\infty \leq 1$, then $|\alpha - \delta| \leq 1$ and $|-\alpha| \leq 1$, or, $-1 + \delta \leq \alpha \leq 1 + \delta$ and $-1 \leq \alpha \leq 1$.

The minimum-time control sequence could be non-unique. The minimum-time MPC feedback law at x_0 uses the first move, $u_0 = [0,\ \alpha - \delta]^{\mathrm{T}}$, resulting in $x_1 = [0,\ \alpha,\ \delta]^{\mathrm{T}}$. Now $\tau^*(x_1) = 1$ and $u_1 = \tilde{u}_1 = [\tilde{u}_{11},\ \tilde{u}_{12}]^{\mathrm{T}}$ leads to $x_2 = [\tilde{u}_{11},\ \alpha + \tilde{u}_{12}, 0]^{\mathrm{T}}$. Hence, the length 1 sequence that brings x_1 to the origin is $\tilde{u}_1 = [0, -\alpha]^{\mathrm{T}}$ and hence $[0, -\alpha]^{\mathrm{T}}$ would be assigned/computed for the MPC feedback law at x_1. Clearly, then $x_2 = [0,\ 0,\ 0]^{\mathrm{T}}$. Note that $\|x_1\|_\infty \geq \alpha$ no matter how small $\delta \neq 0$ is chosen. We conclude that even though the origin is finite-time attractive under the MPC feedback law, it is not Lyapunov stable.

Note also that in this case, even for a control set U that is both compact and convex, D_1 and D_2 are unbounded, as any initial condition of the form $[0,\ 0,\ \delta]^{\mathrm{T}},\ \delta \neq 0$ lies in D_1 and any initial condition of the form $[\delta_1,\ 0, \delta_2]^{\mathrm{T}},\ \delta_i \neq 0$ lies in D_2.

Consider now another example,

$$A = \begin{bmatrix} 1 & 1 \\ 0 & 1 \end{bmatrix}, \quad B = \begin{bmatrix} 0 \\ 1 \end{bmatrix}, \quad x_0 = \begin{bmatrix} x_{01} \\ x_{02} \end{bmatrix}. \tag{5.15}$$

Then, $x_1 = [x_{01} + x_{02},\ u_0 + x_{02}]^{\mathrm{T}}$, $x_2 = [u_0 + x_{01} + 2x_{02},\ u_0 + u_1 + x_{02}]^{\mathrm{T}}$. Absent control constraints, $\tau^*(x_0) = 2$ for almost all x_0; consider an $x_0 = [x_{01}, x_{02}]^{\mathrm{T}}$ that is small enough

in magnitude that control constraints are inactive, and define

$$\begin{aligned} u_0 &= -x_{01} - 2x_{02}, \\ u_1 &= -u_0 - x_{02} = x_{01} + 2x_{02} - x_{02} = x_{01} + x_{02}. \end{aligned} \tag{5.16}$$

Note that the sequence that brings the state to the origin in two moves,

$$\{u_0,\ u_1\} = \{-x_{01} - 2x_{02},\ x_{01} + x_{02}\}, \tag{5.17}$$

is unique. For x_0, the MPC feedback law uses $-x_{01} - 2x_{02}$, resulting in $x_1 = [x_{01} + x_{02},\ -x_{01} - x_{02}]^{\mathrm{T}}$. Now $\tau^*(x_1) = 1$ and we look for a length 1 control sequence $\{\tilde{u}_1\}$ that brings the state to the origin:

$$x_2 = \begin{bmatrix} 1 & 1 \\ 0 & 1 \end{bmatrix} \begin{bmatrix} x_{01} + x_{02} \\ -x_{01} - x_{02} \end{bmatrix} + \begin{bmatrix} 0 \\ \tilde{u}_1 \end{bmatrix} = \begin{bmatrix} 0 \\ -x_{01} - x_{02} + \tilde{u}_1 \end{bmatrix}. \tag{5.18}$$

Hence, at time instant $k = 1$, the MPC feedback law would use $\tilde{u}_1 = x_{01} + x_{02}$, resulting in $x_2 = 0$. Based on the expression for x_1, the origin of the closed loop system under MPC feedback law is both Lyapunov stable and finite-time attractive.

Based on the above examples, it appears that non-uniqueness of the optimal control sequence can lead to a discontinuous control action (such as $u_0 = [0,\ \alpha - \delta]^{\mathrm{T}}$ where α does not depend on δ in our example) and loss of Lyapunov stability. For such cases, a lexicographic minimum-time optimal control approach is proposed.

Suppose $x_0 \in D_n$, where $n = \tau^*(x_0) \geq 1$ is the minimum discrete-time to reach the origin. Suppose the system model is of the form (5.1) with constraints (5.2), (5.3), where the function f is continuous, $0 \in \text{int}(U)$, $0 \in \text{int}(X)$ and $f(0,0) = 0$. Let $\mathcal{U}_n =$

$[u_0^{\mathrm{T}}, \cdots, u_{n-1}^{\mathrm{T}}]^{\mathrm{T}} \in \mathbb{R}^{n_u \times n}$, and consider the optimization problem (where n is fixed),

$$\begin{aligned} \min_{\mathcal{U}_n} \quad & \|\mathcal{U}_n\|_2^2, \\ \text{subj to.:} \ & x_n = 0, \\ & x_{k+1} = f(x_k, u_k), \ k = 0, 1, \cdots, n-1, \\ & x_k \in X, \ k = 1, 2, \cdots, n, \\ & u_k \in U, \ k = 0, 1, \cdots, n-1. \end{aligned} \tag{5.19}$$

The optimization problem picks the minimum-norm control sequence to reduce the cumulative control effort, in the case the minimum-time control sequence is non-unique.

In lexicographic optimization, there are two or more objectives with different priorities. In our case, the primary objective is to minimize n, and the secondary objective is to minimize the norm of the control sequence.

Define,

$$u_{MPC}(x_0) = \begin{cases} 0, & \text{if } x_0 \in D_0 = \{0\} \\ \mathcal{U}_{n,0}^*, & \text{if } x_0 \in D_n, \ \tau^*(x_0) = D_n, \end{cases} \tag{5.20}$$

where $n = 1, 2, \cdots, \mathcal{U}_{n,0}^*$ is the first control input given by the solution, $\mathcal{U}_n^*$, to (5.19). Note that if f is affine and X and U are convex, such a solution is unique.

Before giving a more general result, we consider the application of the lexicographic optimization to the previous example where, due to non-uniqueness of the optimal control, a control selection can be made that lacks Lyapunov stability. In revisiting this example, the assumption that control constraints are satisfied at each step by the optimal control sequence is carried forward.

We have that

$$x_0 \in D_1 \setminus D_0 \Rightarrow x_1 = \begin{bmatrix} u_{01} \\ x_{02} + u_{02} \\ 0 \end{bmatrix} \Rightarrow u_0^* = \begin{bmatrix} 0 \\ -x_{02} \end{bmatrix}. \tag{5.21}$$

For $x_0 \in D_2$, $\tau^*(x_0) = 2$, the lexicographic optimization takes the form:

$$\begin{aligned} &\min\ u_{02}^2 + u_{12}^2, \\ &\text{s.t. } x_{02} + u_{02} + u_{12} = 0. \end{aligned} \tag{5.22}$$

To solve this problem, we use the Karush-Kuhn-Tucker (KKT) conditions [102], which are both necessary and sufficient since the problem is convex.

Let $\mathcal{L} = u_{02}^2 + u_{12}^2 + \lambda(x_{02} + u_{02} + u_{12})$ be the Lagrangian. Then, the stationarity conditions lead to:

$$\begin{aligned} 2u_{02} + \lambda = 0, \\ 2u_{12} + \lambda = 0, \end{aligned} \tag{5.23}$$

with solution $u_{02} = u_{12} = -0.5\lambda$. Then, $x_{02} + u_{02} + u_{12} = 0$ implies that $\lambda = x_{02}$, and the first move is defined by $u_0^* = [u_{01}^*,\ u_{02}^*]^{\mathrm{T}} = [0, -0.5x_{02}]^{\mathrm{T}}$. Now, the lexicographic MPC

feedback law is defined by:

$$u_{\mathrm{MPC}}(x_0) = \begin{cases} 0, \text{ if } x \in D_0, \\ \begin{bmatrix} 0 \\ -x_{02} \end{bmatrix}, \text{ if } x \in D_1,\ \tau^*(x_0) = 1, \\ \begin{bmatrix} 0 \\ -0.5x_{02} \end{bmatrix}, \text{ if } x \in D_2,\ \tau^*(x_0) = 2. \end{cases} \tag{5.24}$$

Note that u_{MPC} is not continuous at $x_0 \in D_1$, i.e., the origin; however, it is continuous at $x_0 = 0$. Hence for all $\epsilon > 0$, there exists $\delta > 0$ such that $\|x_0\| \leq \delta$ implies $\|u_{\mathrm{MPC}}(x_0)\| \leq \epsilon$. Further note that for $x_0 \in D_1,\ \tau^*(x_0) = 1$ or for $x_0 \in D_2,\ \tau^*(x_0) = 2$, u_{MPC} is a linear function of x_0.

Consider a closed-loop trajectory emanating from $x_0 \in D_2$ under the MPC feedback law:

$$x_0 \in D_2,\ x_1 = \begin{bmatrix} 0 \\ 0.5x_{02} \\ x_{01} \end{bmatrix},\ x_2 = \begin{bmatrix} 0 \\ 0 \\ 0 \end{bmatrix},\ x_3 = x_4 = \cdots = \begin{bmatrix} 0 \\ 0 \\ 0 \end{bmatrix}. \tag{5.25}$$

Consider now a closed-loop trajectory emanating from $x_0 \in D_1$ under the MPC feedback law:

$$x_0 \in D_1,\ x_1 = \begin{bmatrix} 0 \\ 0 \\ 0 \end{bmatrix},\ x_2 = x_3 = \cdots = \begin{bmatrix} 0 \\ 0 \\ 0 \end{bmatrix}. \tag{5.26}$$

Finally, $x_0 \in D_0,\ x_1 = x_2 = x_3 = \cdots = [0,\ 0,\ 0]^{\mathrm{T}}$.

By inspection, it is clear that the closed-loop system under lexicographic minimum-time MPC feedback law is Lyapunov stable at the origin. Indeed, given $\epsilon > 0$, for $\|x_0\| \leq$

0.5ϵ, it follows that $\|x_k\| \leq \epsilon$ for all $k \geq 0$.

We are now ready to generalize from this example.

Assumption (5.A1): There exists $n^* \in \mathbb{Z}_{\geq 0}$ such that $0 \in \text{int}(\bar{D}_{n^*})$, $\bar{D}_{n^*} = \bigcup_{k=0}^{n^*} D_k$, and the feedback law, u_{MPC}, defined by (5.20), is continuous at the origin.

Theorem 5.2: Under the above assumptions including (A1), the origin is a Lyapunov stable equilibrium for the closed-loop system with the MPC feedback law.

Sketch of the Proof: Since $0 \in \text{int}(\bar{D}_{n^*})$, for all x_0 in a sufficiently small neighborhood $S \subset \bar{D}_{n^*}$ of the origin, u_{MPC} is defined. Consider $x_0 \in S$, then $x_0 \in D_n$ for some n, $0 \leq n \leq n^*$. The state sequence resulting from x_0 under the MPC feedback law is of the form

$$\begin{aligned} x_1 &= f(x_0, u_{\text{MPC}}(x_0)), \\ x_2 &= f(x_1, u_{\text{MPC}}(x_1)), \\ &\vdots \\ x_{n-1} &= f(x_{n-2}, u_{\text{MPC}}(x_{n-2})), \\ x_n &= 0, \\ x_k &= 0, \ k > n. \end{aligned} \tag{5.27}$$

By (5.A1), continuity of f, and properties of MPC feedback law (Theorem 5.1), we conclude that $x_k \in \bar{D}_{n^*}$, $k \geq 0$, and can be made arbitrarily small in norm by selecting x_0 sufficiently small in norm. ■

Consider now the case when $f(x,u) = Ax + Bu$, $0 \in \text{int}(U)$, $0 \in \text{int}(X)$. Let $x_0 \in D_n$ and $n = \tau^*(x_0)$. Note that $x_n = A^n x_0 + [B \ AB \ \cdots \ A^{n-1}B]\mathcal{U}_n = L_n x_0 + G_n \mathcal{U}_n$. Consider optimization problem (5.19) without the state and control constraints:

$$\begin{aligned} \|\mathcal{U}_n\|_2^2 &\to \min, \\ L_n x_0 + G_n \mathcal{U}_n &= 0. \end{aligned} \tag{5.28}$$

Since $x_0 \in D_n$, (5.28) has a feasible solution $\bar{\mathcal{U}}_n$. As the set $\{\mathcal{U}_n |\ L_n x_0 + G_n \mathcal{U}_n = 0\} \cap \{\mathcal{U}_n |\ \|\mathcal{U}_n\|_2^2 \leq \|\bar{\mathcal{U}}_n\|_2^2\}$ is compact, by a corollary to the Weierstrass theorem a minimizer exists for this problem. Since the objective function of (5.28) is strictly convex and the optimization is over a convex set defined by affine constraints, the minimizer in (5.28) is unique and KKT conditions are both necessary and sufficient.

Let us analyze the KKT conditions: The Lagrangian is given by

$$\mathcal{L} = \|\mathcal{U}_n\|_2^2 + \lambda^{\mathrm{T}}(L_n x_0 + G_n \mathcal{U}_n), \tag{5.29}$$

where λ is the vector of Lagrange multipliers of the same dimension as x. The KKT conditions (stationarity and equality constraints) are:

$$\begin{aligned} 2\mathcal{U}_n + G_n^{\mathrm{T}} \lambda = 0, \\ L_n x_0 + G_n \mathcal{U}_n = 0. \end{aligned} \tag{5.30}$$

Note that (5.30) is a system of linear algebraic equations. System (5.30) has a unique solution, and the solution mapping $x_0 \rightarrow (\mathcal{U}_n^*,\ \lambda^*)$ is linear. Indeed, if $\mathcal{U}_n^1,\ \mathcal{U}_n^2, \lambda^1,\ \lambda^2$ are solutions for x_0^1 and x_0^2 respectively, then $q_1\mathcal{U}_n^1 + q_2\mathcal{U}_n^2$, $q_1\lambda^1 + q_2\lambda^2$ satisfy (5.30) if $q_1 x_0^1 + q_2 x_0^2$ replaces x_0 in (5.30). Thus,

$$\mathcal{U}_n^* = \Sigma_n x_0, \tag{5.31}$$

for some matrix Σ_n.

Note that if x_0 is sufficiently close to the origin, then the solution (5.31) of (5.28) satisfies the state and control constraints as $0 \in \text{int}(X)$, $0 \in \text{int}(U)$. Hence, (5.31) is also the solution to (5.19) for x_0 sufficiently close to the origin. Considering the first move of the sequence in (5.31), $\mathcal{U}_{n,0}^*$, it is also a linear function of x_0 such that $\mathcal{U}_n^*(x_0) \rightarrow 0$ as $x_0 \rightarrow 0$.

If we now assume that the pair $(A,\ B)$ is controllable, it follows that Assumption A1 is satisfied in the linear system case. Thus, the application of lexicographic minimum-time MPC to linear controllable systems yields a Lyapunov stable closed loop system at the origin, the trajectories of which are finite-time convergent with the basin of attraction given by $\bar{D}_\infty$ in (5.8).

We also note that in the above linear system setting, given the uniqueness of the control sequence, and assuming no model mismatch or disturbances, the principle of optimality which typically does not hold for the conventional MPC does hold for the minimum time MPC. In particular, the MPC feedback law will reproduce the elements of the initially computed optimal open-loop control sequence.

5.4 Numerical Simulations

In this section we consider an application of minimum time MPC to control of spacecraft relative motion in proximity to a nominal orbital position on a circular orbit. The linearized Clohessy-Wiltshire equations [70] for relative motion of spacecraft in the orbital plane have the following form,

$$\begin{aligned} \dot{r}_x &= v_x, \\ \dot{v}_x &= 3n^2 r_x + 2n v_y + \frac{u_1}{m}, \\ \dot{r}_y &= v_y, \\ \dot{v}_y &= -2n v_x + \frac{u_2}{m}, \end{aligned} \tag{5.32}$$

where r_x and r_y are spacecraft coordinates in Hill's frame, $m = 140$ kg is the spacecraft mass, and u_1, u_2 are thrust force components. A discrete-time model is obtained assuming a time step of 30 sec. The nominal orbit is circular with a 500 km altitude, corresponding to low-Earth orbit, and a mean motion of $n = 0.0011085\ s^{-1}$. The objective is to bring the spacecraft to the origin ($D_0 = \{0\}$) while satisfying control constraints with $U =$

$[-0.01,\ 0.01] \times [-0.01,\ 0.01]\ kN$.

Based on the theoretical results, the origin can be made an asymptotically stable and finite-time attractive equilibrium of the closed-loop system while the sets D_k are convex and compact.

The sets D_k are constructed recursively using the following procedure [92]. Assuming that D_{k-1} is polyhedral, D_k is obtained as a convex hull of the set of points which are generated by backward propagation of vertices of D_{k-1} under the control values at the vertices of U, i.e., $D_k = \text{convh}\{z :\ z = A^{-1}(x - Bu),\ x \in \text{vert}(D_{k-1}),\ u \in \text{vert}(U)\}$. The convex hull was computed using Matlab's *convhull* command.

Consider an initial state $x_0 = [-8\text{ km}, 0\text{ km}, 0.03\text{ km/s}, 0.01\text{ km/s}]^{\text{T}}$ for which $\tau^*(x_0) = 15$ and $x_0 \in D_{15}$. In the simulations, to illustrate the robustness properties of the minimum time MPC, we consider additive disturbances in the discrete-time update equations for each state drawn from the uniform distribution over the set $[-0.01,\ 0.01] \times [-0.01,\ 0.01] \times [-0.001,\ 0.001] \times [-0.001,\ 0,001]$.

Figures 5.3-5.6 compare closed-loop trajectories with and without the additive disturbance, projected into the $r_x - r_y$, $r_x - v_x$, and $r_y - v_y$ phase planes. The boundaries of the sets D_k are also shown.

5.5 Summary

This chapter formulated and treated an optimal control problem in which a discrete-time system is driven to the origin in minimum-time. The solution involves the use of sets defining the basin of attraction for the origin of the system, with relevant properties of the basin sets highlighted and demonstrated. A time-optimal MPC controller was formulated to solve the optimal control problem.

Minimum-time MPC is of interest for a range of applications to agile maneuvering. Lyapunov stability of the equilibrium may not hold under the minimum-time MPC feed-

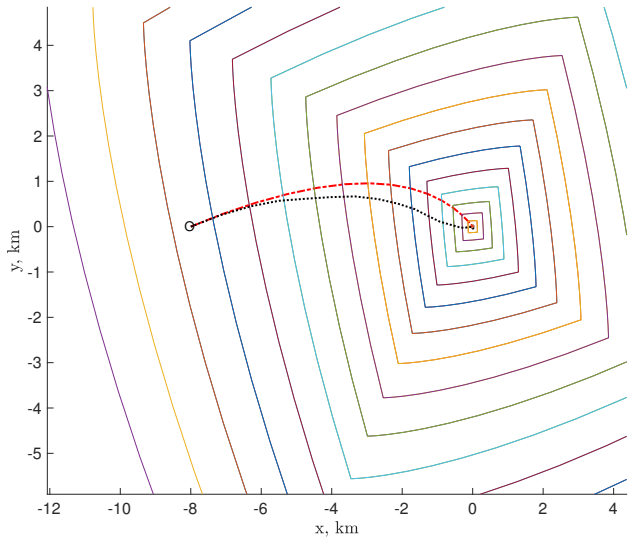

Figure 5.3: Non-perturbed (dashed) and perturbed (dotted) closed-loop trajectories in the r_x-r_y phase plane. The 'o' represents the initial state, and the target state is the origin.

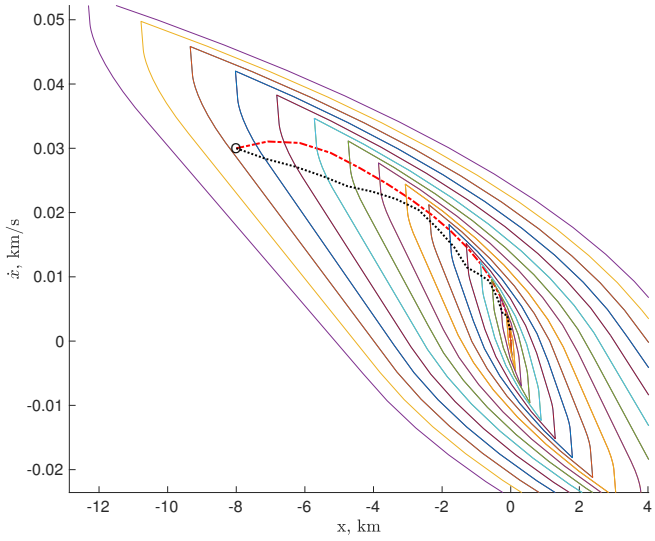

Figure 5.4: Non-perturbed (dashed) and perturbed (dotted) closed-loop trajectories in the r_x-v_x phase plane. The 'o' represents the initial state, and the target state is the origin.

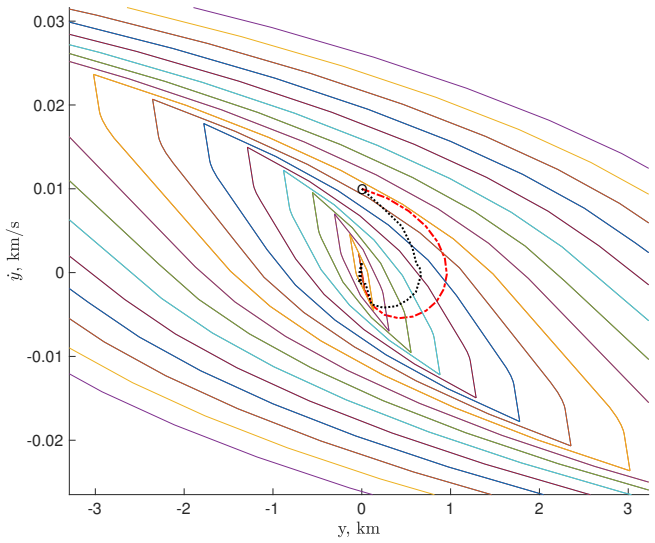

Figure 5.5: Non-perturbed (dashed) and perturbed (dotted) closed-loop trajectories in the r_y-v_y phase plane. The 'o' represents the initial state, and the target state is the origin.

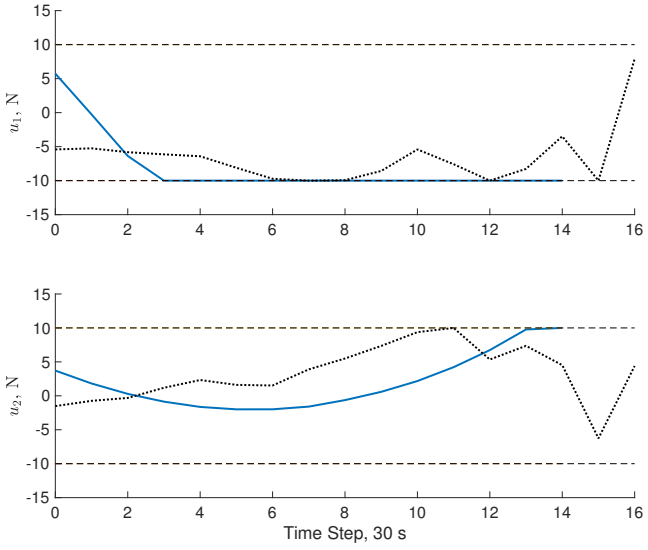

Figure 5.6: The time histories of the control input sequences $u_{1,k}$, $u_{2,k}$ generated by the lexicographic MPC. The dashed lines represent the constraint set U. Non-perturbed trajectory is solid and perturbed trajectory is dashed.

back due to the non-uniqueness of the optimal control sequence. Lyapunov stability can be recovered through a lexicographic MPC approach, which picks a minimum norm control sequence.

CHAPTER 6

Conclusions and Future Work

6.1 Conclusions

This dissertation focused on two kinds of problems. The first problem, Disjunctive Sensing and Control (DSC), concerned the design of switching sequences between mutually-exclusive actuation and estimation modes. The second problem, time-optimal control in an MPC setting, was inspired by requirements for imaging satellites to slew through as many ground targets as possible in a given time frame. For both classes of problem, theoretical and methodological results were developed and simulation results that demonstrated the viability and efficiency of the control techniques used for spacecraft control applications were reported. In addition, comprehensive control solution was developed for a magnetically actuated cubesat attitude control.

Chapter 2 treated the magnetically actuated satellite control problem in detail, with proofs of time-varying controllability and an analysis of the effects on the dynamics caused by the augmentation of the passive atmospheric drag panels. The reliance of the satellite on magnetic actuators as well as magnetic sensors created an untenable amount of magnetic noise in the sensors when both subsystems were activated together; a discrete-time LQR control scheme was developed that switched between the magnetic sensors and magnetic control rods at regular intervals, to allow the noise to dissipate. The passive actuation provided by the drag panels allowed for the development of a second, reduced-order discrete-

time LQR controller that allowed for faster control calculations, vital on a small platform such as a cubesat with limited computational resources. The discrete-time LQR controller was expanded into a model predictive controller, and simulation results were presented that supported the disturbance-rejection properties of the closed-loop predictive controller despite the switching logic implemented.

In Chapter 3, motivated by the satellite control problem, the more general problem of Disjunctive Sensing and Control (DSC) was considered. The stability properties of this more general class of switched systems were analyzed, and conditions for ensuring convergence to a limit set were derived. The efficacy of these conditions were demonstrated with simulation results. Further conditions were derived for ensuring that the limit set of the trajectory satisfied chance constraints, ensuring that desired behavior was maintained to a high probability despite random disturbance effects. Additional results and algorithms were also introduced to speed up the search for switching sequences with acceptable properties.

Chapter 4 switched the focus to the time-optimal waypoint following problem which it approached using a modified MPC scheme. As compared to the open-loop solution, the use of MPC improved robustness to unmodeled disturbances as well as dynamic model mismatch that can arise due to the application of a controller based on a linearized approximation to a non-linear dynamic system. To solve the problem computationally, a Mixed-Integer Linear Program (MILP) reformulation was defined with the binary integer state introduced to indicate if the state had entered a pre-defined target set. Simulations were provided for spacecraft attitude maneuvering with multiple waypoints, demonstrating the controller's ability to update to new waypoints in a multi-point trajectory plan. The problem was further extended by the addition of non-convex exclusion zones (obstacles) in the state space which the trajectory had to avoid. Additional binary integer optimization variables and suitable constraints were introduced to capture the obstacle avoidance requirements. While the exclusion zone handling has been shown to be possible within the same framework, it was noted that the growth in the computation time caused by the

addition of the exclusion zones is exponential. As another extension, the spacecraft attitude dynamics were further amended to include a set of flexible appendages, which were constrained from bending deflections exceeding particular limits. Simulations were presented that demonstrated the controller's ability to constrain the elastic deflections while still completing the maneuver in the minimum time.

Chapter 5 added a further consideration to the treatment of the minimum-time MPC of Chapter 4 which is the loss of Lyapunov stability of the target equilibrium if the optimal control sequence in the minimum-time MPC problem is non-unique. To recover Lyapunov stability, a lexicographic optimization approach was proposed. In this approach, a secondary objective function was minimized once the minimum time-to-go was determined. By selecting the secondary objective function to be convex, such as the 2-norm over the entire control sequence, the lexicographic optimizer returned a single, unique control sequence that restored Lyapunov stability of the equilibrium. A method of efficiently determining the minimum-time horizon was proposed, in which backward reachable sets were constructed recursively, starting at the target set and using a backwards-in-time propagation of the dynamics. Numerical simulations were presented that demonstrated the Lyapunov stability of the origin and robust operation in the presence of disturbances for a spacecraft relative motion example. From a practicl perspective, a possible alternative approach to lexicographic optimization is a blended-cost objective function that reflects both the minimum-time and minimum-effort goals in a single cost function with a much larger weight on the time-to-go; such a method is implemented in, for example, [103].

6.2 Future Work

Many topics and avenues for future work remain.

6.2.1 Disjunctive Sensing and Control (DSC)

In the DSC case, it is assumed that, of the two subsystems, one is always active. In addition, the existence of residual actuation effects was disregarded. In real satellite missions, there are multiple other subsystems, such as a radio, scientific experiments, and others. Furthermore, when actuators are activated and deactivated, the switch is not instantaneous; there is some required ramp up and ramp down time. Mission objectives and power limitation constraints could also force both the sensors and actuators offline while a third system is active. Expanding the periodic sequences to account for other systems, or to allow for residual actuation decay, while maintaining the same chance constraint guarantees should be further examined; in particular, the sequences could be modified by the addition of a third state ("act-sense-think"). In the current work, it is also assumed that the dynamic matrices are time-invariant; a further avenue of study is the case when the dynamics are time-varying, i.e., a formulation, $x_{k+1} = A(t_k)x_k + B(t_k)u_k$.

6.2.2 Waypoint-Following MPC

In the MILP solver, the addition of exclusion zones causes an exponential increase in the number of binary optimization variables and a corresponding increase in the total computation time. Finding ways to mitigate this growth in complexity without violating constraints and while maintaining close to optimal time-to-go is left as the subject for future work. In addition, while disturbance effects have been introduced in the simulations, the question of input-to-state stability with respect to additive disturbance effects is an important consideration that has received some attention in the literature [98] and which should be considered in depth in future work. Further, under the given problem formulation, it is assumed that each target set in the waypoint sequence is a robust, forward control-invariant set, that is, each target set is a "reach-and-remain" type waypoint. Given multiple waypoints, there may be an improved overall solution in which intermediate waypoints are treated as "pass-through" waypoints, without the assumption of control invariance. A MILP formulation

that accounts for “pass-through” waypoints should be considered.

APPENDIX A

Derivation of Linearized Equations of Motion

We repeat (2.5) and (2.6), which express the full combined kinematics and dynamics in terms of the state variables:

$$\begin{bmatrix} \dot{\phi} \\ \dot{\theta} \\ \dot{\psi} \end{bmatrix} = C_{\phi\theta}^{-1} \left(\begin{bmatrix} \omega_1 \\ \omega_2 \\ \omega_3 \end{bmatrix} + n \begin{bmatrix} c_\theta s_\psi \\ s_\phi s_\theta s_\psi + c_\phi c_\psi \\ c_\phi s_\theta s_\psi - s_\phi c_\psi \end{bmatrix} \right), \tag{A.1}$$

$$\mathbf{J}_b^{\mathcal{B}c} \dot{\boldsymbol{\omega}}_b^{bg} + S[\boldsymbol{\omega}_b^{bg}] \mathbf{J}_b^{\mathcal{B}c} \boldsymbol{\omega}_b^{bg} = \boldsymbol{\tau}_b^{\mathcal{B}c}. \tag{A.2}$$

where

$$C_{\phi\theta}^{-1} = \left(\frac{1}{c_\theta} \right) \begin{bmatrix} c_\theta & s_\phi s_\theta & c_\phi s_\theta \\ 0 & c_\phi c_\theta & -s_\phi c_\theta \\ 0 & s_\phi & c_\phi \end{bmatrix}.$$

A.0.1 Linearized Kinematics

By design, the desired equilibrium state is such that [ϕ, θ, ψ] = [0, 0, 0], thus we can use small angle approximations ($c_\phi \approx 1$, $s_\phi \approx \phi$) to simplify (A.1),

$$\begin{bmatrix} \dot{\phi} \\ \dot{\theta} \\ \dot{\psi} \end{bmatrix} \approx \begin{bmatrix} 1 & \phi\theta & \theta \\ 0 & 1 & -\phi \\ 0 & \phi & 1 \end{bmatrix} \left(\begin{bmatrix} \omega_1 \\ \omega_2 \\ \omega_3 \end{bmatrix} + n \begin{bmatrix} \psi \\ \phi\theta\psi + 1 \\ \theta\psi - \phi \end{bmatrix} \right). \tag{A.3}$$

Applying the equilibrium values for the Euler angles and Euler angle rates, we can easily verify that the equilibrium angular velocity values must satisfy [ω_1, ω_2, ω_3] = [0, $-n$, 0]. Expanding (A.3):

$$\begin{aligned}
\dot{\phi} &= \omega_1 + \phi\theta\omega_2 + \theta\omega_3 + n\psi(1 + \phi^2\theta^2 + \theta^2), \\
\dot{\theta} &= \omega_2 - \phi\omega_3 + n(1 + \phi^2), \\
\dot{\psi} &= \phi\omega_2 + \omega_3 + n(1 + \phi^2)\theta\psi.
\end{aligned} \tag{A.4}$$

Then, taking the partial derivative in each state variable, we get the following sets of equations:

$$\begin{aligned}
\frac{\partial\dot{\phi}}{\partial\phi} &= \theta\omega_2 + 2n\phi\theta^2\psi, \\
\frac{\partial\dot{\phi}}{\partial\theta} &= \phi\omega_2 + 2n(1 + \phi^2)\theta\psi + \omega_3, \\
\frac{\partial\dot{\phi}}{\partial\psi} &= n(1 + \phi^2\theta^2 + \theta^2), \\
\frac{\partial\dot{\phi}}{\partial\omega_1} &= 1, \quad \frac{\partial\dot{\phi}}{\partial\omega_2} = \phi\theta, \quad \frac{\partial\dot{\phi}}{\partial\omega_3} = \theta,
\end{aligned} \tag{A.5}$$

$$\begin{aligned}
\frac{\partial\dot{\theta}}{\partial\phi} &= -\omega_3 + 2n\phi, \\
\frac{\partial\dot{\theta}}{\partial\theta} &= \frac{\partial\dot{\theta}}{\partial\psi} = \frac{\partial\dot{\theta}}{\partial\omega_1} = 0, \\
\frac{\partial\dot{\theta}}{\partial\omega_2} &= 1, \quad \frac{\partial\dot{\theta}}{\partial\omega_3} = -\phi,
\end{aligned} \tag{A.6}$$

$$\begin{aligned}
\frac{\partial\dot{\psi}}{\partial\phi} &= \omega_2 + 2n\phi\theta\psi, \\
\frac{\partial\dot{\psi}}{\partial\theta} &= n(1 + \phi^2)\psi, \\
\frac{\partial\dot{\psi}}{\partial\psi} &= n(1 + \phi^2)\theta, \\
\frac{\partial\dot{\psi}}{\partial\omega_1} &= 0, \quad \frac{\partial\dot{\psi}}{\partial\omega_2} = \phi, \quad \frac{\partial\dot{\psi}}{\partial\omega_3} = 1.
\end{aligned} \tag{A.7}$$

We complete the linearization of the kinematics by plugging the equilibrium values into

the partial derivatives of the system:

$$\begin{bmatrix} \dot{\phi} \\ \dot{\theta} \\ \dot{\psi} \end{bmatrix} = \begin{bmatrix} 0 & 0 & n & 1 & 0 & 0 \\ 0 & 0 & 0 & 0 & 1 & 0 \\ -n & 0 & 0 & 0 & 0 & 1 \end{bmatrix} \begin{bmatrix} \phi \\ \theta \\ \psi \\ \omega_1 \\ \omega_2 + n \\ \omega_3 \end{bmatrix}. \tag{A.8}$$

A.0.2 Linearized Dynamics

We are treating the case of the ideal, uncontrolled dynamics, so the only external torque effect to consider is the gravity gradient. Thus, we can replace the $\tau_b^{\mathcal{B}c}$ term above with the equivalent τ_b^{gg}. Then, the dynamics can be be expressed as:

$$J\dot{\omega} + \mathrm{S}\left[\omega\right] J\omega = 3n^2 \begin{bmatrix} -(J_2 - J_3)c_\phi s_\phi c_\theta^2 \\ (J_3 - J_1)c_\phi c_\theta s_\theta \\ (J_1 - J_2)s_\phi c_\theta s_\theta \end{bmatrix}. \tag{A.9}$$

This equation simplifies to:

$$\begin{aligned} \dot{\omega}_1 &= J_{23}(\omega_2\omega_3 - 3n^2 c_\phi s_\phi c_\theta^2), \\ \dot{\omega}_2 &= J_{31}(\omega_3\omega_1 + 3n^2 c_\phi c_\theta s_\theta), \\ \dot{\omega}_3 &= J_{12}(\omega_1\omega_2 + 3n^2 s_\phi c_\theta s_\theta), \end{aligned} \tag{A.10}$$

where $J_{12} := (J_1 - J_2)/J_3$, $J_{31} := (J_3 - J_1)/J_2$, and $J_{23} := (J_2 - J_3)/J_1$.

As with the kinematics, we now apply the small-angle approximations for the Euler an-

gle terms:

$$\begin{aligned}\dot{\omega}_1 &= J_{23}(\omega_2\omega_3 - 3n^2\phi),\\ \dot{\omega}_2 &= J_{31}(\omega_3\omega_1 + 3n^2\theta),\\ \dot{\omega}_3 &= J_{12}(\omega_1\omega_2 + 3n^2\phi\theta).\end{aligned} \tag{A.11}$$

We form the Jacobian of the small-angle system by taking the first-order partial derivatives in each state variable:

$$\begin{aligned}&\frac{\partial\dot{\omega}_1}{\partial\phi} = -3n^2J_{23},\\ &\frac{\partial\dot{\omega}_1}{\partial\theta} = \frac{\partial\dot{\omega}_1}{\partial\psi} = \frac{\partial\dot{\omega}_1}{\partial\omega_1} = 0,\\ &\frac{\partial\dot{\omega}_1}{\partial\omega_2} = J_{23}\omega_3,\ \ \frac{\partial\dot{\omega}_1}{\partial\omega_3} = J_{23}\omega_2.\end{aligned} \tag{A.12}$$

$$\begin{aligned}&\frac{\partial\dot{\omega}_2}{\partial\phi} = \frac{\partial\dot{\omega}_2}{\partial\psi} = \frac{\partial\dot{\omega}_2}{\partial\omega_2} = 0,\\ &\frac{\partial\dot{\omega}_2}{\partial\theta} = 3n^2J_{31},\\ &\frac{\partial\dot{\omega}_2}{\partial\omega_1} = J_{31}\omega_3,\ \ \frac{\partial\dot{\omega}_2}{\partial\omega_3} = J_{31}\omega_1,\end{aligned} \tag{A.13}$$

$$\begin{aligned}&\frac{\partial\dot{\omega}_3}{\partial\phi} = 3n^2J_{12}\theta,\ \ \frac{\partial\dot{\omega}_3}{\partial\theta} = 3n^2J_{12}\phi,\\ &\frac{\partial\dot{\omega}_3}{\partial\psi} = \frac{\partial\dot{\omega}_3}{\partial\omega_3} = 0,\\ &\frac{\partial\dot{\omega}_3}{\partial\omega_1} = J_{12}\omega_2,\ \ \frac{\partial\dot{\omega}_3}{\partial\omega_2} = J_{12}\omega_1,\end{aligned} \tag{A.14}$$

We complete the linearization by substituting the equilibrium values into the partial derivatives:

$$\begin{bmatrix} \dot{\omega}_1 \\ \dot{\omega}_2 \\ \dot{\omega}_3 \end{bmatrix} = \begin{bmatrix} -3n^2 J_{23} & 0 & 0 & 0 & 0 & -nJ_{23} \\ 0 & 3n^2 J_{31} & 0 & 0 & 0 & 0 \\ 0 & 0 & 0 & -nJ_{12} & 0 & 0 \end{bmatrix} \begin{bmatrix} \phi \\ \theta \\ \psi \\ \omega_1 \\ \omega_2 + n \\ \omega_3 \end{bmatrix} \tag{A.15}$$

The combined linearized kinematics and dynamics equations can now be expressed by the A_c matrix that appears in (2.17).

APPENDIX B

Algebraic Riccati Equation Solution Algorithm Formulation

For implementation of the LQR controller in the satellite, we chose to follow a zero-order hold discrete-time formulation identical to (2.20), with equations repeated here for convenience. Let $t \in \mathbb{R}_{\geq 0}$ be the current time instant and A_c, $B_c(t)$ be the continuous-time dynamics defined in (2.17), (2.18). For $\Delta t > 0$, the discrete-time model predicts the state $\mathbf{x}_k$ at time $t + k\Delta t, k \in \mathbb{Z}_{\geq 0}$, according to the following model with the "frozen-in-time" magnetic field:

$$\begin{aligned} \mathbf{x}_{k+1} &= A_d \mathbf{x}_k + B_d(t)\mathbf{u}_k, \\ A_d &= e^{A_c \Delta t}, \\ B_d(t) &= -A_c^{-1}\left(\mathbf{I}_6 - A_d\right) B_c(t), \\ \mathbf{x}_0 &= \mathbf{x}(t). \end{aligned} \tag{B.1}$$

The pair $(A_d, B_d(t))$ can be verified to be controllable for all t for our orbit and choices of Δt. For the difference equation (2.20), we define the infinite-horizon cost functional J:

$$J = \sum_{k=0}^{\infty} \left(\mathbf{x}_k^T Q \mathbf{x}_k + \mathbf{u}_k^T R \mathbf{u}_k\right), \tag{B.2}$$

where $R = R^T \in \mathbb{R}^3$ is a positive definite matrix, and $Q = Q^T \in \mathbb{R}^6$ is a positive semi-definite matrix satisfying the usual detectability assumption. Then, the optimal feedback control sequence $\mathbf{u}_k = -K(t)\mathbf{x}_k$ that minimizes J has the solution:

$$K(t) = \left(R + B_d(t)^T P(t) B_d(t)\right)^{-1} B_d(t)^T P(t) A_d, \tag{B.3}$$

$$P(t) = A_d^T P(t) A_d + Q - A_d^T P(t) B_d(t) K(t). \tag{B.4}$$

Note that (2.23) can have multiple solutions; the $P(t)$ of interest to us is the unique positive definite solution. Also note that $B_d(t)$ changes throughout the orbit, thus (2.23) is solved at different instants t in time and the gain $K(t)$ in (2.22) is time-varying. The control $\mathbf{u}(t+\sigma) = K(t)\mathbf{x}(t)$ is applied for $0 \leq \sigma < \Delta t$ and then recomputed.

B.0.1 Gain Computation

Upon generating the discrete-time model in (B.1), we define the following two matrices [104]:

$$\begin{aligned} N &:= \begin{bmatrix} A_d & \mathbf{0}_{6\times 6} \\ -Q & \mathbf{I}_6 \end{bmatrix}, \\ L &:= \begin{bmatrix} \mathbf{I}_6 & B_d R^{-1} B_d^T \\ \mathbf{0}_{6\times 6} & A_d^T \end{bmatrix}, \end{aligned} \tag{B.5}$$

where $A_d \in \mathbb{R}^{6\times 6}$ and $B_d = B_d(t) \in \mathbb{R}^{6\times 3}$. From these, we form the Hamiltonian matrix

$$H = (N + L)^{-1} (N - L). \tag{B.6}$$

We require the positive square root of H^2, and employ a Newton-Raphson iteration process to compute it. We begin with an initial guess of $S_0 = \mathbf{I}_6$, the identity matrix, and then

iterate according to the following scheme:

$$S_{k+1} = 0.5\left(S_k + S_k^{-1}H^2\right). \tag{B.7}$$

Upon reaching desired convergence in S_k, we can then extract the unique positive-definite solution $P(t)$ to (2.23) from the first column of the matrix

$$\begin{bmatrix} X_1 & \sim \\ X_2 & \sim \end{bmatrix} = H - S, \tag{B.8}$$

as

$$P(t) = X_2 X_1^{-1}. \tag{B.9}$$

Given $P(t)$, we then compute

$$K(t) = \left(R + B_d(t)^T P(t) B_d(t)\right)^{-1} B_d(t)^T P(t) A_d. \tag{B.10}$$

This solution algorithm is suitable for use even on our resource-limited cubesat platform, as the necessary matrix inverses can be computed very efficiently through a decomposition scheme; in our case, we applied an LU-decomposition, as described in Anton & Rorres [105]. Furthermore, since the solution between time steps does not change significantly in this slowly-varying system, after the first gains are computed then future solutions can be "warm started", i.e., the initialization S_0 takes the value of the solution from the previous time step. This has the benefit of reducing the number of iterations required to obtain convergence. Once the solution matrix $P(t)$ is found, it is then a simple matter to compute the LQR gain matrix $K(t)$. Note that A_d, Q, and R^{-1} are invariant and do not depend on the magnetic field, hence are precomputed and stored in memory.

We measure the accuracy of the algorithm's output by taking the 2-norm of the difference between the approximate solutions, denoted $P_D(t)$, with the exact solutions $P(t)$

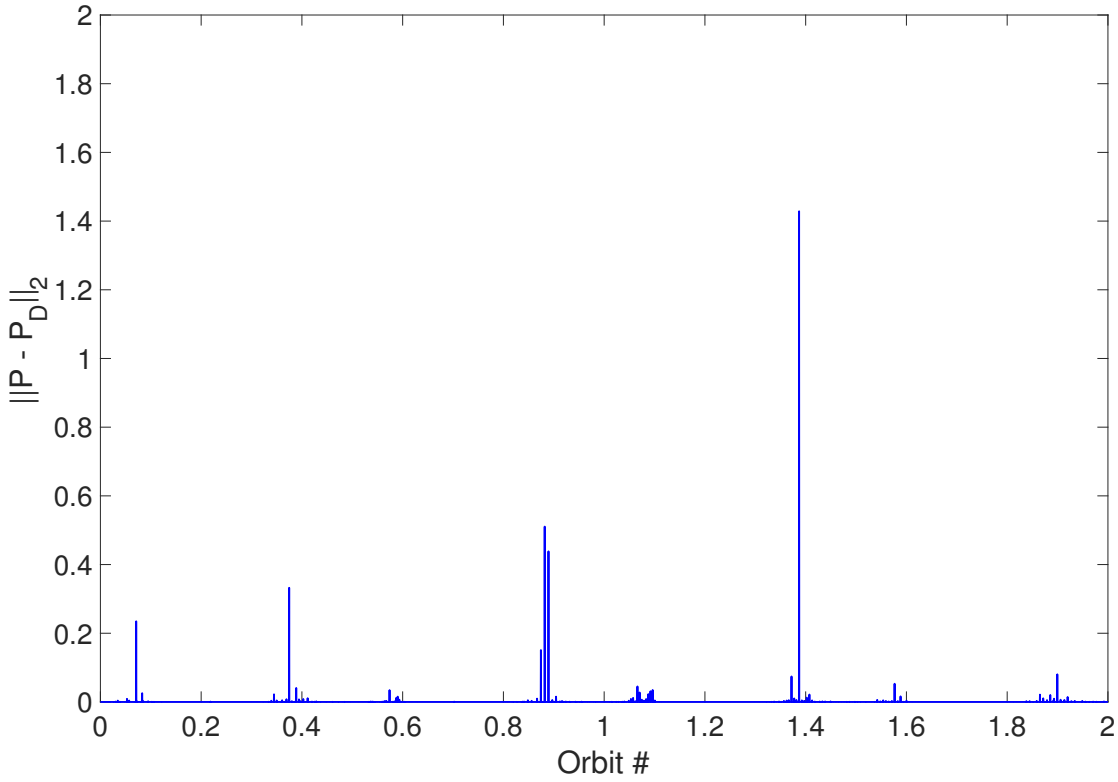

Figure B.1: 2-norm of the difference between the exact solution to the Discrete-Time Algebraic Riccati Equation and the approximate solution returned by the algorithm.

returned by Matlab's *dlqr* command over two simulated orbits. See Figure B.1. The norms are generally close to zero, indicating very strong agreement between the approximate and exact solutions, validating the use of the described algorithm.

APPENDIX C

Proof of Theorem 2.1

LTV controllability holds if the controllability matrix analogue $\mathcal{K} = [K_0,\ K_1,\ K_2]$ has full row rank for some $t_c \in [0,\ T]$ [47], where $K_j = \frac{\partial^j}{\partial \tau^j}[\Phi(t,\tau)B(\tau)]_{\tau=t}$ and $\Phi(t,\tau)$ is the state transition matrix for the A matrix. We form this matrix and show that non-singularity holds for $t_c = T/4$ under the above conditions.

Suppose the satellite's orbit aligns with the magnetic Equator, so that $i_m = 0$. Then, for all t, $b_1(t) = b_3(t) = 0$ and $b_2(t)$ is constant. Then, B is constant and takes the form

$$B = \begin{bmatrix} & \mathbf{0}_{3\times 3} & \\ b_\alpha & 0 & 0 \\ 0 & 0 & 0 \\ 0 & 0 & b_\gamma \end{bmatrix}. \tag{C.1}$$

In this case, the lack of controllability can be shown by forming the standard controllability matrix for LTI systems, $\mathcal{C} = \begin{bmatrix} B & AB & A^2B \end{bmatrix} \in \mathbb{R}^{6\times 9}$, and showing that it does not have full row rank. Each of B, AB, and A^2B has all zero entries in the fifth row, thus $\mathcal{C}$ has all zero entries in the fifth row. Thus, the row rank of $\mathcal{C}$ is at most $5 < 6$, $\mathcal{C}$ does not have full row rank, and the associated LTI system is not controllable.

Now assume that the satellite's orbit is inclined relative to the magnetic Equator. B is

time-varying, thus we must form the time-varying controllability analogue,

$$\mathcal{K} = \left[B(t) \;\; \dot{B}(t) - AB(t) \;\; A^2B(t) - 2A\dot{B}(t) + \ddot{B}(t) \right], \tag{C.2}$$

and show that the matrix $\mathcal{K}$ has full row rank for some $t_c \in [0,\ T]$. For convenience, select $t_c = T/4$, as then $nt_c = \pi/2$ and the trigonometric terms in the magnetic field approximation simplify greatly. Following Yang [47], we express the A and B matrices as follows,

$$A = \begin{bmatrix} \Sigma_1 & \mathbf{I}_3 \\ \Lambda & \Sigma_2 \end{bmatrix},\ B = \begin{bmatrix} \mathbf{0}_{3\times 3} \\ B_2 \end{bmatrix}, \tag{C.3}$$

so that $\mathcal{K}$ can then be expressed as

$$\mathcal{K} = \begin{bmatrix} \mathbf{0}_{3\times 3} & -B_2 & (\Sigma_1 + \Sigma_2)\, B_2 - 2\dot{B}_2 \\ B_2 & -\Sigma_2 B_2 + \dot{B}_2 & (\Lambda + \Sigma_2^2)\, B_2 - 2\Sigma_2\dot{B}_2 + \ddot{B}_2 \end{bmatrix}. \tag{C.4}$$

We now look for a submatrix of $\mathcal{K}$ in $\mathbb{R}^{6\times 6}$ that is non-singular. We can simplify $\mathcal{K}$ with a row reduction by premultiplying the top row by $-\Sigma_2$ and adding the result to the second row to get

$$\begin{aligned} \mathcal{K}_2 &= \begin{bmatrix} \mathbf{0}_{3\times 3} & -B_2 & (\Sigma_1 + \Sigma_2)\, B_2 - 2\dot{B}_2 \\ B_2 & \dot{B}_2 & (\Lambda - \Sigma_2\Sigma_1)\, B_2 + \ddot{B}_2 \end{bmatrix} \\ &= \begin{bmatrix} \mathbf{0}_{3\times 3} & -B_2 & M_1 \\ B_2 & \dot{B}_2 & M_2 \end{bmatrix}. \end{aligned} \tag{C.5}$$

$\mathcal{K}_2$ having a non-singular submatrix is equivalent to $\mathcal{K}$ having one, so we now work

with the new matrix instead. At the chosen time instant, we have

$$\begin{aligned} b_1(t_c) &= 0,\ \dot{b}_1(t_c) = -n\frac{\mu_f}{a^3}s_{i_m},\ \ddot{b}_1(t_c) = -n^2\frac{\mu_f}{a^3}s_{i_m} \\ b_2(t_c) &= -\frac{\mu_f}{a^3}c_{i_m},\ \dot{b}_2(t_c) = 0,\ \ddot{b}_2(t_c) = 0 \\ b_3(t_c) &= 2\frac{\mu_f}{a^3}s_{i_m},\ \dot{b}_3(t_c) = 0,\ \ddot{b}_3(t_c) = -n^2\frac{\mu_f}{a^3}s_{i_m}. \end{aligned} \tag{C.6}$$

Define $p_1 = (\mu_f/a^3)s_{i_m}$, $p_2 = (\mu_f/a^3)c_{i_m}$, $p_3 = 2(\mu_f/a^3)s_{i_m} = 2p_1$, and $p_{jk} = p_j/J_k$. Then, $\mathcal{K}_2$ takes the form,

$$\mathcal{K}_2 = \begin{bmatrix} 0 & 0 & 0 & 0 & -p_{31} & p_{21} & m_{11} & 0 & 0 \\ 0 & 0 & 0 & p_{32} & 0 & 0 & 0 & 0 & m_{12} \\ 0 & 0 & 0 & -p_{23} & 0 & 0 & 0 & m_{13} & m_{14} \\ 0 & p_{31} & -p_{21} & 0 & 0 & 0 & 0 & m_{21} & m_{22} \\ -p_{32} & 0 & 0 & 0 & 0 & np_{12} & m_{23} & 0 & 0 \\ p_{23} & 0 & 0 & 0 & -np_{13} & 0 & m_{24} & 0 & 0 \end{bmatrix}, \tag{C.7}$$

and we form a submatrix $\mathcal{K}_3$ from columns 1, 2, 4, 5, 7, and 8.

$$\mathcal{K}_3 = \begin{bmatrix} 0 & 0 & 0 & -p_{31} & m_{11} & 0 \\ 0 & 0 & p_{32} & 0 & 0 & 0 \\ 0 & 0 & -p_{23} & 0 & 0 & m_{13} \\ 0 & p_{31} & 0 & 0 & 0 & m_{21} \\ -p_{32} & 0 & 0 & 0 & m_{23} & 0 \\ p_{23} & 0 & 0 & -np_{13} & m_{24} & 0 \end{bmatrix}, \tag{C.8}$$

which we can row-reduce to,

$$\mathcal{K}_4 = \begin{bmatrix} 0 & 0 & 0 & -p_{31} & m_{11} & 0 \\ 0 & 0 & p_{32} & 0 & 0 & 0 \\ 0 & 0 & 0 & 0 & 0 & m_{13} \\ 0 & p_{31} & 0 & 0 & 0 & 0 \\ -p_{32} & 0 & 0 & 0 & m_{23} & 0 \\ p_{23} & 0 & 0 & -np_{13} & m_{24} & 0 \end{bmatrix}, \tag{C.9}$$

which has determinant $\det(\mathcal{K}_4) = (-p_{32})(-m_{13})(p_{31})(m_{24}p_{31}p_{32} - m_{23}(-p_{31})p_{23} + m_{11}p_{32}nb_{13})$. The LTV system is then controllable if this determinant is nonzero. Each p term is already nonzero, thus we seek $m_{13} \neq 0$ and $\det(\mathcal{K}_5) = m_{24}p_{31}p_{32} + m_{23}p_{31}p_{23} - m_{11}p_{32}np_{13} \neq 0$. We have:

$$\begin{aligned} m_{13} &= \frac{-2np_1}{J_3} - \frac{n(-J_3 + J_2 - J_1)p_3}{J_1 J_3} \\ &= \left(\frac{-2np_1}{J_1 J_3}\right)(J_1 - J_3 + J_2 - J_1) \\ &= \left(\frac{-2np_1}{J_1 J_3}\right)(J_2 - J_3) \\ &\neq 0 \end{aligned} \tag{C.10}$$

which, as $n \neq 0$ and $p_1 \neq 0$, implies that $J_2 \neq J_3$.

Next,

$$\begin{aligned}
m_{11}p_{32}np_{13} &= \frac{-np_1}{J_3}\frac{p_3}{J_2}\frac{p_2}{J_3}\left(\frac{nJ_1+n(J_3-J_2)}{J_1}\right) \\
&= \left(\frac{p_2p_3^2n^2}{J_1J_2J_3}\right)\left(\frac{-J_1+J_2-J_3}{2J_3}\right), \\
m_{23}p_{31}p_{23} &= \frac{p_3}{J_2}\frac{p_3}{J_1}\frac{p_2}{J_3}\left(3n^2\frac{J_3-J_1}{J_2}+n^2\frac{\Gamma}{J_2}-n^2\right) \\
&= \left(\frac{p_2p_3^2n^2}{J_1J_2J_3}\right)\left(\frac{3(J_3-J_1)+\Gamma-J_2}{J_2}\right), \\
m_{24}p_{31}p_{32} &= \frac{-p_2}{J_3}\frac{p_3}{J_1}\frac{p_3}{J_2}\left(n^2\frac{\Gamma}{J_3}-n^2\frac{J_2-J_1}{J_3}\right) \\
&= \left(\frac{p_2p_3^2n^2}{J_1J_2J_3}\right)\left(\frac{J_2-J_1-\Gamma}{J_3}\right),
\end{aligned} \tag{C.11}$$

thus, the condition

$$\det(\mathcal{K}_5) \neq 0 \tag{C.12}$$

implies, after some regrouping, that

$$J_3\left(6(J_3-J_1)+2\Gamma\right) \neq J_2\left(J_1-J_2+J_3-2\Gamma\right). \tag{C.13}$$

BIBLIOGRAPHY

[1] Giancoli, D., *Physics: Principles with Applications*, Prentice Hall, 3rd ed., 1991.

[2] Sun, Z. and Ge, S., *Switched Linear Systems: Control and Design*, Springer-Verlag, 2005.

[3] Teel, A., Subbaraman, A., and Sferlazza, A., "Stability analysis for stochastic hybrid systems: A survey," *Automatica*, Vol. 50, 2014, pp. 2435–2456.

[4] van der Schaft, A. and Schumacher, H., *An Introduction to Hybrid Dynamical Systems*, Dutch Institute of Systems and Control, 1999.

[5] Acary, V. and Brogliato, B., *Numerical Methods for Nonsmooth Dynamical Systems: Applications in Mechanics and Electronics*, Springer-Verlag, 2008.

[6] White, D., Wozniak, J., and Lawrence, D., "Missile autopilot design using a gain scheduling technique," *Proceedings of the 26th Southeastern Symposium on System Theory*, 1994, pp. 606–610.

[7] Liberzon, D. and Morse, A., "Basic problems in stability and design of switched systems," *IEEE Control Systems Magazine*, Vol. 19, October 1999, pp. 59–70.

[8] Camacho, E. and Alba, C., *Model Predictive Control*, Springer Science & Business Media, 2013.

[9] Frey, G., *Advances in Constrained Spacecraft Relative Motion Planning*, Ph.D. thesis, University of Michigan - Ann Arbor, 2018.

[10] Richards, A. and How, J., "Mixed-integer Programming for Control," *Proceedings of the 2005 American Control Conference*, June 2005, pp. 2676–2683.

[11] Bertsimas, D. and Tsitsiklis, J., *Introduction to Linear Optimization*, Athena Scientific, 1997.

[12] Linderoth, J. and Savelsbergh, M., "A computational study of branch and bound search strategies for mixed integer programming," *INFORMS Journal on Computing*, Vol. 11, 1999, pp. 173–187.

[13] Barnhart, C., Johnson, E., Nemhauser, G., Savelsbergh, M., and Vance, P., "Branch-and-price: column generation for solving huge integer programs," *Operations Research*, Vol. 46, 1998, pp. 316–329.

[14] Harjunkoski, I., Kabore, P., and Fahl, M., "An efficient MILP-heuristic approach for solving large-scale multi-stage scheduling problems," *Proceedings of the AIChE Annual Meeting*, 2004.

[15] Glover, F. and Laguna, M., *Tabu search*, Kluwer Academic Publishers, 1997.

[16] Pantelides, C., Realff, M., and Shah, N., "Short-Term Scheduling of Pipeless Batch Plants," *Chemical Engineering Research and Design*, Vol. 75, 1997, pp. S156–S169.

[17] Johnson, D. and McGeoch, L., *Local Search in Combinatorial Optimization*, John Wiley & sons, 1997.

[18] Zidek, R., *Drift Counteraction Optimal Control: Theory and Applications to Autonomous Cars and Spacecraft*, Ph.D. thesis, University of Michigan - Ann Arbor, 2017.

[19] Bertsekas, D., *Dynamic Programming and Optimal Control*, Vol. 1, Athena Scientific, 2005.

[20] Kolmanovsky, I., Lezhnev, L., and Maizenberg, T., "Discrete-time drift counteraction stochastic optimal control," *Automatica*, Vol. 44, No. 1, 2008, pp. 177–184.

[21] Balasubramanian, K. and Kolmanovsky, I., "Range maximization of a direct methanol fuel cell powered mini air vehicle using stochastic drift counteraction optimal control," *Proceedings of the 2012 American Control Conference*, June 2012.

[22] Kolmanovsky, I. and Menezes, A., "A stochastic drift counteraction optimal control approach to glider flight management," *Proceedings of the 2011 American Control Conference*, 2011, pp. 1009–1014.

[23] Tedesco, F., Raimondo, D., and Casavola, A., "Collision avoidance command governor for multi-vehicle unmanned systems," *International Journal of Robust and Nonlinear Control*, Vol. 24, No. 16, 2014, pp. 2309–2330.

[24] Sutherland, R., Kolmanovsky, I., and Girard, A., "Attitude Control of a 2U Cubesat by Magnetic and Air Drag Torques," *IEEE Transactions on Control Systems Technology*, 2018.

[25] Sutherland, R., Kolmanovsky, I., Girard, A., Leve, F., and Petersen, C., "Optimal strategies for disjunctive sensing and control," *arXiv e-prints*, September 2018, pp. 1–6.

[26] Sutherland, R., Kolmanovsky, I., and Girard, A., "LQ Attitude Control of a 2U Cubesat by Magnetic Actuation," *Proceedings of the Space Flight Mechanics Meeting*, February 2017.

[27] Sutherland, R., Kolmanovsky, I., Girard, A., Leve, F., and Petersen, C., "Optimal Strategies for Disjunctive Sensing and Control," *Proceedings of the 2018 IEEE American Control Conference*, 2018, pp. 4712–4717.

[28] Sutherland, R., Kolmanovsky, I., Girard, A., Leve, F., and Petersen, C., "Minimum-time Model Predictive Spacecraft Attitude Control for Waypoint Following and Exclusion Zone Avoidance," *Proceedings of the AIAA SciTech Forum*, January 2019.

[29] Sutherland, R., Kolmanovsky, I., Girard, A., Leve, F., and Petersen, C., "On Closed-loop Lyapunov Stability with Minimum-time MPC Feedback Laws for Discrete-time Systems," *Proceedings of the 58th Conference on Decision and Control (submitted)*, December 2019, pp. 1–7.

[30] "QB50 - The Project - Scientific Research," https://www.qb50.eu/index.php/project-description-obj, Last Accessed: Oct 4, 2016.

[31] "University of Michigan Sends Satellite into Space," http://www.fox2detroit.com/news/local-news/254297170-story, Last Accessed: May 19, 2017.

[32] Krishnan, H., McClamroch, N., and Reyhanoglu, M., "Attitude Stabilization of a Rigid Spacecraft Using Two Momentum Wheel Actuators," *Journal of Guidance, Control, and Dynamics*, Vol. 18, March 1995, pp. 256–263.

[33] Krishnan, H., Reyhanoglu, M., and McClamroch, N., "Attitude Stabilization of a Rigid Spacecraft Using Two Control Torques: A Nonlinear Control Approach based on the Spacecraft Attitude Dynamics," *Automatica*, Vol. 30, 1994, pp. 1023–1027.

[34] Crouch, P., "Spacecraft Attitude Control and Stabilization: Applications of Geometric Control Theory to Rigid Body Models," *Transactions on Automatic Control*, Vol. 29, 1984, pp. 321–332.

[35] Petersen, C., Leve, F., and Kolmanovsky, I., "Model Predictive Control of an Underactuated Spacecraft with Two Reaction Wheels," *AIAA Journal of Guidance, Control, and Dynamics*, to appear.

[36] Ferreira, L. and Cruz, J., "Attitude and Spin Rate Control of a Spinning Satellite Using Geomagnetic Field," *Journal of Guidance, Control, and Dynamics*, Vol. 14, January 1991, pp. 216–218.

[37] Rodden, J., "Closed-Loop Magnetic Control of a Spin-Stabilized Satellite," *Automatica*, Vol. 20, 1984, pp. 729–735.

[38] Wisniewski, R. and Blanke, M., "Fully-Magnetic Attitude Control for Spacecraft Subject to Gravity-Gradient," *Automatica*, Vol. 35, 1999, pp. 1201–1214.

[39] Steyn, W., "Comparison of Low-Earth-Orbit Satellite Attitude Controllers Submitted to Controllability Constraints," *Journal of Guidance, Control, and Dynamics*, Vol. 17, No. 4, July-August 1994, pp. 795–804.

[40] Psiaki, M., "Magnetic Torquer Attitude Control via Asymptotic Periodic Linear Quadratic Regulation," *Journal of Guidance, Control, and Dynamics*, Vol. 24, March/April 2001, pp. 386–394.

[41] Psiaki, M., "Nanosatellite Attitude Stabilization Using Passive Aerodynamics and Active Magnetic Torquing," *Journal of Guidance, Control, and Dynamics*, Vol. 27, May/June 2004, pp. 347–355.

[42] Lovera, M. and Astolfi, A., "Spacecraft Attitude Control using Magnetic Actuators," *Automatica*, Vol. 40, August 2004, pp. 1405–1414.

[43] De Ruiter, A., Damaren, C., and Forbes, J., *Spacecraft Dynamics and Control: An Introduction*, Wiley, West Sussex, United Kingdom, 2013.

[44] Slabaugh, G., "Computing Euler Angles From a Rotation Matrix," http://www.staff.city.ac.uk/~sbbh653/publications/euler.pdf, Last Accessed: Nov 6, 2017.

[45] Weiss, A., *Predictive, Adaptive, and Time-Varying Control of Spacecraft Orbits and Attitude*, Ph.D. thesis, University of Michigan, 2013.

[46] Wie, B., *Space Vehicle Dynamics and Control*, American Institute of Aeronautics and Astronautics, Reston, VA, 2008.

[47] Yang, Y., "Controllability of Spacecraft using only Magnetic Torques," *IEEE Transactions on Aerospace and Electronic Systems*, Vol. 52, April 2016, pp. 954–961.

[48] Yang, Y., "An Efficient Algorithm for Periodic Riccati Equation with Periodically Time-Varying Input Matrix," *Automatica*, Vol. 78, 2017, pp. 103–109.

[49] Vermillion, C., Grunnagle, T., Lim, R., and Kolmanovsky, I., "Model-based Plant Design and Hierarchical Control of a Prototype Lighter-than-Air Wind Energy System, with Experimental Flight Test Results," *IEEE Transactions on Control Systems Technology*, Vol. 22, No. 2, March 2014, pp. 531–542.

[50] Mostaza-Prieto, D. and Roberts, P., "Methodology to Analyze Attitude Stability of Satellites Subjected to Aerodynamic Torques," *Journal of Guidance, Control, and Dynamics*, Vol. 39, 2016, pp. 437–449.

[51] Gombosi, T., *Physics of the Space Environment*, Cambridge University Press, Cambridge, 1998.

[52] Wertz, J., *Spacecraft Attitude Determination and Control*, Reidel, Netherlands, 1978.

[53] "International Geomagnetic Reference Field," http://www.ngdc.noaa.gov/IAGA/vmod/igrf.html, Revised 2014-12-22, Accessed 2016-06-01.

[54] Mazzini, L., *Flexible Spacecraft Dynamics, Control, and Guidance*, Springer, 2016.

[55] Fehse, W., *Automated Rendezvous and Docking of Spacecraft*, Cambridge University Press, 2003.

[56] Liberzon, D., *Switching in Systems and Control*, Birkhauser Boston, 2003.

[57] Sun, Z., *Switched Linear Systems: Control and Design*, Springer Science & Business Media, 2006.

[58] Bittanti, S. and Colaneri, P., *Periodic Systems: Filtering and Control*, Springer, 2009.

[59] Sadkane, M. and Grammont, L., "A Note on the Lyapunov Stability of Periodic Discrete-Time Systems," *Journal of Computational and Applied Mathematics*, Vol. 176, 2005, pp. 463–466.

[60] Zhou, B., Zheng, W., and Duan, G., "Stability and Stabilization of Discrete-Time Periodic Linear Systems with Actuator Saturation," *Automatica*, Vol. 47, 2011, pp. 1813–1820.

[61] Heemels, W., Johansson, K., and Tabuada, P., "An Introduction to Event-Triggered and Self-Triggered Control," *Proceedings of the 51st annual Conference on Decision and Control*, 2012.

[62] Liu, S., Fardad, M., Masazade, E., and Varshney, P., "Optimal Periodic Sensor Scheduling in Networks of Dynamical Systems," *IEEE Transactions on Signal Processing*, Vol. 62, 2014, pp. 3055–3068.

[63] Sunberg, Z., Chakravorty, S., and Erwin, R., "Information Space Receding Horizon Control," *IEEE Transactions on Cybernetics*, Vol. 43, No. 6, 2013, pp. 2255–2260.

[64] Chen, C., *Linear System Theory and Design*, Oxford University Press, 3rd ed., 1999.

[65] Halanay, A. and Rasvan, V., *Stability and Stable Oscillations in Discrete-Time Systems*, Gordon and Breach Science Publishers, 2000.

[66] Yu, Q. and Zhao, X., "Stability Analysis of Discrete-Time Switched Linear Systems with Unstable Subsystems," *Applied Mathematics and Computation*, Vol. 273, 2016, pp. 718–725.

[67] Lax, P. D., *Functional Analysis*, Wiley, 2002.

[68] Navarro, J., "A very simple proof of the multivariate Chebyshev's inequality," *Communications in Statistics - Theory and Methods*, Vol. 45, 2016, pp. 3458–3463.

[69] Chen, X., "A New Generalization of Chebyshev Inequality for Random Vectors," *arXiv preprint*, Vol. arXiv:0707.0805, 2011, pp. 1–7.

[70] Clohessy, W. and Wiltshire, R., "Terminal Guidance System for Satellite Rendezvous," *Journal of the Aerospace Sciences*, Vol. 4, No. 9, 1960, pp. 653–658.

[71] Tóth, R., Heuberger, P., and Van den Hof, P., "Discretisation of Linear Parameter-Varying State-Space Representations," *IET Control Theory and Applications*, Vol. 4, 2010, pp. 2082–2096.

[72] Karpenko, M. and Ross, I., "Flight Implementation of Shortest-Time Maneuvers for Imaging Satellites," *Journal of Guidance, Control, and Dynamics*, Vol. 37, No. 4, July-August 2014, pp. 1069–1079.

[73] Rawlings, J. B. and Mayne, D. Q., *Model Predictive Control: Theory and Design*, Nob Hill Pub., 2009.

[74] Borrelli, F., Bemporad, A., and Morari, M., *Predictive Control for Linear and Hybrid Systems*, Cambridge University Press, 2017.

[75] Floudas, C., *Nonlinear and Mixed-Integer Optimization - Fundamentals and Applications*, Oxford University Press, 1995.

[76] Richards, A. and How, J., "Model Predictive Control of Vehicle Maneuvers with Guaranteed Completion Time and Robust Feasibility," *Proceedings of the 2003 American Control Conference*, 2003, pp. 4034–4040.

[77] Zidek, R., Petersen, C., Bemporad, A., and Kolmanovsky, I., "Receding Horizon Drift Counteraction and its Application to Spacecraft Attitude Control," *Proceedings of 27th AAS/AIAA Space Flight Mechanics Meeting, February 5-9, 2017, San Antonio, Texas, published in Advances in the Astronautical Science*, Vol. 160, Univelt Inc., 2017, pp. 3865–3879.

[78] Zidek, R., Bemporad, A., and Kolmanovsky, I., "Optimal and Receding Horizon Drift Counteraction Control: Linear Programming Approaches," *Proceedings of American Control Conference (ACC), 2017*, 2017, pp. 2636–2641.

[79] Zidek, R., Kolmanovsky, I., and Bemporad, A., "Spacecraft Drift Counteraction Optimal Control: Open-loop and Receding Horizon Solutions," *Journal of Guidance, Control, and Dynamics*, Vol. 41, No. 9, 2018, pp. 1859–1872.

[80] Park, H., Kolmanovsky, I., and Sun, J., "Parametric Integrated Perturbation nalysis-Sequential Quadratic Programming pproach for Minimum-Time Model Predictive Control," *Proceedings of 19th IFAC World Congress, Cape Town, South Africa, IFAC Proceedings Volumes*, Vol. 47, IFAC, 2014, pp. 1922–1927.

[81] Petersen, C., Baldwin, M., and Kolmanovsky, I., "Model Predictive Control Guidance with Extended Command Governor Inner-Loop Flight Control for Hypersonic Vehicles," *Proceedings of AIAA Guidance, Navigation, and Control Conference*, AIAA, 2013, pp. 1–20.

[82] Starek, J. and Kolmanovsky, I., "Nonlinear Model Predictive Control Strategy for Low-thrust Spacecraft Missions," *Optimal Control Applications and Methods*, Vol. 35, 2014, pp. 1–20.

[83] Richards, A., Schouwenaars, T., How, J., and Feron, E., "Spacecraft Trajectory Planning with Avoidance Constraints Using Mixed-Integer Linear Programming," *Journal of Guidance, Control, and Dynamics*, Vol. 25, No. 4, 2002, pp. 755–764.

[84] ILOG Inc., Mountain View, C., "ILOG AMPL CPLEX System Version 10.0 Users Guide," https://ampl.com/BOOKLETS/amplcplex100userguide.pdf, Retrieved 2 Apr 2019.

[85] Zhang, L., Zhou, Z., and Zhang, F., "Mixed Integer Linear Programming for UAV Trajectory Planning Problem," *Applied Mechanics and Materials*, Vol. 541-542, 2014, pp. 1473–1477.

[86] Shekhar, R., Kearney, M., and Shames, I., "Robust Model Predictive Control of Unmanned Aerial Vehicles Using Waysets," *Journal of Guidance, Control, and Dynamics*, Vol. 38, No. 10, 2015, pp. 1898–1907.

[87] Di Gennaro, S., "Passive Attitude Control of Flexible Spacecraft from Quaternion Measurements," *Journal of Optimization Theory and Applications*, Vol. 116, No. 1, 2003, pp. 41–60.

[88] Ton, C. and Petersen, C., "Continuous Fixed-Time Sliding Mode Control for Spacecraft with Flexible Appendages," *IFAC Papers Online*, Vol. 51, 2018, pp. 1–5.

[89] Ngo, T. and Sultan, C., "Model Predictive Control for Helicopter Shipboard Operations in the Ship Airwakes," *Journal of Guidance, Control, and Dynamics*, Vol. 38, No. 12, 2015, pp. 574–589.

[90] Hartley, E., "A Tutorial on Model Predictive Control for Spacecraft Rendezvous," *Proceedings of the European Control Conference*, 2015, pp. 1355–1361.

[91] Tsiotras, P. and Mesbahi, M., "Toward an Algorithmic Control Theory," *Journal of Guidance, Control, and Dynamics*, Vol. 40, No. 2, 2017, pp. 194–196.

[92] Keerthi, S. and Gilbert, E., "Computation of Minimum-time Feedback Control Laws for Discrete-Time Systems with State-Control Constraint," *IEEE Transactions on Automatic Control*, Vol. 32, No. 5, 1987, pp. 432–435.

[93] Mayne, D. and Schroeder, W., "Robust time-optimal control of constrained linear systems," *Automatica*, Vol. 33, No. 12, 1997, pp. 2103–2118.

[94] Rothwangl, H., "Numerical synthesis of the time optimal nonlinear state controller via mixed integer programming," *Proceedings of 2001 American Control Conference*, 2001, pp. 3201–3205.

[95] Verschueren, R., Ferreau, H., Zanarini, A., Mercangöz, M., and Diehl, M., "A Stabilizing Nonlinear Model Predictive Control Scheme for Time-optimal Point-to-point Motions," *Proceedings of 56th IEEE Annual Conference on Decision and Control*, 2017, pp. 2525–2530.

[96] Grieder, P., Kvasnica, M., Baotic, M., and Morari, M., "Stabilizing low complexity feedback control of constrained piecewise affine systems," *Automatica*, Vol. 41, 2005, pp. 1683–1694.

[97] Zidek, R. A., Kolmanovsky, I., and Bemporad, A., "Spacecraft Drift Counteraction Optimal Control: Open-Loop and Receding Horizon Solutions," *Journal of Guidance, Control, and Dynamics*, Vol. 41, No. 9, 2018, pp. 1859–1872.

[98] Anderson, A., González, A., Ferramosca, A., and Kofman, E., "Finite-time Convergence Results in Robust Model Predictive Control," *Optimal Control Applications and Methods*, Vol. 39, 2018, pp. 1627–1637.

[99] Kerrigan, E. and Maciejowski, J., "Designing Model Predictive Controllers with Prioritised Constraints and Objectives," *Proceedings of IEEE International Symposium on Computer Aided Control System Design*, 2002, pp. 33–38.

[100] He, D., Wang, L., and Sun, J., "On Stability of Multiobjective NMPC with Objective Prioritization," *Automatica*, Vol. 57, 2015, pp. 189–198.

[101] Anilkumar, M., Padhiyar, N., and Moudgalya, K., "Lexicographic optimization based MPC: Simulation and experimental study," *Computers and Chemical Engineering*, Vol. 88, 2016, pp. 135–144.

[102] Lange, K., *Optimization*, chap. 5, Springer-Verlag, 2nd ed., 2013, pp. 107–135.

[103] Liu, G., Ceylan, O., Xiao, B., Starke, M., Ollis, T., King, D., Irminger, P., and Tomsovic, K., "Advanced Energy Storage Management in Distribution Network," *Proceedings of the 49th Hawaii International Conference on System Sciences*, January 2016, pp. 1–9.

[104] Lu, L. and W., L., "An Iterative Algorithm for the Solution of the Discrete-Time Algebraic Riccati Equation," *Linear Algebra and its Applications*, Vol. 188-189, July-August 1993, pp. 465–488.

[105] Anton, H. and Rorres, C., *Elementary Linear Algebra: Applications Version*, Wiley, New York, 2000.